

FIAN TD31/00

UCRHEP-E273

April 7, 2000

(revised September 18, 2000)

## HADRON MULTIPLICITIES

I.M. Dremin<sup>1</sup>, J.W. Gary<sup>2</sup><sup>1</sup>*Lebedev Physical Institute, Moscow 117924, Russia*<sup>2</sup>*Department of Physics, University of California, Riverside CA 92521,  
USA*

### Abstract

We review results on hadron multiplicities in high energy particle collisions. Both theory and experiment are discussed. The general procedures used to describe particle multiplicity in Quantum Chromodynamics (QCD) are summarized. The QCD equations for the generating functions of the multiplicity distributions are presented both for fixed and running coupling strengths. The mean multiplicities of gluon and quark jets, their ratio, higher moments, and the slopes of multiplicities as a function of energy scale, are among the main global features of multiplicity for which QCD results exist. Recent data from high energy  $e^+e^-$  experiments, including results for separated quark and gluon jets, allow rather direct tests of these results. The theoretical predictions are generally quite successful when confronted with data. Jet and subjet multiplicities are described. Multiplicity in limited regions of phase space is discussed in the context of intermittency and fractality. The problem of singularities in the generating functions is formulated. Some special features of average multiplicities in heavy quark jets are described.

# Contents

<b>1</b>	<b>Introduction</b>	<b>4</b>
<b>2</b>	<b>Definitions and notation</b>	<b>9</b>
<b>3</b>	<b>Phenomenology</b>	<b>13</b>
3.1	KNO scaling and $F$ scaling . . . . .	14
3.2	Entropy scaling . . . . .	15
3.3	Conventional distributions . . . . .	17
3.3.1	The Poisson distribution . . . . .	17
3.3.2	The negative binomial distribution and its generaliza- tions . . . . .	18
3.3.3	The fixed multiplicity and Gaussian distributions . . .	21
3.4	Some models . . . . .	24
3.5	Experimental phenomenology . . . . .	26
<b>4</b>	<b>Equations of Quantum Chromodynamics</b>	<b>29</b>
<b>5</b>	<b>Gluodynamics</b>	<b>33</b>
5.1	Approximate solutions of equations with fixed coupling con- stant and the shape of the KNO function . . . . .	33
5.2	Higher order approximations with a running coupling constant	39
<b>6</b>	<b>Perturbative solutions of QCD equations with a running cou- pling constant</b>	<b>44</b>
6.1	Average multiplicities and their slopes . . . . .	46
6.2	Widths of the distributions . . . . .	53
<b>7</b>	<b>Computer solutions</b>	<b>58</b>
<b>8</b>	<b>Exact solutions of QCD equations with a fixed coupling con- stant</b>	<b>60</b>
8.1	First moments and the ratio of average multiplicities in gluon jets to those in quark jets . . . . .	60
8.2	Widths and higher rank moments of multiplicity distributions in gluon and quark jets . . . . .	65

<b>9</b>	<b>Non-perturbative modifications of QCD equations</b>	<b>73</b>
<b>10</b>	<b>Singularities of the generating functions</b>	<b>74</b>
<b>11</b>	<b>Measurements of mean multiplicity, slopes, and higher moments</b>	<b>77</b>
11.1	Mean multiplicity . . . . .	80
11.2	Multiplicity ratio . . . . .	86
11.3	Slopes . . . . .	90
11.4	Higher moments . . . . .	91
11.5	Oscillating $H_q$ moments . . . . .	97
11.6	Soft particles . . . . .	99
<b>12</b>	<b>Jet and subjet multiplicities</b>	<b>106</b>
<b>13</b>	<b>Multiplicity of three-jet events</b>	<b>111</b>
<b>14</b>	<b>Evolution of distributions with decreasing phase space: intermittency and fractality</b>	<b>113</b>
<b>15</b>	<b>Heavy quark jets</b>	<b>122</b>
<b>16</b>	<b>Conclusions</b>	<b>126</b>
<b>17</b>	<b>Acknowledgments</b>	<b>128</b>

# 1 Introduction

The number of hadrons created in high energy inelastic collisions varies from one event to another. The distribution of the number of produced hadrons (the multiplicity distribution, for short) provides a basic means to characterize the events. The multiplicity distribution contains information about multiparticle correlations in an integrated form, providing a general and sensitive means to probe the dynamics of the interaction.

Here, we would like to review the main theoretical approaches and experimental results concerning hadron multiplicities. Much precise experimental information on multiplicities has become available in recent years from  $e^+e^-$ , hadron, and nucleus collisions. The experimental progress has stimulated additional theoretical developments. Therefore, the time seems appropriate for a review. The theoretical results summarized here represent an expanded and updated version of an earlier work [1].

After introducing basic definitions and notation in Section 2, we turn in Section 3 to describe some phenomenological approaches to multiplicity. The phenomenological methods are based on simplified ideas about particle emission, exploiting widely used distributions from probability theory (see e.g. Ref. [2]). Among them, the negative binomial distribution is especially popular because it describes experimental data reasonably well for various reactions over a wide energy interval.

The discovery of asymptotic freedom, in conjunction with the parton model used to characterize deep inelastic and  $e^+e^-$  data, led to the development of the theory of strong interactions, Quantum Chromodynamics (QCD). QCD provides a means to apply perturbative techniques to hadronic processes with large transferred momenta, with quarks and gluons playing the role of partons [3]-[7]. The current state of affairs concerning multiplicity in quark and gluon jets as predicted by QCD and measured by experiment forms the bulk of our review, presented in Sections 4-15.

Lattice calculations imply that hadronization – the transition of quarks and gluons to hadrons at the final stage of evolution – is an inherent property of QCD. Nonetheless, we are still unable to treat hadronization in an unambiguous manner since the problem of confinement has yet to be solved mathematically. Simplified estimates suggest either that hadronization does not drastically alter the parton level results or else that its effects can be estimated from the energy dependence of experimental observables. Phe-

nomenologically, the distributions of partons and hadrons are often found to be remarkably similar. This implies that the study of the partonic stage of an event is of utmost importance since the properties of high energy multi-hadronic events are primarily determined at that level.

The probabilistic equations of QCD for the parton cascade can be solved within the perturbative approach. The parton shower framework allows the use of sub-series of the perturbative expansion, with terms ordered according to their energy behavior. The zero order approximation already involves an arbitrary number of produced particles. Higher order approximations lead to detailed predictions for multiplicity distributions which can be tested through comparison with experiment. Before proceeding to details in the following sections, however, we wish to note two problematic areas and then briefly comment on the main topics we address.

First, QCD yields results on partons, and not hadrons, as already mentioned. Therefore an assumption about hadronization must be made in any comparison of experiment with theory. A common assumption is local parton-hadron duality (LPHD) [8], which states that parton distributions are simply renormalized in the process of hadronization, without changing their shape. LPHD originated from the idea of soft preconfinement [9], whereby partons group in colorless clusters without disturbing the initial spectra. Phenomenological models of hadronization have been incorporated into Monte Carlo simulations of inelastic processes and in most cases support the approximate property of LPHD.

Second, perturbative analysis has limitations in the context of any specific approximation. Formally speaking, perturbation theory should be used only when the coupling constant is very small compared to unity. This condition is fulfilled by QCD only for extremely large transferred momenta, however, often for energies much larger than present experimental conditions. In any QCD process, the energies of cascading partons degrade during their evolution, and a proper accounting for soft partons, their recoil due to interaction, and energy-momentum conservation laws, should be included. All these considerations are neglected in the lowest order approximation, for which only processes with a rather large gradient of energies and emission angles at each stage of the evolution are considered (the so-called double-logarithmic approximation, DLA<sup>1</sup>). Account is taken of soft partons and strict transverse

---

<sup>1</sup>Also referred to as leading order (LO).

momentum ordering in subsequent terms of the perturbative series, such as the modified leading-logarithmic approximation (MLLA<sup>2</sup>). Recoil effects and conservation laws can be incorporated at the next-to-next-to-leading order (NNLO), the next-to-next-to-next-to-leading order (3NLO), and higher order stages. The conservation laws are more accurately included, the higher the order of the perturbative approximation.

In most cases these corrections are under control, being about 10-20% percent of the main terms at present energies. In spite of their rather small total contribution, they are often very important and change the qualitative theoretical description in regions where the corresponding functions are small. For example, they are crucial for the proper description of the multiparticle production process. This manifests itself mathematically as a new expansion parameter equal to the product of the QCD coupling constant (or, more precisely, of its square root) and the rank of the moment of the distribution. Thus it is for large ranks, i.e. high multiplicities, that the corrections are most important. These problems are discussed in detail in Sections 4-8.

The first results on the multiplicity distributions of partons were obtained using the double-logarithmic approximation (for reviews, see Refs. [7, 10]). They yielded asymptotic Koba-Nielsen-Olesen (KNO) scaling [11]. According to the KNO hypothesis [12], the multiplicity distribution depends only on the ratio of the number of particles to the average multiplicity (see Section 3). KNO scaling failed to be valid in the higher order approximations, however, i.e. the asymptotic realm is too far from present energies. At the same time, the width of the asymptotic KNO function was found to be much larger than experimental distributions. This problem was resolved [13, 14] through consideration of the higher order effects mentioned above. The increase of average multiplicity with energy was found to depend on the coupling constant in a manner which is faster than any logarithmic function and slower than any power-like one (if the running coupling constant is used), in agreement with experimental findings. One can now state that an overall agreement between theory and data has been achieved, at least qualitatively.

Moreover, some qualitative predictions of perturbative QCD (pQCD) were found to be unexpectedly well suited for “soft” hadronic processes as well. Given the large value of the expansion parameter at small scales, this may seem puzzling. However, higher order corrections should account for

---

<sup>2</sup>Also referred to as next-to-leading-order (NLO).

ever softer partons in a consistent manner, implying a more general correspondence between soft and hard processes than is usually considered in theoretical schemes. For example, the newly discovered feature of the oscillation of cumulant moments (see Section 5.2), prompted by solutions of the QCD equations, were experimentally observed in  $e^+e^-$ , hadron-, and nucleus-induced reactions. These oscillations were found to be extremely sensitive to small details of the multiplicity distributions.

Many discussions are devoted to the value of the ratio of average multiplicities between gluon and quark jets,  $r$ . The value obtained in the double-logarithmic approximation is  $r=9/4$ . The simplest corrections reduce this value by about 10%. An even larger decrease of  $r$  is predicted by the exact solution of the equations for the generating functions in the case of a fixed coupling constant, by the analytic higher order approximations with a running coupling constant, and by computer solutions of these equations. These results are discussed in Sections 6-8. A proper accounting for the boundary between the perturbative and non-perturbative regions appears to be crucial for this quantity. The energy dependence of the average multiplicities, i.e. their slopes, is considered in Section 6. The ratios of the slopes and of the corresponding curvatures are found to be less sensitive to higher order corrections than the ratio of multiplicities itself. Some attempts to account for non-perturbative effects in evolving jets are briefly described in Section 9.

The behavior of the moments of multiplicity is strongly influenced by the nature of the singularities of the generating function, which are not yet known. Approaches to this problem are discussed in Section 10.

Experimental measurements of multiplicity as they relate to tests of the QCD predictions are described in Section 11. Especially noteworthy are recent data from  $e^+e^-$  annihilation experiments operating on the  $Z^0$  peak, namely the four experiments ALEPH, DELPHI, L3 and OPAL at the LEP storage ring at CERN and the SLD experiment at the SLC collider at SLAC. The simplicity of the hadronic production process in  $e^+e^-$  events, along with the large data samples collected by these experiments, has resulted in an unprecedented level of experimental precision for multiplicity related quantities, leading to the possibility, for example, of examining multiplicity in small phase space windows. Recent progress in distinguishing quark and gluon jets by these experiments has made it possible to study their properties separately. In particular, the multiplicity distributions for each set have recently been analyzed for the first time [15].

The evolution of jets can be studied by resolving subjets, and by determining the subjet multiplicity rate as a function of the resolution scale. Theoretical and experiment results on subjet multiplicities are described in Section 12. This is followed in Section 13 by a brief discussion of particle multiplicity in  $e^+e^-$  three-jet events.

It is of interest to study multiplicity not only in total phase space but also in small subregions. These studies are generally focused on the intermittency phenomenon and on the fractality of particle distributions within a selected phase space volume (for a recent review, see [16]), related to a relative widening of the multiplicity distribution for smaller phase space volumes. Intermittency gives rise to an increase of multiplicity moments in a power-like manner as the phase space window decreases. Such tendencies have been experimentally observed. Quantum Chromodynamics provides a qualitative description of the increase of the moments, relates the intermittency exponents (or fractal dimensions) directly to the QCD anomalous dimension (i.e. the coupling constant), and clearly delineates the region of applicability of the regularities, indicating the scales at which one should consider the coupling constant to be running or at which it can be treated as approximately fixed. Theoretical and experimental aspects of intermittency and fractality are described in Section 14.

A deeper understanding of specific features of multiplicity can be gained if inclusive distributions of particles and their mutual correlations are considered. The quantum mechanical origin of the interacting partons reveals itself in various interference effects. They lead to the hump-backed plateau of rapidity distributions, to correlations of partons in energies and azimuthal angles, to the string (or drag) effect in three-jet events, and to interference phenomena in the production of heavy bosons and lepton pairs at large transverse momenta. We do not describe these results here, instead referring the reader to monographs [3, 7] and to a recent review [17]. Nonetheless, we discuss one interference effect, namely the suppression of the forward production of accompanying particles in processes with heavy quarks. Inclusion of this topic is justified here because it directly affects the relation between the mean multiplicities in heavy- and light-quark jets. A summary of theoretical and experimental results on multiplicity in heavy quark jets is given in Section 15.

To keep this review to a reasonable length, we do not describe the interactions of hadrons, nuclei or polarized quarks except in passing. These



topics merit their own review. Our main purpose is to present a coherent, updated overview of the theoretical and experimental status of multiplicity in high energy hadron jets. We apologize to the authors of papers whose contributions have not been mentioned. These omissions are unintentional.

## 2 Definitions and notation

The multiplicity distribution is defined by the formula

$$P_n = \frac{\sigma_n}{\sum_{n=0}^{\infty} \sigma_n} = \frac{\sigma_n}{\sigma_{inel}}, \quad (1)$$

where  $\sigma_n$  is the cross section of an  $n$ -particle production process (the so-called topological cross section),  $\sigma_{inel}$  is the inelastic cross section, and the sum is over all possible values of  $n$  so that

$$\sum_{n=0}^{\infty} P_n = 1. \quad (2)$$

It is often more convenient to represent the multiplicity distribution by its moments, i.e. by another set of numbers obtained from it by a definite algorithm. All such sets can be obtained from the so-called generating function defined by the formula

$$G(y, z) = \sum_{n=0}^{\infty} P_n(y) (1+z)^n, \quad (3)$$

which substitutes an analytic function of  $z$  in place of the set of numbers  $P_n(y)$  at a fixed energy  $y$ .

In what follows, use will often be made of the (normalized) factorial moments  $F_q$  and cumulants  $K_q$  determined from the generating function  $G(z)$  by the relations

$$F_q = \frac{\sum_n P_n n(n-1)\dots(n-q+1)}{(\sum_n P_n n)^q} = \frac{1}{\langle n \rangle^q} \cdot \left. \frac{d^q G(z)}{dz^q} \right|_{z=0}, \quad (4)$$

$$K_q = \frac{1}{\langle n \rangle^q} \cdot \left. \frac{d^q \ln G(z)}{dz^q} \right|_{z=0}, \quad (5)$$

where

$$\langle n \rangle = \sum_{n=0}^{\infty} P_n n \quad (6)$$

is the average multiplicity. The expression for  $G(z)$  can be written as

$$G(z) = \sum_{q=0}^{\infty} \frac{z^q}{q!} \langle n \rangle^q F_q \quad (F_0 = F_1 = 1), \quad (7)$$

$$\ln G(z) = \sum_{q=1}^{\infty} \frac{z^q}{q!} \langle n \rangle^q K_q \quad (K_1 = 1). \quad (8)$$

The distribution  $P_n$  and its ordinary moments  $C_q$  can be derived from the generating function  $G(z)$  using the formulas

$$P_n = \frac{1}{n!} \cdot \left. \frac{d^n G(z)}{dz^n} \right|_{z=-1}, \quad (9)$$

$$C_q = \frac{\sum_{n=0}^{\infty} P_n n^q}{\langle n \rangle^q} = \frac{1}{\langle n \rangle^q} \cdot \left. \frac{d^q G(e^z - 1)}{dz^q} \right|_{z=0}. \quad (10)$$

All the moments are connected by definite relations that can be derived from their definitions given above. For example, the factorial moments and cumulants are related to each other through the identities

$$F_q = \sum_{m=0}^{q-1} C_{q-1}^m K_{q-m} F_m, \quad (11)$$

which are nothing other than the relations between the derivatives of a function and its logarithm at the point where the function itself equals unity. Here

$$C_{q-1}^m = \frac{(q-1)!}{m!(q-m-1)!} = \frac{\Gamma(q)}{\Gamma(m+1)\Gamma(q-m)} = \frac{1}{mB(q, m)} \quad (12)$$

are the binomial coefficients, and  $\Gamma$  and  $B$  denote the gamma and beta functions, respectively. There are only numerical coefficients in the recurrence relations (11). Therefore iterative solution yields all cumulants if the factorial moments are given, and vice versa. In this sense, cumulants and factorial

moments are equally suitable. The relations between them for the lowest ranks are

$$\begin{aligned}
F_1 &= K_1 = 1, \\
F_2 &= K_2 + 1, \\
F_3 &= K_3 + 3K_2 + 1, \\
F_4 &= K_4 + 4K_3 + 3K_2^2 + 6K_2 + 1, \\
F_5 &= K_5 + 5K_4 + 10K_3K_2 + 10K_3 + 15K_2^2 + 10K_2 + 1.
\end{aligned} \tag{13}$$

The physical meaning of these moments can be seen from their definitions if they are presented in the form of integrals of correlation functions (for a review, see Ref. [16]). Let the single symbol  $y$  represent all kinematic variables needed to specify the position of each particle in the phase space volume  $\Omega$ . A sequence of inclusive  $q$ -particle differential cross sections  $d^q\sigma/dy_1 \dots dy_q$  defines the factorial moments in the following manner:

$$F_q = \frac{1}{\sigma_{inel} \langle n \rangle^q} \int_{\Omega} dy_1 \dots \int_{\Omega} dy_q \frac{d^q\sigma}{dy_1 \dots dy_q}. \tag{14}$$

Therefore, the factorial moments include in integrated form all correlations within the system of particles under consideration. The corresponding expressions for cumulants are more complicated as can be seen from relations (11) and (13). Therefore we do not present them here but instead remark that analogous relations exist in quantum field theory where formulas similar to eqs. (4) and (5) define the complete set of Feynman graphs (both connected and disconnected) and the subset of connected diagrams, respectively (see e.g. Ref. [3]). Thus, factorial moments represent integral characteristics of any correlation between the particles whereas cumulants of rank  $q$  represent genuine  $q$ -particle correlations not reducible to the product of lower order correlations.<sup>3</sup> To be more precise, all  $q$  particles are connected to each other in the  $q$ th cumulant and cannot be split into disconnected groups. One can say they form a  $q$ -particle cluster which is not divisible into smaller clusters, in analogy with Mayer cluster decomposition in statistical mechanics.

---

<sup>3</sup>This interpretation is valid, however, only for moments with a rank smaller than the average multiplicity at a given energy (for more details, see Ref. [16]).

It is a common feature of distributions in particle physics that their factorial moments and cumulants increase rapidly as the rank  $q$  increases. Therefore it is often convenient to consider their ratio introduced in Ref. [14]:

$$H_q = \frac{K_q}{F_q}, \quad (15)$$

which does not share this feature. At the same time the  $H_q$  ratios exhibit all the qualitative features of the cumulants. As will be discussed below, the ratios  $H_q$  appear in a natural manner as the solution of the QCD equations for the generating functions [14].

From eq. (4), one can derive the relation between the factorial moments  $F_q$  and the ordinary moments  $C_q$  with the same or lower ranks. The two types of moments are found to differ by terms which depend only on the mean multiplicity so that, for example,

$$F_2 = \frac{\langle n(n-1) \rangle}{\langle n \rangle^2} = C_2 - \langle n \rangle^{-1}. \quad (16)$$

Thus ordinary and factorial moments have a different energy dependence, since  $\langle n \rangle^{-1}$  is energy dependent. In general, factorial moments differ from ordinary moments by lower order correlation terms suppressed by the inverse power of the mean multiplicity to the corresponding power. Thus ordinary and factorial moments coincide asymptotically.

The generating function contains the same physical information as the multiplicity distribution. This information is also contained in the unnormalized moments and their ratio. For normalized moments, the average multiplicity at a given energy also needs to be specified. Note that higher rank moments emphasize higher multiplicity events, i.e. multiplicities  $n \geq q$  contribute to factorial moments of (integer) rank  $q$ , as seen from eq. (4). If the distribution is truncated at some  $n = n_{max}$ , all factorial moments with rank  $q > n_{max}$  are zero, whereas they are positive for smaller  $q$ . The cumulants may be either positive or negative if the distribution is truncated.

An emphasis on low multiplicity events can be made by considering derivatives of the generating functions at  $z=-1$ . For example, the so-called combinants [18, 19], defined by

$$Q_n = \frac{1}{n!} \left. \frac{d^n \ln G(z)}{dz^n} \right|_{z=-1}, \quad (17)$$

measure correlations within the low multiplicity part of the distribution.

Of potential interest would be moments with an exponentially damped high-multiplicity tail, defined by

$$D_q = \frac{1}{\langle n \rangle^q} \left. \frac{d^q G(e^z - 1)}{dz^q} \right|_{z=-1} \quad (18)$$

(see the expression for the ordinary moments  $C_q$  given by eq. (10)). Events with multiplicity  $n=q$  are enhanced in these moments. This type of moment has not yet been studied, however.

To this point we have assumed that the rank of a moment is a positive integer. However, the definitions (4), (5) and (10) can be easily generalized to non-integer moments [20], by re-expressing the factorial moments as

$$F_q = \frac{1}{\langle n \rangle^q} \sum_{n=0}^{\infty} P_n \frac{\Gamma(n+1)}{\Gamma(n-q+1)}, \quad (19)$$

which is valid for any real value of  $q$ . This result can also be obtained using a more general approach, by forming the derivative of any real order  $q$  of the generating function, i.e. by using fractional calculus. Fractional moments have not yet found much application in particle physics (see section 3.3.2, however). Therefore, we refer the reader to Refs. [1], [21]-[23] for further discussion.

The method of generating functions is a particular realization of the more general method of generating functionals. The latter approach considers the probability to find a certain  $n$ -particle distribution inside the phase space volume, in place of  $P_n$  in eq. (3), and therefore utilizes functions  $z(y_i)$  instead of the variable  $z$ , where the  $z(y_i)$  depend on the phase space variables  $y_i$ . The corresponding distributions and correlation functions are obtained by taking the variational derivatives of the generating functional over the probing functions  $z(y_i)$ . The moments of the multiplicity distribution are related to the integrals of the correlation functions, as seen from eq. (14). For more details, see Refs. [16, 17].

### 3 Phenomenology

### 3.1 KNO scaling and $F$ scaling

A principal phenomenological issue is the energy dependence of multiplicity for different colliding particles and nuclei. One of the most successful assumptions about the shape of the multiplicity distribution at high energies is the hypothesis that its energy dependence is determined by the average multiplicity in such a manner that  $P_n$  may be represented as:

$$P_n = \frac{1}{\langle n \rangle} f\left(\frac{n}{\langle n \rangle}\right). \quad (20)$$

This property is called KNO scaling after the names of its authors [12], who proposed it on the basis of the Feynman plateau of rapidity distributions. Earlier, a similar relation was obtained in the framework of conformal field theories [24]. KNO scaling is usually considered to be an asymptotic property, i.e. valid in the limit  $\langle n \rangle \rightarrow \infty$ . The multiplicity distribution is restored from the asymptotic function  $f(x)$  through the Poisson transform

$$P(n) = \int_0^\infty f(x) \frac{(\langle n \rangle x)^n}{n!} e^{-\langle n \rangle x} dx. \quad (21)$$

The function  $f(x)$  is unspecified.

The normalization conditions are

$$\int_0^\infty f(x) dx = 1, \quad \int_0^\infty x f(x) dx = 1. \quad (22)$$

It is clear that the ordinary moments of the KNO distribution, eq. (20), do not depend on energy and are just functions of their rank  $q$ :

$$C_q = \int_0^\infty x^q f(x) dx = \text{independent of } E. \quad (23)$$

In contrast, the factorial moments of the KNO distribution do depend on energy, as follows from eq. (16) for  $F_2$ , tending to constant values only at asymptotically high energies. Constancy of the factorial moments is called  $F$  scaling. Therefore  $F$  scaling coincides with KNO scaling asymptotically. The generating function depends on the average multiplicity in both cases as seen from the definitions (3), (7) and (8).

If Feynman scaling is approximate, KNO scaling is violated, suggesting the replacement of eq. (20) by other functions. In particular, it has been

proposed [25] to utilize the set of relations with arbitrary functions  $f_k$

$$P(n) = \frac{\langle n^k \rangle^2}{n^k \langle n^{k+1} \rangle} f_k \left( \frac{n \langle n^k \rangle}{\langle n^{k+1} \rangle} \right), \quad (24)$$

which reduces to KNO result for  $k=0$ .

Another proposal is based on the scaling properties of systems undergoing a second order phase transition, and yields [26, 27]

$$P(n) = \frac{1}{\langle n \rangle^\delta} \phi \left( \frac{n - \langle n \rangle}{\langle n \rangle^\delta} \right), \quad (25)$$

which reduces to KNO case for  $\delta=1$ . It has been argued that solutions of this type appear for QCD equations when they are modified by non-perturbative terms (see Section 9). It has also been proposed to consider so-called log-KNO scaling [28], which has the general form

$$P(n) = \frac{1}{\lambda(s)} \varphi \left( \frac{\ln n + c(s)}{\lambda(s)} \right), \quad (26)$$

which amounts to a scale- and power-transform of multiplicity.

In eq. (20), a continuous function  $f$  is used to approximate the discrete distribution  $P_n$ . This procedure is justified for  $\langle n \rangle \gg 1$ . The procedure to restore the discrete distribution  $P_n$  from the continuous function  $f$  is [29]

$$P_n = \int_n^{n+1} \frac{dm}{\langle m \rangle} f \left( \frac{m}{\langle m \rangle} \right). \quad (27)$$

Note that  $\langle m \rangle$  is slightly shifted compared to  $\langle n \rangle$ , i.e.  $\langle m \rangle \approx \langle n \rangle + 0.5$ .

### 3.2 Entropy scaling

A convenient means to study the energy dependence of multiplicity in an integrated form is provided by the so-called information entropy [30], defined by

$$S = - \sum_{n=0}^{\infty} P_n \ln P_n. \quad (28)$$

Information entropy possesses some peculiar properties (see Refs. [31, 32]), viz.:

- The entropy of  $k$  statistically independent sources equals the sum of the entropies of the individual sources:  $S = \sum_{m=1}^k S_m$ .
- The entropy is invariant under an arbitrary distortion of the multiplicity scale, in particular if a subsample of particles is chosen such as the charged particles.
- There exists a relationship between the entropy  $S$ , the average multiplicity  $\langle n \rangle$ , and the KNO function  $f(x)$ , as long as the KNO form eq. (20) is valid:

$$S - \ln \langle n \rangle = \int_0^\infty f(x) \ln \frac{1}{f(x)} dx. \quad (29)$$

- For functions satisfying the normalization conditions (22), the right hand side of eq. (29) does not exceed unity. Therefore the following inequality is valid:

$$\frac{S}{\ln \langle n \rangle} \leq 1 + \frac{1}{\ln \langle n \rangle}. \quad (30)$$

From eq. (30) we see that KNO scaling is equivalent to scaling of the ratio  $S/\ln \langle n \rangle$  in the limit of asymptotics, and that the approach to this limit is very slow, of order  $\mathcal{O}(1/\ln \langle n \rangle)$ . In contrast, the ratio of the entropy  $S$  to the total available rapidity range, namely  $S/\ln(\sqrt{s}/m_\pi)$ , has been shown to exhibit scaling at experimentally accessible scales. The observed constancy of  $S/\ln(\sqrt{s}/m_\pi)$  is called entropy scaling [31]. If correct, entropy scaling implies a violation of KNO scaling unless the average multiplicity increases as a power of energy.

If subsamples of particles are chosen, it is necessary to employ the proper mean values of the subset multiplicities and the correspondingly normalized KNO functions in eqs. (29) and (30) (for more details, see [32]). The values of entropy are the same for the subsamples as for the full sample, as noted above.

The above treatment can be generalized [33] using the so-called Rényi information entropy of  $q$ th order:

$$I_q = \frac{1}{1-q} \ln \sum_{n=0}^{\infty} (P_n)^q. \quad (31)$$



Entropy  $S$  is obtained from eq. (31) by setting  $q=1$ . Such a generalization is reminiscent of the moments approach to multiplicity described in Section 2. The relation between  $I_q$  and the KNO function is

$$I_q - \ln\langle n \rangle = \frac{1}{1-q} \ln \int_0^\infty f^q(z) dz. \quad (32)$$

Asymptotically, KNO scaling therefore corresponds to scaling of the ratio  $I_q/\ln\langle n \rangle$ , analogous to the result discussed above for the ratio  $S/\ln\langle n \rangle$ .

The entropy approach is also valid for smaller regions of phase space [33, 34] and can be formulated in terms of the fractals discussed in Section 14. Here we merely note that a multi-fractal character of the multiparticle production process requires violation of KNO scaling, and predicts a widening of the KNO function  $f(x)$  and an increase of its maximum as energy increases [33].

### 3.3 Conventional distributions

The purely phenomenological study of multiplicity is based on the use of well known functions from probability theory. Here we consider three functions for which analytic expressions for the generating functions and all moments can be derived [35, 36]. These will serve as a starting point for our discussion of the QCD results presented in Sections 4-8.

#### 3.3.1 The Poisson distribution

The presence of correlations in a process is conventionally described by the difference between its typical distribution and the Poisson distribution, which is written as

$$P_n = \frac{\langle n \rangle^n}{n!} \exp(-\langle n \rangle). \quad (33)$$

The generating function is (see eq. (3))

$$G^{(P)}(z) = \exp(\langle n \rangle z), \quad (34)$$

where, from eqs. (4) and (5),

$$F_q = 1, \quad K_q = H_q = \delta_{q1}. \quad (35)$$

Therefore the measure of correlations can be defined as the difference between  $F_q$  and 1, or, equivalently, between  $K_q$  (or  $H_q$ ) and 0. The Poisson distribution exhibits exact  $F$  scaling and asymptotic KNO scaling.

### 3.3.2 The negative binomial distribution and its generalizations

The negative binomial distribution (NBD) deserves special attention. The NBD [37] has been used to describe experimental measurements of multiplicity in a wide variety of processes and over a large energy range. In particular, the NBD qualitatively describes the distribution of multiplicity in almost all inelastic, high energy processes, except for data at the highest available energies. The NBD is given by

$$P_n = \frac{\Gamma(n+k)}{\Gamma(n+1)\Gamma(k)} \left(\frac{\langle n \rangle}{k}\right)^n \left(1 + \frac{\langle n \rangle}{k}\right)^{-n-k}, \quad (36)$$

where  $k$  is an adjustable parameter with the physical meaning of the number of independent sources. The Bose-Einstein distribution is a special case of the NBD with  $k=1$ . The Poisson distribution is obtained from eq. (36) in the limit  $k \rightarrow \infty$ .

The generating function is

$$G^{(NBD)}(z) = \left(1 - \frac{z\langle n \rangle}{k}\right)^{-k}. \quad (37)$$

The integer rank moments are

$$F_q = \frac{\Gamma(k+q)}{\Gamma(k)k^q}, \quad (38)$$

$$K_q = \frac{\Gamma(q)}{k^{q-1}}, \quad (39)$$

$$H_q = \frac{\Gamma(q)\Gamma(k+1)}{\Gamma(k+q)} = kB(q, k). \quad (40)$$

For a fixed value of  $k$ , the rate of increase of the factorial moments with  $q$  is larger than exponential. As  $q$  increases, the cumulants at first decrease, reaching a minimum at  $q \approx k$ , after which they increase. The cumulants are all positive. The product of several generating functions of negative binomial distributions with different parameters also yields positive cumulants since the unnormalized total cumulant is just the sum of unnormalized individual cumulants. Similarly, the ratio  $H_q$  is always positive. The  $H_q$  moments decreases monotonically and are proportional to  $q^{-k}$  at large  $q$ .

Fig. 1 shows the behavior of  $\ln F_q$ ,  $\ln K_q$  and  $\ln H_q$  as a function of  $q$  for  $k=5$  and 10. The function  $P_n$  becomes narrower as  $k$  increases. This explains the slower rise of  $F_q$  for  $k=10$  compared to  $k=5$ . The dependence of  $K_q$  on  $k$  is seen to be more pronounced than for  $H_q$ . These properties are characteristic of the NBD and not of QCD (see e.g. Section 5.2).

The negative binomial distribution with fixed parameter  $k$  exhibits  $F$  scaling and asymptotic KNO scaling. For large  $n$ , the KNO function with fixed  $k$  behaves as

$$f(x) = \frac{k^k}{(k-1)!} x^{k-1} e^{-kx}, \quad (41)$$

where  $x=n/\langle n \rangle$ . This distribution is wider than the Poisson distribution for all  $k$ . The generating function eq. (37) is singular for  $z=k/\langle n \rangle \rightarrow 0$  if  $\langle n \rangle \rightarrow \infty$  and  $k$  is constant. Therefore, it is necessary to approach the singularity when calculating the derivatives of the generating function at  $z=0$ , i.e. the factorial moments (see eq. (4)). The singularity moves closer to  $z=0$  as the energy increases.

The generalized negative binomial distribution can be represented as the Poisson transform of the generalized gamma distribution [38], given by the special scaling function (see eq. (20))

$$f(x) = \frac{|\mu|}{\Gamma(k)} \lambda^{\mu k} x^{\mu k-1} \exp(-[\lambda x]^\mu) \quad (42)$$

with three adjustable parameters. The Poisson transform of eq. (42) leads to a multiplicity distribution which can be expressed in terms of different Fox functions in various intervals of the parameter  $\mu$ , as was studied in Ref. [39]. The notion of fractional moments is quite useful when considering the generalized NBD because its integer order moments are formally equivalent to the fractional moments of the ordinary NBD (see Ref. [38]).

The so-called modified negative binomial distribution with the generating function

$$G^{(MNBD)}(z) = \left( \frac{1 - \Delta z}{1 - \chi z} \right)^k \quad (43)$$

has also been used to describe data [40]. The number of adjustable parameters is again three. They are related to the average multiplicity through the relation  $\langle n \rangle = k(\chi - \Delta)$ . The negative binomial distribution corresponds to  $\Delta=0$ . Such fits of multiplicity usually yield better results than the NBD,

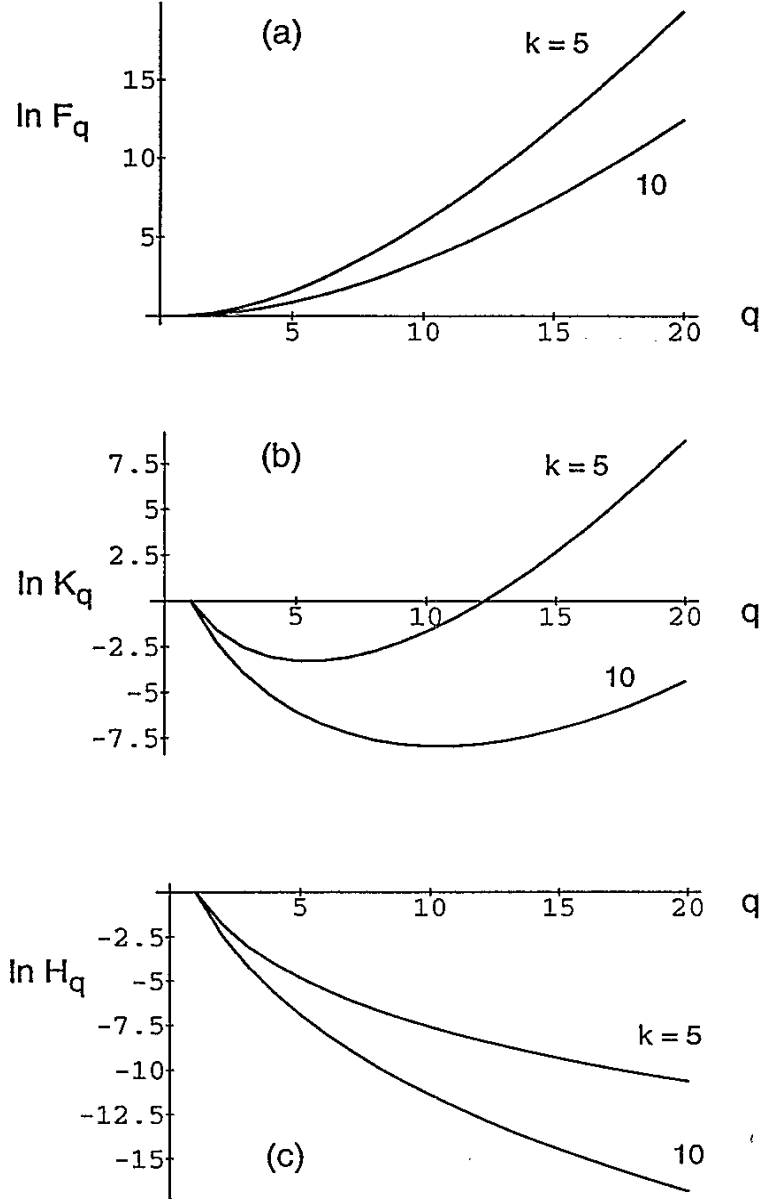


Figure 1: Moments of the negative binomial distribution [36] for  $k=5$  and 10, calculated for integer values of rank  $q$ : (a)  $\ln F_q$ , (b)  $\ln K_q$ , (c)  $\ln H_q$ . The curves are drawn to guide the eye.

which is no surprise given the larger number of parameters. On the other hand, it is difficult to give a physical interpretation to these parameters. The cumulants derived from eq. (43) are

$$K_q^{MNBD} = k^{1-q}(q-1)!(\chi^q - \Delta^q)/(\chi - \Delta)^q, \quad (44)$$

which change sign at each subsequent integer  $q$  for the range of parameters  $\chi$  and  $\Delta$  given in [40]. This differs from QCD results described below. Moreover negative probabilities appear at large  $n$  which is forbidden.

A three parameter fit also has been attempted in the framework of the Saleh-Teich distribution [41], with the claim that it perfectly describes the observed shape of the distribution at high multiplicities, including the shoulder (see Section 3.5). Moments of the multiplicity distribution have not been studied using this approach, however.

A combination of two NBDs has also been used in some fits. This also enlarges the number of adjustable parameters.

We will also mention the log-normal distribution which describes the Gaussian distribution of the logarithms of the variable. The discrete probability distribution for charged particle multiplicity  $n$  is defined by

$$P_n(\mu, \sigma, c) = N \int_n^{n+\delta n} \frac{dn'}{n' + c} \exp\left(-\frac{[\ln(n' + c) - \mu]^2}{2\sigma^2}\right), \quad (45)$$

where  $\mu$ ,  $\sigma$  and  $c$  are adjustable parameters and  $N$  is a normalization factor. The integration parameter is  $\delta n=2$  for full phase space. In restricted rapidity intervals, where both even and odd multiplicities contribute,  $\delta n=1$ . This distribution corresponds to a scale invariant stochastic branching process (for details see Refs. [42, 43]).

### 3.3.3 The fixed multiplicity and Gaussian distributions

We next consider the example of fixed multiplicity. Fixed multiplicity demonstrates how severely experimental selection criteria can influence moments. Events with a given multiplicity have often been studied in the past, the so-called semi-inclusive events. In this case one deals with the distribution

$$P_n = \delta_{nn_0} \quad (n_0 = \text{const}). \quad (46)$$

The generating function is

$$G^{(F)}(z) = (1 + z)^{n_0}. \quad (47)$$

Since  $\langle n \rangle = n_0$ , one obtains

$$F_q = \frac{n_0!}{n_0^q (n_0 - q)!} = \frac{\Gamma(n_0) n_0^{1-q}}{\Gamma(n_0 - q + 1)}, \quad 1 < q \leq n_0, \quad (48)$$

$$F_q = 0, \quad q > n_0, \quad (49)$$

$$K_q = (-n_0)^{1-q} (q-1)! = (-n_0)^{1-q} \Gamma(q), \quad (50)$$

$$H_q = (-1)^{1-q} n_0 B(q, n_0 - q + 1). \quad (51)$$

The factorial moments decrease monotonically with  $q$  until  $q=n_0$ . All factorial moments with rank larger than  $n_0$  are zero. Thus the  $H_q$  ratios are defined for  $q \leq n_0$  only. The integer order cumulants alternate in sign for successive ranks, being positive at odd values of  $q$  and negative at even values: therefore the cumulants “oscillate.” As  $q$  increases, the amplitude of the oscillations decreases until  $q=n_0$ , after which the amplitude increases.

Oscillations of the cumulants are also observed in QCD but with a different periodicity (see Section 5.2). Furthermore, in QCD, the factorial moments increase rapidly with  $q$ .

Fig. 2 shows the  $F_q$ ,  $K_q$  and  $H_q$  moments of the fixed multiplicity distribution for  $n_0=10$ . The insets show  $\ln |K_q|$  and  $\ln |H_q|$ .

For fixed multiplicity, the oscillations of the cumulant moments are entirely a consequence of the event selection procedure. This is easy to recognize when one selects, for example, 10-particle events from a set of events which are distributed according to the Poisson distribution. Then we obtain alternating sign cumulants at integer ranks instead of cumulants equal to zero. The amplitude of the oscillations preserves information about the original distribution as long as the normalization is not changed.

A similar behavior of cumulants is observed for the Gaussian distribution

$$P_n = \frac{1}{\sqrt{2\pi\sigma^2}} \exp\left[-\frac{(n - \langle n \rangle)^2}{2\sigma^2}\right]. \quad (52)$$

If  $\sigma \propto \langle n \rangle$ , the Gaussian exhibits KNO scaling. Its generating function is

$$G(z) = \exp\left[\langle n \rangle \ln(z+1) + \frac{\sigma^2}{2} \ln^2(z+1)\right]. \quad (53)$$

For  $\sigma \rightarrow 0$ , the generating function tends to the fixed multiplicity case, i.e. the cumulants are positive for odd ranks and negative for even ranks. For  $\sigma^2 > \langle n \rangle$ , the cumulants are positive for even ranks and negative for odd ranks.

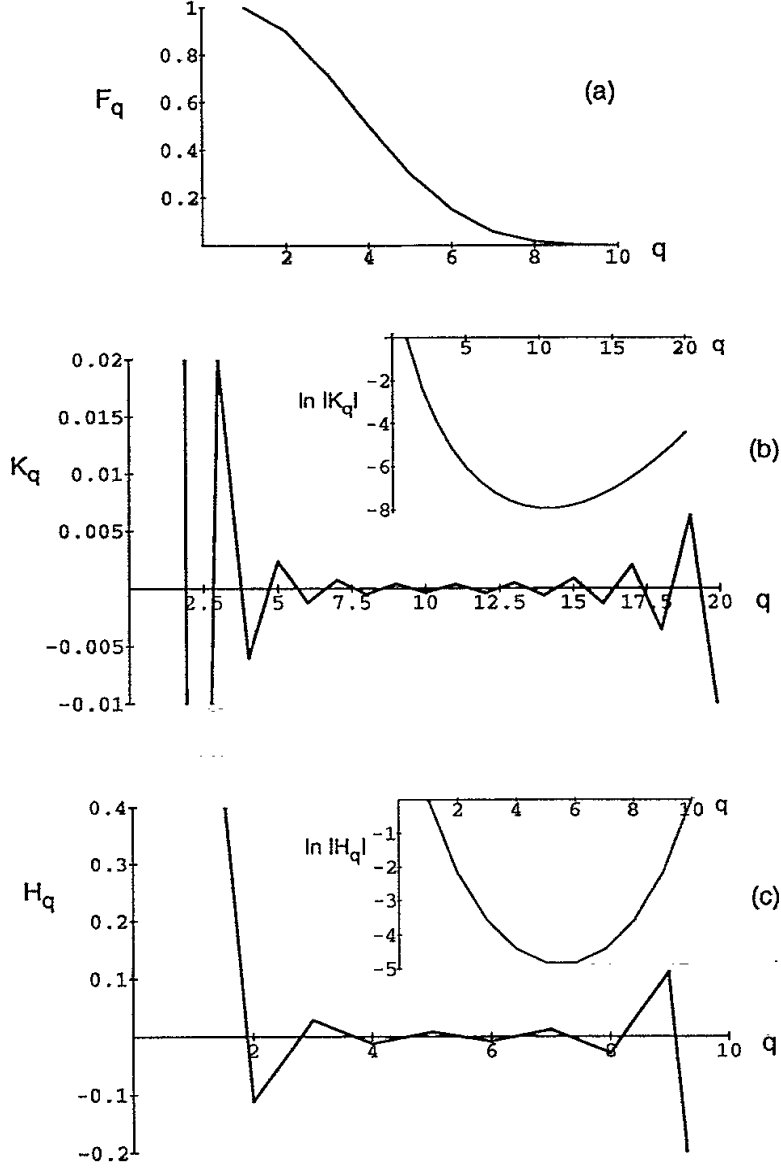


Figure 2: Moments of the fixed multiplicity distribution [36] for  $n_0=10$ , calculated for integer values of rank  $q$ : (a)  $F_q$ , (b)  $K_q$ ,  $\ln |K_q|$ , (c)  $H_q$ ,  $\ln |H_q|$ . The curves are drawn to guide the eye.

### 3.4 Some models

The distributions discussed above are well known from probability theory. In particle physics, they have been used in the context of cluster or clan [2] models and in the multiperipheral cluster model [44] with one particle exchange.

At first sight, the graph-theoretic description of multiparticle production seems entirely different between  $e^+e^-$  and hadron initiated processes. In the former case, the main graphs are tree-like, with a highly virtual initial time-like parton. In the latter case, one used to consider a sequence of multiperipheral-type graphs with low space-like virtualities and rather complicated topologies. A more general and unifying picture emerges by considering strings to be stretched between the color charges (cf. the Lund model [45, 46], dual topological model [47, 48], and the quark-gluon string model [49, 50]) and by introducing models for final particle clusterization (the multiperipheral cluster model [44], clans [2, 51], etc.). The multiplicity distributions in these models are not usually described by a single analytic formula but are formed from a combination of distributions. For example, the multiperipheral model with a single ladder (chain, string) is based on the Poisson distribution for the particle emission centers (resonances, fireballs, clusters, clans, etc.). In general, the resulting distribution is obtained by convolution of the Poisson distribution, which specifies the number of sources, with the decay distribution of the sources. If one chooses a logarithmic distribution to describe the decay multiplicity, the distribution of final particle multiplicity is given by the NBD. This model does not incorporate energy-momentum conservation, however, which would almost certainly modify the simplicity of this result.

The simultaneous creation of several ladders yields a more complicated distribution. Particles produced in different chains are treated as uncorrelated. For each configuration, the multiplicity distributions of different ladders are convoluted. Averaging over all multiple scattering processes yields the final multiplicity distribution.

The multiplicity is sometimes approximated by a sum of negative binomials with different parameters, resulting in a distribution with “shoulders” or “quasi-oscillations” imposed on a smooth curve. (The possible relation between these oscillations and those of the  $H_q$  moments discussed below in Sections 5.2 and 11.5 is considered in Refs. [52, 53].) In particular, the mul-



tiplicity distribution within a single jet in  $e^+e^-$  annihilation is sometimes approximated by a single NBD, while the superposition of several jets yields a distribution with a shoulder [54] in qualitative agreement with experiment (see Section 3.5). However, the solutions of QCD equations do not support the hypothesis of superimposed NBDs, as we discuss below. The detailed study of semi-phenomenological models is usually performed using Monte Carlo computations, involving assumptions about hadronization. It is possible that the discrepancy between the QCD solutions and the results of the phenomenological approaches is related to these assumptions.

In hadron-induced reactions, one generally describes multiparticle production as proceeding through a set of clusters created through the exchange of some mean transferred momentum between the colliding constituents. The general kinematic relation between the primary energy  $s$ , the cluster masses  $s_i$ , and the effective transferred momentum  $p_t^2$  is easily obtained by iteration of the formula  $s = s_1 s_2 / p_t^2$  [55]. For equal cluster masses and transferred momenta, this relation can be written as  $s/p_t^2 \approx (s_i/p_t^2)^N$  or, in terms of mean multiplicities, as

$$\langle n(y) \rangle = \frac{y - L_p}{y_i - L_p} \langle n(y_i) \rangle \approx \frac{y}{y_i - L_p} \langle n(y_i) \rangle, \quad (54)$$

where  $y = \ln s$ ,  $y_i = \ln s_i$ , and  $L_p = \ln p_t^2$  (with  $s$ ,  $s_i$  and  $p_t^2$  appropriately normalized by, say,  $1 \text{ GeV}^2$ ), and  $N = \langle n(y) \rangle / \langle n(y_i) \rangle$  is the number of clusters. The traditional multiperipheral approach assumes constant values of  $y_i$  and  $L_p$  and therefore constant  $\langle n(y_i) \rangle$ . Thus  $\langle n(y) \rangle \propto y$ , i.e. the mean multiplicity is predicted to increase logarithmically with energy. A faster than logarithmic rise is observed experimentally, however. According to eq. (54), this implies that the ratio of  $s_i$  to  $p_t^2$  tends to unity at high energies, an effect which is also observed by experiment. The model of classical fields as applied to nucleus-nucleus collisions (see Refs. [56, 57]) should yield similar features if interpreted in terms of clusters.

Another important consideration in the comparison of theory with hadron-hadron data is that the phase space is relatively unoccupied in typical events, i.e. for events with multiplicities close to the mean, because the phase space volume is proportional to the primary energy  $\sqrt{s}$  whereas the mean multiplicity increases more slowly, as  $\exp(c\sqrt{\log s})$  according to perturbative QCD or as a power of  $\log s$  according to some phenomenological models. At present, we describe these data using peripheral-like ladder type processes

with reggeons or reggeized gluon exchange. The phase space is elongated along the axis of the impinging hadrons and fixed in the transverse direction. For the tail of the multiplicity distribution at very high multiplicities, the phase space becomes saturated. Which dynamics governs this region is not yet clear. Surely, the longitudinal momenta will decrease compared to typical events because of conservation laws. However it is unclear whether the transverse momenta are the same or larger than in than in typical events. This latter possibility has been suggested by some theoretical speculations. In the former case, one should employ non-perturbative approaches while in the latter case perturbative solutions can be found. Additional experimental and theoretical effort is required in this area, which could result in the observation of new physical effects or at least a deeper understanding of the dynamics. The Fermi statistical model [58, 59] and the Landau hydrodynamical model [60] (or their modifications), popular in the 1950s, could apply here. A statistical approach to the description of very high multiplicity processes based on the generating function technique is proposed in [61].

The treatment of nucleus-nucleus interactions is even more complicated, involving an extremely large number of exchanged ladders between numerous colliding nucleons, yielding a much wider multiplicity distribution than hadron-hadron collisions. This feature is in qualitative agreement with experiment. In central heavy ion collisions, particle production is described by multi-ladder exchange in the reggeon approach. This implies that the number of partons emitted by colliding nuclei is very large, and that their combined action can be treated as a source of some classical field which creates the final-state particles [56]. The multiplicity distribution is a Gaussian type [57] and exhibits KNO scaling, i.e.  $\sigma \propto \langle n \rangle$  in eq. (52). The cumulants change sign at each subsequent rank. However, such a classical field model is found to be applicable only to the tail of the observed multiplicity distribution.

Despite its greater complexity, collisions involving nuclei share some features with the simpler hadron-hadron and  $e^+e^-$  collisions, as we discuss in the following sections.

### 3.5 Experimental phenomenology

When KNO scaling was first proposed [12], experimental data were available at comparatively low energies only. The available data from hadron collisions

approximately satisfied the KNO scaling condition. A slight deficiency of the fits at low multiplicities was cured by use of the correct relation between discrete and continuous distributions [29]. It was only when UA5 data became available in 1985 [62], with energies of several hundred GeV, that violation of KNO scaling was clearly observed. The negative binomial distribution was then used to fit the UA5 data. However, a shoulder structure was present in the data which could not be reproduced using a single NBD.

The situation in  $e^+e^-$  annihilations followed a similar path, with suggestions at low energies that KNO scaling was valid followed by observations at higher energies that it was not. A shoulder structure in the multiplicity distribution, similar to that observed in hadron collisions, was also observed here. The shoulder is ascribed to the multi-source nature of the processes, either from additional ladders in hadron reactions or to multi-jet emission in the  $e^+e^-$  events.

A universal energy dependence of average multiplicities in reactions initiated by different particles was proposed [63, 64]. It was argued that the scale for hadron-initiated reactions should be the so-called effective energy, obtained by subtracting the energy of leading particles from the total event energy. The effective energy corresponds to the notion of inelasticity coefficients in cosmic ray studies. The mean multiplicities of  $e^+e^-$  and hadron reactions were found to coincide up to ISR energies ( $\sqrt{s} \sim 50$  GeV) if the effective energy was used in the latter case. This correspondance has not yet been checked for higher energies, however, where it is known that multiplicity sensitive quantities such as rapidity differ between the two processes.

With the advent of high statistics  $e^+e^-$  experiments at the  $Z^0$  energy, it became possible to analyze multiplicity not only in full phase space but in limited phase space regions. As an example, Fig. 3 shows results from the ALEPH Collaboration at LEP for the distribution of charged particle multiplicity in hadronic  $Z^0$  decays [65]. The data are shown for full phase space and in limited phase space intervals defined by rapidity  $|Y| \leq 2.0$  and  $|Y| \leq 0.5$ . The data are compared to the results of the negative binomial and log-normal distributions. Overall, the log-normal result is in somewhat better agreement with data than the NBD. The shoulder structure, especially pronounced in the data for multiplicities  $n \approx 30$  in the  $|Y| \leq 2.0$  rapidity bin, is not well described by either model, however. Concerning factorial moments, the NBD underestimates the experimental results whereas the log-normal distribution overestimates them [66, 67]. Further analysis of factorial moments reveals

disagreement between the data and the log-normal distribution both in small intervals and full phase space [67]. This is an example of how moment analysis can reveal small differences between theory and data in a more clear manner than a direct fit of multiplicity. Neither the modified negative binomial distribution nor the so-called pure birth stochastic model [68] improve the situation.

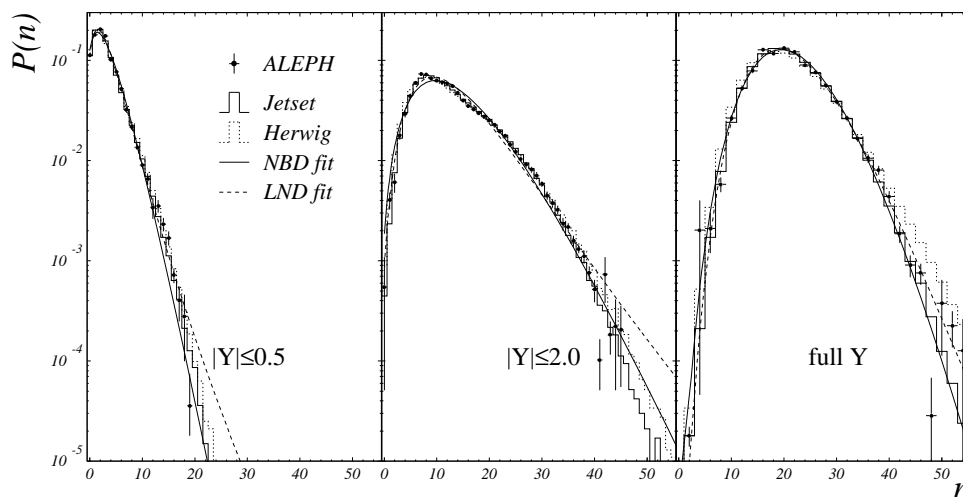


Figure 3: The measured charged particle multiplicity distribution in  $e^+e^-$  hadronic  $Z^0$  decays [65], for small ( $|Y| \leq 0.5$ , left) and intermediate ( $|Y| \leq 2.0$ , center) rapidity windows, and in full phase space (right), in comparison to various models.

The predictions of the JETSET [69] and HERWIG [70] parton shower Monte Carlo event generators are included in Fig. 3. These two programs, along with the ARIADNE parton shower Monte Carlo [71], are widely used to interpret  $e^+e^-$  data (see, for example, Ref. [72]). The Monte Carlo results are seen to describe the data quite well, presumably because they account for hard gluon emission relevant for the shoulder. Monte Carlo studies based on the quark-gluon string model and the dual topological model similarly provide a rather successful guide to experimental distributions from hadron- and nucleus-initiated reactions.

As a final remark we note that other phenomenological distributions have been used to describe experimental data on multiplicity, such as the so-called modified gamma distribution [73].

## 4 Equations of Quantum Chromodynamics

Multiparticle production in Quantum Chromodynamics arises from the interactions of quarks and gluons. The interactions lead to the creation of additional quarks and gluons and eventually to the formation of hadrons. The most characteristic features of QCD processes are determined by the vector nature of the massless gluons and by the dimensionless coupling constant. Gluons carry color charge and therefore emit gluons in addition to quark-antiquark pairs. The development of quark and gluon jets is described by evolution equations. The main parameter of the evolution is the angle of divergence of the jet or, more precisely, its transverse momentum. The essential difference between Quantum Electrodynamics and Quantum Chromodynamics – due to the triple gluon coupling – can be traced to the lowest order graphs in which two colliding electrons (or quarks) emit a single photon (or gluon). In the latter case there exists an additional graph with a gluon emitted by the exchanged gluon. The interference of this graph with the others leads to transverse momentum ordering, in contrast to pure angular ordering as in Quantum Electrodynamics (see e.g. Ref. [74]).

The subsequent emission of gluons and quarks within the jet fills in the internal regions of cones defined by the previous emissions (transverse momentum ordering). This remarkable property of “angular ordering” can be exploited to formulate a probabilistic scheme for the development of the jet as a whole. In this case the evolution equations are reminiscent of the well known classical Markovian equations for “birth-death” or “mother-daughter” processes. (For a detailed discussion of this approach, based on the coherence phenomenon, see Refs. [7, 75]).

The system of two equations for the generating functions  $G_F$  and  $G_G$  of quark and gluon jets, respectively, is (with  $A, B, C = F, G$ ) [3, 7, 76]

$$\begin{aligned} G_A(y, z) &= e^{-w_A(y)} z \\ &+ \frac{1}{2} \sum_{B,C} \int^y dy' \int_0^1 dx \exp[-w_A(y) + w_A(y')] \end{aligned}$$

$$\times \frac{\alpha_S}{2\pi} K_A^{BC}(x) G_B[y' + \ln(x), z] G_C[y' + \ln(1-x), z], \quad (55)$$

where

$$y = \ln(p\Theta/Q_0) = \ln(2Q/Q_0) = \ln(Q/\Lambda), \quad (56)$$

with  $p$  the initial momentum,  $\Theta$  the angle of divergence of the jet (the initial jet opening angle), assumed here to be small,  $Q$  the jet virtuality,  $Q_0$  a constant which defines the limit of perturbative evolution, and  $\alpha_S$  the strong interaction coupling strength or “constant.”  $\Lambda$  is the so-called scale parameter of QCD, related to  $Q_0$  by  $\Lambda = Q_0/2$ .<sup>4</sup> The scale parameter  $\Lambda$  is strongly related to  $\Lambda_{\overline{\text{MS}}}$  [79, 80] but is not, in general, the same. We shall consider both running and fixed  $\alpha_S$ . An effective infrared safe coupling constant is sometimes used as a substitute for the phenomenological parameter  $Q_0$  (see [17, 81]). Here, we use the more traditional approach, however.

The first term on the right hand side of eq. (55) corresponds to the propagation of the primary parton without interaction, and is described by the form factor  $\exp[-w_A(y)]$ . The second term describes the creation of two jets  $B$  and  $C$  which carry proportions  $x$  and  $1-x$  of the primary energy after their production at the vertex  $K_A^{BC}$ , which is reached by the primary parton after it evolves to scale  $y'$  without splitting, as dictated by the factor  $\exp[-w_A(y) + w_A(y')]$ . Iteration of eq. (55) generates all tree graphs of the perturbation series, ordered by transverse momentum.

Considering just terms of order  $(\alpha_S \log^2 s)^n$ , where  $s \approx 4p^2$  is the cms energy squared, and then summing, leads to the so-called DGLAP evolution equation (see Ref. [82]) with kernels explicitly written below. The approximation in which only these terms are taken into account is the double-logarithmic approximation (DLA). Adding further terms with lower powers of  $\log s$  yields the modified leading-logarithmic approximation (MLLA). Adding yet lower powers of  $\log s$ , one obtains the next-to-next-to-leading order approximation (NNLO), and so on. Even the lowest order approximation includes processes with an arbitrary number of partons and is described by a sub-series of the perturbative expansion with different powers of the coupling constant. Thus the classification of approximations is not based simply on powers of  $\alpha_S$  but rather on the product of  $\alpha_S^n$  with the corresponding power of  $\log s$ . This explains why terms from different sub-series are combined when

---

<sup>4</sup> Note that the relationship between  $Q_0$  and  $\Lambda$  is not unique; other relationships have been chosen (see e.g. Refs. [77, 78]) and they are often treated as independent variables.

the conservation laws (e.g. energy conservation) are included, as discussed in more detail below (see Section 5.2).

Multiplying both sides of eq. (55) by  $\exp[w_A(y)]$  and then differentiating by  $y$ , we eliminate the form factors and obtain the final system of equations [3, 7, 76]<sup>5</sup>:

$$\begin{aligned} G'_G &= \int_0^1 dx K_G^G(x) \gamma_0^2 [G_G(y + \ln x) G_G(y + \ln(1-x)) - G_G(y)] \\ &+ n_f \int_0^1 dx K_G^F(x) \gamma_0^2 [G_F(y + \ln x) G_F(y + \ln(1-x)) - G_G(y)], \end{aligned} \quad (57)$$

$$G'_F = \int_0^1 dx K_F^G(x) \gamma_0^2 [G_G(y + \ln x) G_F(y + \ln(1-x)) - G_F(y)], \quad (58)$$

where  $G'(y) = dG/dy$ ,  $n_f$  is the number of active quark flavors, and

$$\gamma_0^2 = \frac{2N_c \alpha_S}{\pi}. \quad (59)$$

The kernels of the equations are

$$K_G^G(x) = \frac{1}{x} - (1-x)[2-x(1-x)], \quad (60)$$

$$K_G^F(x) = \frac{1}{4N_c} [x^2 + (1-x)^2], \quad (61)$$

$$K_F^G(x) = \frac{C_F}{N_c} \left[ \frac{1}{x} - 1 + \frac{x}{2} \right], \quad (62)$$

with  $N_c=3$  the number of colors and  $C_F=(N_c^2-1)/2N_c=4/3$  in QCD.

The variable  $z$  has been omitted in eqs. (57) and (58). It should be remembered, however, that derivation of the equations for moments relies on the expansions (7) and (8) of the above equations.

A typical feature of any field theory with a dimensionless coupling constant, and of QCD in particular, is the presence of singular terms at  $x \rightarrow 0$  in the kernels of the equations. These singularities imply an uneven sharing of energy between the newly created jets and play an important role in the jet

---

<sup>5</sup>The system of eq. (6.29) in Ref. [3] is the same as the system of eqs. (57) and (58) in the present work, using a slightly different notation; the notion of the generating function in this context was first introduced in Ref. [76] as is also mentioned in Ref. [7].

evolution, giving rise to a larger average multiplicity compared to the case of equal sharing of energy (the non-singular case).

The system of equations (57) and (58) is physically appealing but not absolutely exact. This last point is clear since, for example, there is no four-gluon interaction term in eqs. (57) and (58). Such a term does not contribute a singularity to the kernels, justifying its omission from the lowest order approximation. Despite this lack of exactness, the modified series of perturbation theory (i.e. with three parton vertices only), is well reproduced by eqs. (57) and (58) up to terms including higher order logarithmic corrections. As shown in Ref. [7], the neglected terms contribute at the level of the product of, at least, five generating functions. The physical interpretation of the corresponding graphs leads to treatment of the “color polarizability” of jets.

There are complications associated with the definition of the evolution parameter, with preasymptotic corrections, etc. (see, e.g., Ref. [83]). For example, the limits of integration in eqs. (57) and (58) are in principle constrained by a restriction on the transverse momentum:

$$k_t = x(1-x)p\Theta' > Q_0/2. \quad (63)$$

This condition originates from the requirement that the formation time of a gluon ( $t_{form} \sim k/k_t^2$ ) be less than its hadronization time ( $t_{had} \sim kR^2 \sim k/Q_0^2$ ). This leads to the requirement that the arguments of the generating functions in eqs. (57) and (58) be positive, which in turn implies that the limits of integration in eqs. (57) and (58) should be  $e^{-y}$  and  $1 - e^{-y}$  rather than 0 and 1. These limits tend to 0 and 1 at high energies. Therefore it seems reasonable to use integration limits of 0 and 1 in eqs. (57) and (58), to study their analytic solutions with high accuracy, and then to account for the neglected terms by considering them to be preasymptotic corrections to these solutions.

This issue of the limits of integration has physical significance. With limits of  $e^{-y}$  and  $1 - e^{-y}$ , the partonic cascade terminates at the virtuality  $Q_0$ , as seen from the arguments of the multiplicities in the integrals. With limits of 0 and 1, the cascade extends into the non-perturbative region with virtualities smaller than  $Q_0/2$ , i.e.  $Q_1 \approx xp\Theta/2$  and  $Q_2 \approx (1-x)p\Theta/2$ . This region contributes terms of the order of  $e^{-y}$ , power-suppressed in energy. It is not known whether the equations and the LPHD hypothesis are valid below the cutoff  $Q_0$ .



## 5 Gluodynamics

It is natural to begin our study of QCD with the case of gluodynamics, in which there are no quarks and only the interactions of gluons are considered. Gluodynamics exhibits all the qualitative features of QCD evolution while being more transparent. In gluodynamics, the system of equations (57) and (58) reduces to the single equation

$$G'(y) = \int_0^1 dx K(x) \gamma_0^2 [G(y + \ln x) G(y + \ln(1 - x)) - G(y)], \quad (64)$$

with  $G(y) \equiv G_G(y)$  and  $K(x) \equiv K_G^G(x)$ . Eq. (64) is a non-linear, integro-differential equation with shifted arguments in the nonlinear term which account for energy conservation in the triple QCD vertex, when one gluon splits into two. As mentioned above,  $k_t$  ordering influences the limits of integration, and instead of 0 and 1 in eq. (64) we should insert  $e^{-y}$  and  $1 - e^{-y}$ . Use of these latter limits leads to preasymptotic power corrections which we neglect for the moment and estimate later. Even though momentum conservation is not, strictly speaking, included, it is taken into account in an approximate manner through a combined action of energy conservation and transverse momentum ordering.

In the lowest order (double-logarithmic) approximation, only the most singular terms in the kernel  $K(x)$  and within the square brackets are retained. Thus  $K \rightarrow 1/x$  and  $\ln(1 - x) \rightarrow 0$  (therefore one neglects energy conservation in the asymptotic limit), while  $\gamma_0^2$  is chosen to be constant.

### 5.1 Approximate solutions of equations with fixed coupling constant and the shape of the KNO function

In Section 8 we describe the exact solutions of the QCD equations for the moments of multiplicity, assuming a fixed coupling strength. We show that the properties of gluon jets do not change appreciably if quarks are included. Therefore it is instructive to examine the more transparent approximate solutions of eq. (64).

Formally, the assumptions of the double-logarithmic approximation are equivalent for the three factors in the integrand of eq. (64) since non-leading terms are neglected. In Quantum Chromodynamics with a fixed coupling

strength,  $F$  scaling is favored over KNO scaling (see Section 8). The difference between  $F$  and KNO scaling is usually neglected, however, since the calculations are often performed for asymptotically high energies. Preasymptotic corrections for the second moment of the multiplicity distribution are discussed in Ref. [84], and for higher moments in Ref. [85].

The generating function for the lowest order solution of eq. (64) is independent of both the energy and coupling constant (see Refs. [7, 86]). In this case eq. (64) reduces to the differential equation (for more details see eq. (77) below)

$$[\ln G(y)]'' = \gamma_0^2(G(y) - 1). \quad (65)$$

The corresponding KNO function  $f(x)$  defined by eq. (20) decreases exponentially at large values of  $x$ :

$$f(x) \sim 2C(Cx - 1 + \frac{1}{3Cx} + \dots) \exp(-Cx); \quad Cx \gg 1, \quad (66)$$

where  $C \approx 2.552$ . For small values of  $x$  its behavior is

$$f(x) \sim x^{-1} \exp(-\ln^2 x/2). \quad (67)$$

The appearance of asymptotic KNO scaling and its independence of the coupling constant in the lowest order approximation are by themselves a success of perturbative Quantum Chromodynamics [11]. The shape of the scaling function (66) does not fit experiment, however. Experiment favors shapes which are much narrower than predicted by eqs. (66) and (67). The corrections of the modified leading-logarithmic approximation yield a function that is less wide [86], reducing the width of  $f(x)$  and introducing a dependence on  $\alpha_S$ .

Detailed studies of the solutions of gluodynamics have been presented in many papers [9]-[11], [13, 14] [36], [83], [87]-[92]. In most cases only moments of low rank are considered, i.e. the average multiplicity and its dispersion. The approximations in these papers do not always allow higher rank moments to be treated, leading to unphysical results such as negative factorial moments of the fifth rank (see Ref. [87]) which are forbidden by the definition, eq. (4). This illustrates the importance of consistency when treating terms of the same order in QCD equations. The role of conservation laws in the shifted arguments of the generating functions is extremely important, providing large corrections. It was shown in Ref. [13] that conservation laws can be taken into

account. However, in Ref. [13] the running property of the coupling constant was disregarded, the non-singular terms in the kernel were neglected (as were some other terms), and the difference between the coupling constant  $\gamma_0$  (eq. (59)) and the QCD anomalous dimension  $\gamma$ , defined as

$$\langle n \rangle = \exp\left(\int^y \gamma(y') dy'\right), \quad (68)$$

was neglected as well.

Eqs. (57) and (58) possess exact solutions for a fixed coupling constant, as discussed in Section 8. To find these solutions requires the numerical solution of some algebraic equations (see Section 8). Therefore we first consider the approximate approach of Ref. [13] because it yields an analytic expression for the KNO function which reveals the importance of the conservation laws, while differing from eq. (66) by predicting a narrower width, in much better agreement with experiment.

First, one obtains a recurrence relation for the factorial moments by substituting expression (7) into eq. (64) and equating the coefficients of  $z^q$  on both sides:

$$(q - q^{-1})F_q = \gamma \sum_{l=1}^{q-1} C_q^l B(\gamma l, \gamma(q-l) + 1) F_{q-l} F_l. \quad (69)$$

This system of equations can be solved<sup>6</sup> using the initial conditions  $F_0=F_1=1$ . The inset in Fig. 4(a) shows the ratio of the resulting moments to their values [13] at large ranks  $q$ :

$$F_q^{as} = \frac{[\Gamma(1 + \gamma)]^q}{\Gamma(1 + \gamma q)} \cdot \frac{2q\Gamma(q + 1)}{C^q}. \quad (70)$$

For large values of  $q\gamma$  one obtains

$$F_q \approx \frac{2\mu D^{-q}}{\sqrt{2\pi\gamma}} \Gamma\left(\frac{3}{2} + \frac{q}{\mu}\right), \quad (71)$$

where

$$\mu = (1 - \gamma)^{-1}, \quad D = C \frac{\gamma^\gamma (1 - \gamma)^{1-\gamma}}{\Gamma(1 + \gamma)}. \quad (72)$$

---

<sup>6</sup>The exact solution of the system of equations for quark and gluon jets in case of the fixed coupling constant is given in Section 8.2.

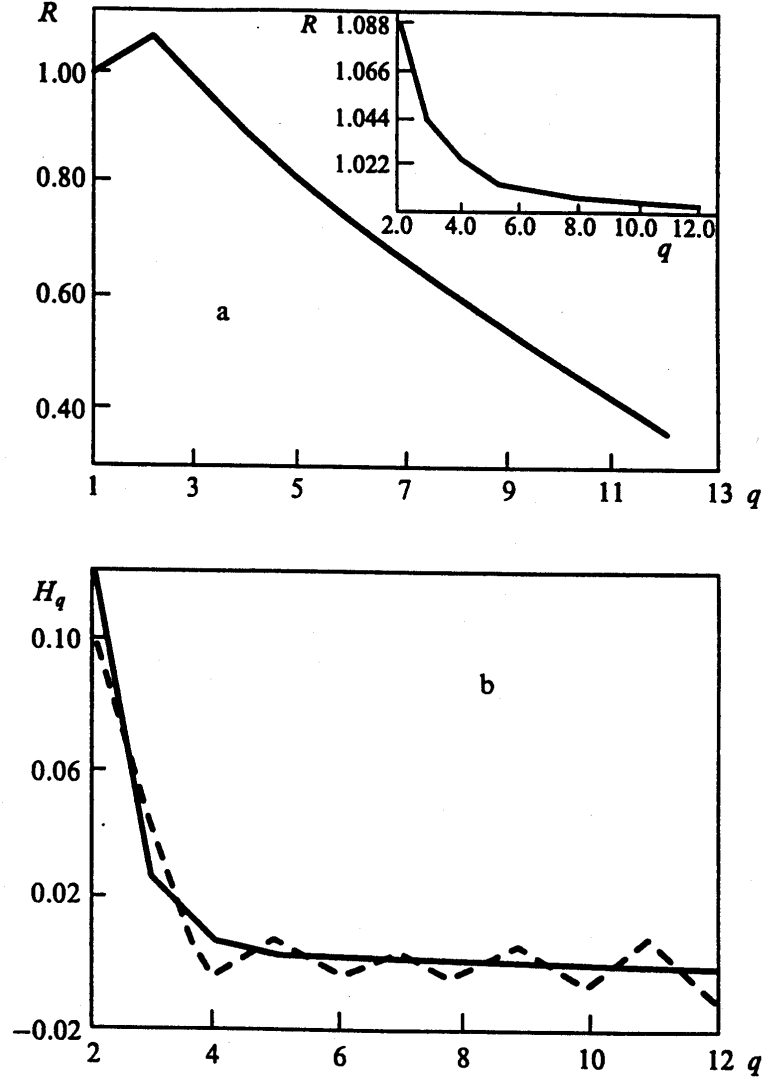


Figure 4: (a) The ratio of factorial moments derived from the KNO curve in Fig. 5 to the asymptotic result of eq. (70); the inset shows the corresponding ratio between the results of eqs. (69) and (70). (b) The ratio  $H_q$  obtained from the modified KNO curve in Fig. 5 (solid line) compared to its NBD counterpart with  $k=7$  (dashed line).

The asymptotic results for  $F_q$  at large ranks determine the asymptotics of the KNO function  $f(x)$  at high multiplicities:

$$f(x) \approx \frac{2\mu^2(Dx)^{3\mu/2}}{x\sqrt{2\pi\gamma}} \exp[-(Dx)^\mu], \quad (\mu - 1)(Dx)^\mu \gg 1. \quad (73)$$

Thus the tail of the distribution at large multiplicities is far more suppressed than in the double-logarithmic approximation, eq. (66). Using the value of  $\gamma \approx 0.4$  at presently accessible energies for which  $\mu = (1 - \gamma)^{-1} \approx 1.6$ , one obtains a Gaussian-like suppression rather than an exponential falloff as in eq. (66). Thus, we conclude that the conservation laws drastically reduce the width of the multiplicity distribution.

This is demonstrated in Fig. 5, where the modified QCD distribution, i.e. the distribution including energy conservation, is compared with the lowest order QCD result. The modified distribution also accounts for some corrections at low multiplicities [13]. The modified distribution (thick solid line) is seen to be much narrower than the DLA distribution (thin solid line). Also shown in Fig. 5 is the result of a fit of the modified distribution by the NBD, with parameters  $k=7$  and  $\langle n \rangle=30$ .

Making use of the modified QCD curve in Fig. 5, the genuine factorial moments can be calculated, i.e. the moments including the corrections at low multiplicities. Their ratio to the asymptotic solution, eq. (70), is shown in the main part of Fig. 4(a). Comparison of the two curves in Fig. 4(a) reveals the importance of the corrections at low multiplicities. Using the genuine factorial moments, one can compute the cumulants and the  $H_q$  ratios. The latter are shown in Fig. 4(b) and compared with the  $H_q$  moments obtained from the fitted NBD curve in Fig. 5. A dramatic difference is seen between the behavior of the modified QCD solution and the NBD. The  $H_q$  ratios in the former case are seen to oscillate as the rank increases. In contrast, the  $H_q$  ratios of the NBD decrease monotonically, as was already seen in Fig. 1(c). These oscillations of the  $H_q$  ratios are reminiscent of the oscillations observed for the fixed multiplicity distribution, Fig. 2(c). Oscillations with a different periodicity are obtained from the solutions to the full QCD generating equations, as discussed below in Sections 7 and 8.

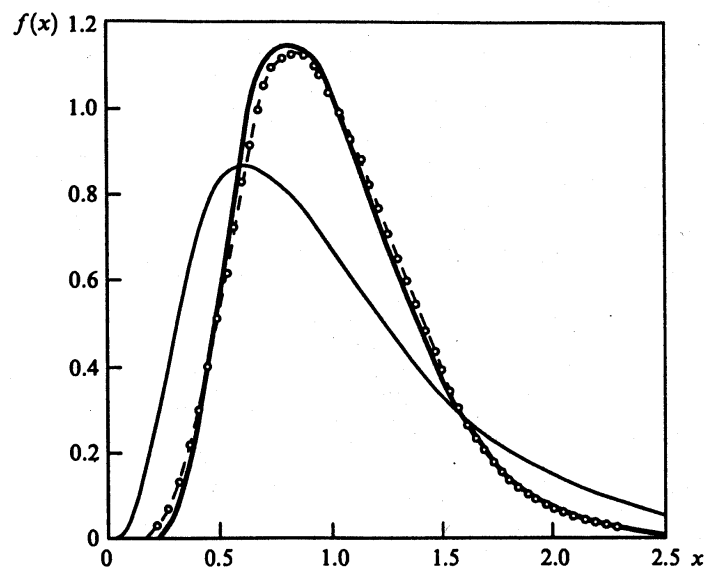


Figure 5: The modified KNO function [13] (thick solid curve) for  $\gamma=0.4$  is much narrower than the lowest order distribution (thin solid curve). The negative binomial distribution with  $k=7$  is shown for comparison (dashed curve).

## 5.2 Higher order approximations with a running coupling constant

Eq. (64) for the generating function in gluodynamics can be solved in a more general approximation [14], by accounting for all terms of the kernel  $K$  including the non-singular ones, by incorporating the running coupling constant, and by using a Taylor series expansion of the generating functions in the nonlinear term at large  $y$ :

$$G(y + \epsilon) \approx G(y) + G'(y)\epsilon + \frac{1}{2}G''(y)\epsilon^2 + \dots \quad (74)$$

This approach illustrates the distinction between the various assumptions and their relative importance.

Each derivative in eq. (74) produces a derivative of  $\langle n \rangle$  which is proportional to the anomalous dimension  $\gamma$  according to eq. (68). In turn, the anomalous dimension  $\gamma$  can be represented by a perturbative series with  $\gamma_0$  as the leading term. Therefore, higher derivatives in the Taylor series give rise to terms of a higher order approximation in the perturbative expansion. The Taylor series leads to a recombination of different order terms in this expansion. It is important to note that energy conservation, accounted for by  $x$  and  $1 - x$  in eqs. (57) and (58), is an essential and integral aspect of the higher order perturbative corrections. At first sight, it may seem odd that the order of the approximation can be changed when energy conservation is included. However, this becomes clear if one considers that energy sharing among partons results in terms with lower powers of  $\log s$  at the same power of  $\alpha_S$ , i.e. in a shift to a higher approximation as seen from eq. (74).

The running coupling strength  $\alpha_S$  should be considered in the two-loop approximation when working in NNLO. It is given by the formula

$$\alpha_S(y) = \frac{2\pi}{\beta_0 y} \left( 1 - \frac{\beta_1}{\beta_0^2} \cdot \frac{\ln 2y}{y} \right) + \mathcal{O}(y^{-3}), \quad (75)$$

with

$$\beta_0 = \frac{11N_c - 2n_f}{3}, \quad \beta_1 = \frac{17N_c^2 - n_f(5N_c + 3C_F)}{3}, \quad (76)$$

where  $n_f$  is the number of active quark flavors (in gluodynamics  $n_f=0$ ), and the difference between the QCD scale  $\Lambda$  and  $Q_0/2$  is neglected in asymptotics.

In MLLA, one can use the one-loop expression, i.e. the first factor of the product in eq. (75) only.

Note that – in contrast to QED – the QCD series is an expansion in the product of the coupling strength and energy dependent ( $\ln s$ ) terms, rather than an expansion in the coupling strength alone. Therefore higher order corrections appearing in the QCD expansion arise not only from higher loop graphs but also from a proper accounting for conservation laws, as mentioned above. In this review, we show that the effects of the latter – resulting in a limitation of the available phase space – are much more important than the two-loop terms of the coupling strength. This explains e.g. why NNLO calculations of the multiplicity ratio  $r$  between gluon and quark jets yield rather different results depending on the accuracy with which energy conservation is included, as we discuss below in Sections 6.1 and 7.

Inserting expression (74) for the generating function into the nonlinear term of eq. (64), dividing both sides of (74) by  $G(y)$  and differentiating with respect to  $y$ , we obtain

$$\begin{aligned} [\ln G(y)]'' &= \gamma_0^2(y)[(1 + 4h_1^2\gamma_0^2(y))(G(y) - 1) - 2h_1G'(y) \\ &+ \sum_{n=2}^{\infty} (-1)^n h_n G^{(n)}(y) + \sum_{m,n=1}^{\infty} (-1)^{m+n} h_{nm} \left( \frac{G^{(m)}G^{(n)}}{G} \right)'] , \end{aligned} \quad (77)$$

where

$$\begin{aligned} h_1 &= 11/24, \\ h_2 &= (67 - 6\pi^2)/36, \\ h_3 &= (4\pi^2 - 15)/24, \quad h_4 = 13/3, \\ h_n &= |2 - 2^{-n} - 3^{-n} - \zeta(n)|, \\ \zeta(n) &= \sum_{m=1}^{\infty} m^{-n}, \quad n \geq 2, \end{aligned} \quad (78)$$

$$h_{mn} = \left| \frac{1}{m!n!} \int_0^1 dx K(x) \ln^n x \ln^m(1-x) \right|. \quad (79)$$

The first term on the right hand side ( $G(y) - 1$ ) without its pre-factor is the well known [7] expression of the double-logarithmic approximation, eq. (65). The additional higher order contribution  $4h_1^2\gamma_0^2$  is due to the derivative of  $\gamma_0^2$ , and is considered in [93] but not in [14]. Similar corrections appear in the



subsequent terms of eq. (77). In particular, the term proportional to  $h_1$  corresponds to the modified leading-logarithmic approximation, while the term proportional to  $h_2$  together with the  $4h_1^2\gamma_0^2$  correction to the first term, mentioned above, corresponds to the next-to-next-to-leading order correction. Actually, the transverse momentum  $k_t$  given by eq. (63) should be used as the argument of  $\alpha_S$  in place of  $y$ , but it can be shown that such a replacement leads to yet higher order corrections than those considered here. Note that the use of the preasymptotic limits of integration, i.e.  $e^{-y}$  and  $1 - e^{-y}$ , do not lead to a differential equation which is as simple as eq. (77) but result in power-like corrections.

A straightforward solution of eq. (77) appears problematic even if only the terms with  $h_1$  and  $h_2$  are included in addition to the double-logarithmic terms. The solution is very simple for the moments of the distributions [14], however, since  $G(z)$  and  $\ln G(z)$  are the generating functions for factorial moments and cumulants, respectively. Using formulas (7) and (8) and assuming asymptotic  $F$  scaling, one obtains the product  $q\gamma$  (and its derivatives) at each differentiation in eq. (77) because the average multiplicity is the only  $y$ -dependent term which remains. The coefficients of  $z^q$  on both sides should be equal. Hence, one obtains in NNLO:

$$H_q = \frac{K_q}{F_q} = \frac{\gamma_0^2[1 - 2h_1q\gamma + 4h_1^2\gamma_0^2 + h_2(q^2\gamma^2 + q\gamma')]}{q^2\gamma^2 + q\gamma'}. \quad (80)$$

The anomalous dimension  $\gamma$  is defined by eq. (68). The condition  $F_1=K_1=1$  determines the relation between  $\gamma$  and  $\gamma_0$ :

$$\gamma \approx \gamma_0 - \frac{1}{2}h_1\gamma_0^2 + \frac{1}{8}(4h_2 + 15h_1^2)\gamma_0^3 + \mathcal{O}(\gamma_0^4), \quad (81)$$

which shows that the increase of the average multiplicity with energy is slower in the modified leading-logarithmic approximation than in the double-logarithmic approximation, since the term with  $h_1$  is negative (see eq. (68)). However, the higher orders reverse this situation. The MLLA and NNLO terms in eq. (81) practically cancel each other for present values of  $\gamma_0$ . Therefore the series (81) essentially yields the asymptotic result. Only at very large energies when  $\gamma_0 \approx 0$  do subsequent terms in the series become smaller than the lower order ones (if only the first term in the expression for  $\alpha_S$  is considered). However, one should keep in mind that in NNLO the value of  $\gamma_0$  itself

acquires a correction, as given by the second term in the brackets in eq. (75). This correction is negative and drastically reduces the value of the coefficient in front of  $\gamma_0^3$  in eq. (81), resulting in a much better convergence of the series. This is discussed below in connection with the NNLO and 3NLO corrections to the expression for the energy dependence of mean multiplicities.

The running property of  $\gamma_0$  was taken into account in expression (81) according to eq. (75):

$$\gamma'_0 \approx -h_1\gamma_0^3 + \mathcal{O}(\gamma_0^5), \quad (82)$$

which leads to

$$\gamma' \approx -h_1\gamma_0^3(1 - h_1\gamma_0) + \mathcal{O}(\gamma_0^5). \quad (83)$$

The lesson we learn from eq. (80) is that in all correction terms (which contain  $h_1, h_2, \dots$ ), the expansion parameter  $\gamma$  appears in a product with the rank, namely the product  $q\gamma$ , which becomes large at high ranks, i.e. at high multiplicities. Therefore, for high multiplicity events one should take into account ever higher order terms in  $\gamma$ . This problem was mentioned a long time ago [7] and is discussed in some detail in Ref. [94], but has only recently been analyzed.

As already mentioned, the double-logarithmic formulas are obtained from eq. (77) by setting  $h_1=h_2=0$ ,  $\gamma=\gamma_0$ , and  $\gamma'=0$ . In this case,

$$H_q = q^{-2}, \quad (84)$$

which is similar to the asymptotic form of the negative binomial distribution with  $k \approx 2$ , corresponding to an extremely wide multiplicity distribution (see eq. (66)). In contrast, experimental data typically yield values of  $k$  in the range from 3.5 to 100. We stress, however, that the NBD result for  $k=2$  is

$$H_q = \frac{2}{q(q+1)}, \quad (85)$$

which shows that the “genuine” correlations are about twice as large in the NBD as in QCD. Therefore the QCD predictions for a single jet do not support the hypothesis of the negative binomial distribution even in asymptotics, not to mention other distinctive features of eq. (80) and its generalization.

It is easy to recognize that eq. (84) is just an asymptotic form (for  $y \rightarrow \infty$ ) of eq. (80) for any fixed rank  $q$ . The value of  $\gamma$  tends to zero as  $y^{-1/2}$  at large  $y$ . In this limit one obtains eq. (84) from eq. (80). The approach to

the asymptotic limit is very slow, however. The omitted terms are of order  $\mathcal{O}(\ln^{-1/2} s)$ . Therefore they should be taken into account at present energies.

Note that the preasymptotic difference between assumed  $F$  scaling and KNO scaling does not alter our conclusions because it is of order  $\mathcal{O}(\langle n \rangle^{-1})$ , i.e. it decreases with energy faster than the terms  $\mathcal{O}(y^{-1/2})$  and  $\mathcal{O}(y^{-1})$  considered.

A more interesting feature of the solutions is the qualitative behavior of  $H_q$  as a function of rank at a given energy, i.e. when  $\gamma_0$  is kept constant in eq. (80). According to eq. (84), the  $H_q$  moments are a smoothly decreasing function of  $q$  in the double-logarithmic approximation. In the modified leading-logarithmic approximation in which the linear  $h_1$  term is kept but the  $h_2$  term and higher order terms are neglected in eqs. (77) and (80),  $H_q$  acquires a minimum at

$$q_{min} \approx \frac{1}{h_1 \gamma_0} + \frac{1}{2} + \mathcal{O}(\gamma_0). \quad (86)$$

Note that the minimum position is shifted to larger rank values at higher energies due to the decrease of  $\gamma_0$ , and to smaller ranks for lower energies or for smaller phase space windows [95] if higher order corrections are neglected (see Section 14). At present energies, with a value of  $\gamma_0$  of about 0.45–0.5, we obtain

$$q_{min} \approx 5 (\pm 1). \quad (87)$$

The uncertainty of  $\pm 1$  for this result is due to the  $\mathcal{O}(\gamma_0)$  correction in eq. (86).

In MLLA, the ratio  $H_q$  crosses the abscissa axis, is negative at the minimum, and tends to zero from below as  $\sim -q^{-1}$  as the rank increases. If one includes the NNLO terms (proportional to  $h_2$ ), the ratio  $H_q$  is shifted up by an amount  $h_2 \gamma_0^2$  independent of  $q$ . The ratio then exhibits a second zero, crosses the abscissa axis again, and tends asymptotically to a positive constant  $h_2 \gamma_0^2$ . The location of the minimum shifts to slightly larger values of  $q$  because of the term with  $h_1^2$  and the two-loop correction to  $\alpha_S$ . If the exact limits of integration  $e^{-y}$  and  $1 - e^{-y}$  are used instead of 0 and 1, the minimum moves back to smaller ranks, however. Thus we conclude that the location of the minimum as approximately given by eqs. (86) and (87) is a rather stable prediction of gluodynamics. Furthermore we see that eq. (80) predicts an oscillation of the  $H_q$  ratio analogous to that found using the more approximate methods of Section 5.1.

One could object that the expansion parameter  $q\gamma$  entering eq. (80) is large at present energies. This, however, is similar to the situation with the expansion of, for example,  $\cos x$  in a Taylor series, for which the higher order terms approximate the function quite well even for large values of  $x$ . As more terms of the Taylor expansion of  $\cos x$  are included, the approximation improves at yet larger values of  $x$ .

A computer solution of eq. (77) [96] also yields an oscillating behavior for  $H_q$  when account is taken of the higher order terms with  $h_3$  and  $h_{11}$ , see Fig. 6. This is consistent with the discussion in the previous paragraph. However, the position of the first minimum is shifted to  $q \approx 4$  in the approximation of Ref. [96], illustrating the sensitivity of  $H_q$  to the various assumptions. In particular, the term with  $h_4$ , important for the proper limit in supersymmetric (SUSY) QCD as shown below, is not included in the results of Ref. [96].

Although the assumptions of the calculation influence the quantitative details of the oscillations, the main qualitative features are stable. An implicit cutoff of the multiplicity distribution at some maximum value due to the restrictions of finite energy produces similar oscillations, although with a smaller amplitude [52, 97]. Our present goal is to discuss the qualitative properties of  $H_q$ . More precise expressions are presented in the following sections. We emphasize that the amplitudes and periodicity of the oscillations are different in the more precise treatment than in the results shown in Figs. 2 and 4.

In this section, we have demonstrated that conservation laws and higher order perturbative corrections lead, in the framework of gluodynamics, to a substantial reduction in the width of the multiplicity distribution and to a qualitative change in the behavior of the cumulant and factorial moments, namely to oscillations of their ratio  $H_q$  as a function of  $q$  which disappear only at extremely high energies.

## 6 Perturbative solutions of QCD equations with a running coupling constant

A discussion of Quantum Chromodynamics, in which quarks are created as well as gluons, leads back to the system of coupled equations (57) and (58) for the generating functions. The structure of these equations does not differ,

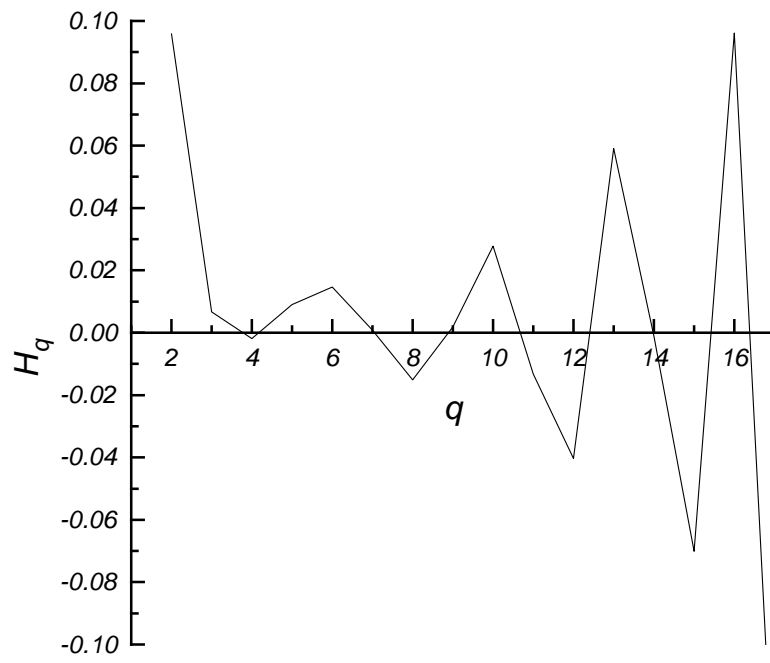


Figure 6: The ratio  $H_q$  as a function of  $q$  reveals oscillations in higher order perturbative QCD [96]. The results shown here correspond to the  $Z^0$  energy.

however, from the equation for gluodynamics, eq. (64). Therefore we shall not present the results for the full solutions (see e.g. Refs. [85, 93], [98]-[100]), but will merely describe them.

In analogy to gluodynamics, one obtains a system of coupled recurrent equations for factorial moments and cumulants when the Taylor series expansion (74) and the formulas (7) and (8) are used. This system of equations has been solved analytically for average multiplicities, accounting for corrections up to  $\mathcal{O}(\gamma_0^3)$ , i.e. the 3NLO approximation [98]. Analytic calculations of the second and third factorial moments have been performed in the same approximation [85]. Numerical solutions are available for yet higher moments [93, 96, 99]. The properties of gluon jets do not change appreciably compared to Section 5, i.e. the gluon jet cumulants and factorial moments are very similar to those determined in gluodynamics. In particular, the ratio  $H_q$  of gluon jets exhibits a minimum at the same value  $q \approx 5$  found in Section 5. The factorial moments of quark jets are determined to be larger than those of gluon jets, i.e. the parton multiplicity distribution of quark jets is wider than that of gluon jets even though the average multiplicity is smaller. This fact was known long ago [101]-[103]. The quark jet cumulants and  $H_q$  ratios are also found to oscillate. The first minimum of the quark jet oscillation is predicted by the analytic solutions to be located at  $q \approx 7-8$ , but it moves to  $q \approx 5$  if the non-asymptotic limits of integration are incorporated [104].

To apply these results to the two jet process of electron-positron annihilations, it is necessary to relate the  $e^+e^-$  generating function to those of quarks and gluons. Bearing in mind the Feynman diagram for the production of two quark jets in  $e^+e^-$  annihilations at a very early stage, one obtains

$$G_{e^+e^-} \approx G_F^2, \quad (88)$$

with further corrections (see, e.g., Ref. [83]). Thus the zeros of the quark jet and  $e^+e^-$  cumulants coincide since the logarithms of their generating functions are proportional to each other (see eq. (5)).

## 6.1 Average multiplicities and their slopes

We now describe the QCD results for average multiplicities [98, 100] in more detail. The equations for the average multiplicities in jets are obtained from the system of equations (57) and (58) by expanding the generating functions

in  $z$  and keeping the terms with  $q=0$  and 1 in the series (7) and (8). They read

$$\begin{aligned} \langle n_G(y) \rangle' &= \int dx \gamma_0^2 [K_G^G(x) (\langle n_G(y + \ln x) \rangle + \langle n_G(y + \ln(1-x)) \rangle - \langle n_G(y) \rangle) \\ &\quad + n_f K_G^F(x) (\langle n_F(y + \ln x) \rangle + \langle n_F(y + \ln(1-x)) \rangle - \langle n_G(y) \rangle)], \end{aligned} \quad (89)$$

$$\langle n_F(y) \rangle' = \int dx \gamma_0^2 K_F^G(x) (\langle n_G(y + \ln x) \rangle + \langle n_F(y + \ln(1-x)) \rangle - \langle n_F(y) \rangle). \quad (90)$$

From these equations one can predict the energy evolution of the ratio of multiplicities  $r$  and the QCD anomalous dimension  $\gamma$  (the slope of the logarithm of the average multiplicity in a gluon jet), defined by

$$r = \frac{\langle n_G \rangle}{\langle n_F \rangle}, \quad \gamma = \frac{\langle n_G \rangle'}{\langle n_G \rangle} = (\ln \langle n_G \rangle)'. \quad (91)$$

The perturbative expansions of  $\gamma$  and  $r$  are

$$\gamma = \gamma_0(1 - a_1\gamma_0 - a_2\gamma_0^2 - a_3\gamma_0^3) + \mathcal{O}(\gamma_0^5), \quad (92)$$

$$r = r_0(1 - r_1\gamma_0 - r_2\gamma_0^2 - r_3\gamma_0^3) + \mathcal{O}(\gamma_0^4). \quad (93)$$

The asymptotic value of  $r$  is  $r_0 = N_c/C_F = 9/4$ , as was first obtained in [105].

Using a Taylor series expansion of  $\langle n \rangle$  at large  $y$  in eqs. (89) and (90), in conjunction with (92) and (93), the coefficients  $a_i$  and  $r_i$  can be determined analytically. Their numerical values are given in Table 1 for various numbers of active quark flavors and for SUSY QCD. In SUSY QCD where  $n_f = N_c = C_F$ , all  $r_i$  are identically zero.

The value of the coefficient  $r_1$  was first reported in Ref. [106] and later in Ref. [87]. The coefficient  $r_2$  was first presented in Ref. [88]. The  $r_2$  results in Ref. [88] do not account for energy conservation in the equations for the generating functions, however, and as a consequence are much smaller than the  $r_2$  values given in Table 1. The larger values of  $r_2$ , i.e. including energy conservation, were first presented in Ref. [93]. Similar results to those in Ref. [93] were subsequently obtained in the framework of the Lund dipole model [107] with cutoff fractal triangles. Large NNLO corrections are also advocated in Ref. [91] using somewhat different reasoning. The energy conservation effects responsible for the large values of  $r_2$  are closely related to the oscillations of higher rank moments discussed below. The 3NLO values

$n_f$	$r_1$	$r_2$	$r_3$	$a_1$	$a_2$	$a_3$
3	0.185	0.426	0.189	0.280	- 0.379	0.209
4	0.191	0.468	0.080	0.297	- 0.339	0.162
5	0.198	0.510	-0.041	0.314	- 0.301	0.112
S	0	0	0	0.188	-0.190	-0.130

Table 1: Numerical values of the perturbative corrections up to order  $\gamma_0^3$  for the multiplicity ratio  $r$  and the QCD anomalous dimension  $\gamma$ , based on integration limits of the generating functions from 0 to 1 (see text).  $n_f$  is the number of active quark flavors while S refers to supersymmetric (SUSY) QCD.

of  $a_3$  and  $r_3$  were first presented in [98] where one can also find analytic expressions for all  $a_i$  and  $r_i$  with  $i \leq 3$ .

According to eq. (93) and the values of  $r_i$  in Table 1,  $r$  at higher orders is much smaller [93] than in the double-logarithmic approximation. On average, it is smaller by about 20%. At the  $Z^0$  resonance, the subsequent terms in eq. (93) diminish the theoretical value of  $r$  compared with its asymptotic value by approximately 10%, 13%, and 1% for  $n_f=4$ , see Section 11.2 and Fig. 18.

Inserting eq. (92) into eq. (68), the energy behavior of the average multiplicity in gluon jets at 3NLO is determined to be [100]

$$\begin{aligned} \langle n_G \rangle = & K y^{-a_1 c^2} \exp(2c\sqrt{y} + \frac{c}{\sqrt{y}}[2a_2 c^2 + \frac{\beta_1}{\beta_0^2}(\ln 2y + 2)] \\ & + \frac{c^2}{y}[a_3 c^2 - \frac{a_1 \beta_1}{\beta_0^2}(\ln 2y + 1)]), \end{aligned} \quad (94)$$

where  $c=(4N_c/\beta_0)^{1/2}=(2B)^{-1/2}$  and  $K$  is a normalization constant. For  $n_f=0$  and  $B=h_1$  this reduces to the corresponding result of gluodynamics. The pre-exponential term and the first term in the exponent correspond to the MLLA expression [108, 109] (for a coupled system of quark and gluon jets, these terms were first found in [92]). The second term in the exponent, proportional to  $c/\sqrt{y}$ , is the NNLO correction. This term can be also written as a small negative correction to the pre-exponent (see Table 1). The third



term in the exponent, proportional to  $c^2/y$ , is the 3NLO result. The role of the 3NLO term in the gluon jet multiplicity is not important compared to the lower order terms because of the smallness of  $a_3$ . Note that the NNLO and 3NLO corrections are almost constant and somewhat compensate each other at currently accessible energies. As a consequence, the MLLA expression for gluon jets is a good approximation to the higher order result, eq. (94).

The solid curves in Fig. 7 show the behavior of the average gluon jet multiplicity as a function of energy (i.e.  $y$ ) as calculated in NNLO using a running coupling constant. The different curves show the results for  $n_f=3, 4$  and 5. The parameter  $Q_0=1.3\Lambda_{\overline{\text{MS}}}$ , with  $\Lambda_{\overline{\text{MS}}}=175$  MeV for  $n_f=5$ , and taken in the proportions 63:100:130 for  $n_f=5:4:3$ , has been chosen as in [110]. For purposes of comparison, we also show the energy dependence of the mean multiplicity for a fixed coupling constant. This is indicated by the dashed curves. At low energies, the multiplicity for fixed coupling increases rather slowly. At higher energies, the rate of increase exceeds that found using the running coupling constant. This is reasonable since the coupling strength in the case of fixed coupling has been evaluated at a rather high scale, namely  $y_{Z^0} \approx 6.6$  corresponding to the mass of  $Z^0$ , yielding a relatively small (fixed) coupling strength. In actuality, the coupling strength should increase during the course of evolution of the jet, while the number of active flavors should decrease. The two trends somewhat compensate each other.

The slope of  $r$ , namely  $r' \equiv dr/dy$ , is extremely sensitive to higher order perturbative corrections. The role of higher order corrections is increased here compared to  $r$  because each  $n$ th order term, proportional to  $\gamma_0^n$ , gets an additional factor of  $n$  in front of it when differentiated, the main constant term disappears, and the large value of the ratio  $r_2/r_1$  becomes crucial [98]:

$$r' = Br_0r_1\gamma_0^3 \left[ 1 + \frac{2r_2\gamma_0}{r_1} + \left( \frac{3r_3}{r_1} + B_1 \right) \gamma_0^2 + \mathcal{O}(\gamma_0^3) \right], \quad (95)$$

where the relation  $\gamma_0' \approx -B\gamma_0^3(1+B_1\gamma_0^2)$  has been used, and where  $B=\beta_0/8N_c$  and  $B_1=\beta_1/4N_c\beta_0$ . The factor in front of the brackets is very small even at present energies:  $Br_0r_1 \approx 0.156$  and  $\gamma_0 \approx 0.5$ . Nonetheless, the numerical estimate of  $r'$  is unreliable because of the expression inside the brackets. Each differentiation leads to a factor  $\alpha_S$  (or  $\gamma_0^2$ ), i.e. to terms of higher order. The values of  $r_1$ ,  $r_2$  and  $r_3$  given in Table 1 for  $n_f=4$  yield  $2r_2/r_1 \approx 4.9$  and  $(3r_3/r_1) + B_1 \approx 1.5$ . Thus the first correction in eq. (95) (proportional to  $\gamma_0$ ) is more than twice as large as unity at present energies, while the next

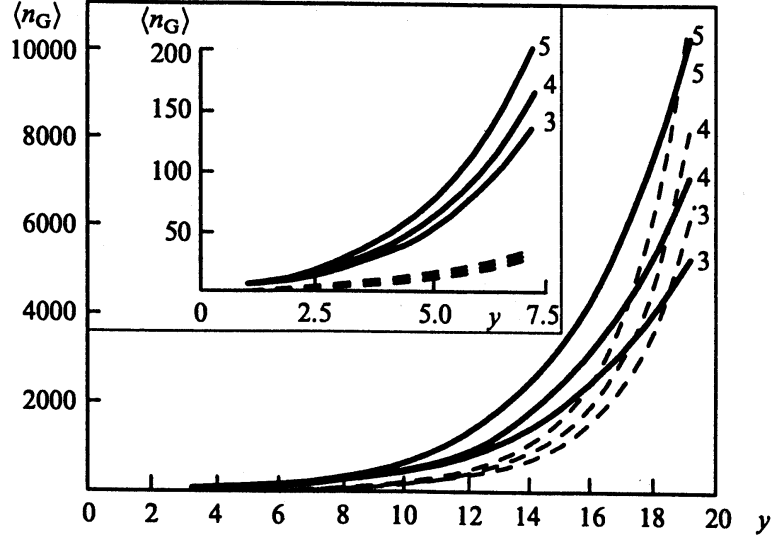


Figure 7: The energy ( $y=\ln(Q/Q_0)$ ) dependence of the average multiplicity of gluon jets, for a running (solid curves) or fixed (dashed curves) coupling constant [93]. The results are shown for different numbers of active flavors,  $n_f=3, 4$ , and 5.

correction (proportional to  $\gamma_0^2$ ) is about 0.4. Therefore even higher order terms are necessary before the perturbative result for  $r'$  can be considered to be reliable.

The slope  $r'$  is 0 for a fixed coupling constant. In the case of the running coupling,  $r'$  evolves rapidly with  $y$  in the lowest perturbative approximation, ranging according to eq. (95) from 0.06 at the  $Z^0$  to 0.25 at the  $\Upsilon$ .

Next we consider the ratios of slopes  $r^{(1)}$  and curvatures  $r^{(2)}$ , defined as

$$r^{(1)} = \frac{\langle n_G \rangle'}{\langle n_F \rangle'}, \quad r^{(2)} = \frac{\langle n_G \rangle''}{\langle n_F \rangle''}. \quad (96)$$

Their ratios to  $r$  can be written as

$$\rho_1 = \frac{r}{r^{(1)}} = 1 - \frac{r'}{\gamma r}, \quad (97)$$

$$\rho_2 = \frac{r}{r^{(2)}} = 1 - \frac{2\gamma r r' + r r'' - 2r'^2}{(\gamma^2 + \gamma')r^2}. \quad (98)$$

Since  $r' \propto \gamma_0^3$ , the asymptotic values of  $r$ ,  $r^{(1)}$  and  $r^{(2)}$  coincide, equaling 2.25. Moreover, the values of  $r$ ,  $r^{(1)}$  and  $r^{(2)}$  coincide in MLLA. The first preasymptotic corrections are very small. They are of order  $\mathcal{O}(\gamma_0^2)$  (NNLO) with a small factor in front and contribute about 2-4% at present energies:

$$\rho_1 = 1 - Br_1\gamma_0^2 \approx 1 - 0.07\gamma_0^2, \quad (99)$$

$$\rho_2 = 1 - 2Br_1\gamma_0^2 \approx 1 - 0.14\gamma_0^2. \quad (100)$$

However, this favorable situation does not persist when the next terms are considered. For  $\rho_1$  the numerical values of the higher order terms are

$$\rho_1 = 1 - 0.07\gamma_0^2(1 + 5.38\gamma_0 + 4.21\gamma_0^2) \quad (n_f = 4), \quad (101)$$

and similarly for  $\rho_2$  (see Ref. [98]). All the correction terms are much smaller than unity. However, the numerical factors inside the brackets are so large that at present values of  $\gamma_0 \approx 0.5$  the subsequent terms are larger than the first one and the sum of the series is unknown. The series can be summed using the simplest Padé approximant (i.e. by assuming the steady decrease of the unaccounted terms in proportions determined by the ratio of two last calculated terms), resulting in

$$\rho_1 = 1 - 0.07\gamma_0^2 \left[ 1 + \frac{5.38\gamma_0}{1 - 0.78\gamma_0} \right]. \quad (102)$$

In contrast to  $\rho_1$ , the perturbative corrections to the ratio of slopes  $r^{(1)}$  are small. The lowest order  $\mathcal{O}(\gamma_0)$  correction to  $r^{(1)}$  is the same as for  $r$  but higher order corrections are smaller because they are negative both in  $r$  and  $\rho_1$  which define  $r^{(1)} = r/\rho_1$ . This explains why experimental values of  $r^{(1)}$  are similar to values of  $r$  calculated in the MLLA approximation (see Section 11), whereas experimental values of  $r$  are about 25% lower than the MLLA prediction. Yet more substantial cancelations of higher order terms should occur for  $r^{(2)}$ . It would be interesting to test this prediction experimentally.

An interesting feature of eq. (101) is that  $\rho_1$  contains terms up to  $\mathcal{O}(\gamma_0^4)$  whereas  $r$  in the numerator of eq. (97) is known to  $\mathcal{O}(\gamma_0^3)$  only. This situation is related to the fact that  $r'/\gamma \sim \mathcal{O}(\gamma_0^2)$ .

The value of  $\rho_1$  also determines the ratio of the slope of the logarithm of the average multiplicity of a quark jet ( $\gamma_F$ ) to that of a gluon jet ( $\gamma$ ):

$$\gamma_F = (\ln \langle n_F \rangle)' = \rho_1 \gamma = \gamma - \frac{r'}{r}. \quad (103)$$

Once again we see that the logarithmic slopes of quark and gluon jets are equal in MLLA. They differ in higher orders in such a manner that  $\gamma_F < \gamma$  since both  $r$  and  $r'$  are positive. Our failure to obtain a precise estimate of  $\rho_1$  implies that we cannot reliably evaluate  $\gamma_F$  either. Thus the ratio of logarithmic slopes  $\rho_1$  is more sensitive to higher order perturbative terms than the ratio of slopes  $r^{(1)}$ .

A high sensitivity of multiplicities in quark jets to higher order terms is especially noticeable if one writes down the expression for their energy dependence, analogous to eq. (94) for gluon jets. Taking into account perturbatively the ratio  $r(y)$  one obtains [98, 100]

$$\begin{aligned} \langle n_F \rangle = \frac{K}{r_0} y^{-a_1 c^2} \exp(2c\sqrt{y} + \frac{c}{\sqrt{y}}[r_1 + 2a_2 c^2 + \frac{\beta_1}{\beta_0^2}(\ln 2y + 2)] \\ + \frac{c^2}{y}[a_3 c^2 + \frac{r_1^2}{2} + r_2 - \frac{a_1 \beta_1}{\beta_0^2}(\ln 2y + 1)]). \end{aligned} \quad (104)$$

Especially striking is the role of the last term which cannot be neglected even at the energy of the  $Z^0$ .

Another representation of this dependence is the direct use of formula (91):

$$\langle n_F \rangle = \frac{\langle n_G \rangle}{r_0(1 - r_1 \gamma_0 - r_2 \gamma_0^2 - r_3 \gamma_0^3)}. \quad (105)$$

However one easily observes that formulas (104) and (105) differ since there is no term with  $r_3$  in eq. (104). This is an important point which emphasizes that the notion of the order of approximations is different in the definitions of  $\gamma$  and  $r$ . The MLLA term of  $r$  (proportional to  $\gamma_0$ ), given by  $r_1$ , appears in the NNLO term of  $\gamma_F$  (proportional to  $\gamma_0^2$ ) in combination with  $a_2$ . This situation is a consequence of the fact that  $r' \sim \mathcal{O}(\gamma_0^3)$ . Therefore the notion of orders is somewhat a question of convention. We conclude that it is improper to use the term with  $r_3$  in eq. (105) until the  $a_4$  contribution to  $\gamma$  is known. By extension this implies that if the MLLA formula is used to

describe multiplicities, as is common practice, the DLA result  $r = r_0$  should be inserted into all formulas to be self consistent within the perturbative approach, leading to the same energy dependence for quark and gluon jets. The NNLO term with  $r_1$  may be included in  $\gamma_F$  only if the  $a_2$  contribution has been incorporated in  $\gamma$ , and so on.

Therefore within the present accuracy of  $\mathcal{O}(\gamma_0^3)$  corrections, the perturbative QCD approach fails in the precise determination of the logarithmic slope of the quark jet multiplicity  $\gamma_F$ , even at the  $Z^0$ , and can be trusted only at much higher energies.

## 6.2 Widths of the distributions

Next we consider higher order corrections for the moments of multiplicity. The normalized factorial moments of any rank  $q$  can be obtained by differentiating the generating functions according to eq. (4) or, equivalently, by using the series (7) and collecting the terms with equal powers of  $z$  on both sides of eqs. (57) and (58). The QCD equations for the moments of multiplicity are given in Refs. [83, 85, 93, 96, 99].

The normalized second factorial moments of gluon and quark jets,  $F_2$ , are given by

$$F_2^G = \frac{\langle n_G(n_G - 1) \rangle}{\langle n_G \rangle^2}, \quad F_2^F = \frac{\langle n_F(n_F - 1) \rangle}{\langle n_F \rangle^2}. \quad (106)$$

The  $F_2$  moments define the widths of the multiplicity distributions, being related to the dispersion  $D^2 = \langle n^2 \rangle - \langle n \rangle^2$  by

$$D^2 = (F_2 - 1)\langle n \rangle^2 + \langle n \rangle = K_2 \langle n \rangle^2 + \langle n \rangle. \quad (107)$$

The perturbative expansions of  $F_2$  up to  $\gamma_0^3$  are

$$F_2^G = \frac{4}{3}(1 - f_1\gamma_0 - f_2\gamma_0^2 - f_3\gamma_0^3), \quad (108)$$

$$F_2^F = (1 + \frac{r_0}{3})(1 - \phi_1\gamma_0 - \phi_2\gamma_0^2 - \phi_3\gamma_0^3). \quad (109)$$

Inserting expressions (108) and (109) into the QCD equations yields predictions for the coefficients  $f_i$  and  $\phi_i$ . The asymptotic ( $\gamma_0 \rightarrow 0$ ) values of  $F_2^G$  and  $F_2^F$  can also be determined by equating the leading terms in  $\gamma_0$  on both sides of the equations. We have presented their explicit expressions in

$n_f$	$f_1$	$f_2$	$f_3$	$\phi_1$	$\phi_2$	$\phi_3$
3	0.364	-0.0279	0.795	0.637	-0.276	2.12
4	0.358	-0.0457	0.740	0.631	-0.286	2.04
5	0.352	-0.0629	0.689	0.625	-0.295	1.95
S	0.313	0.310	-0.120	0.313	0.310	-0.120

Table 2: Numerical values of the perturbative corrections up to order  $\gamma_0^3$  for the normalized second factorial moments of gluon ( $f_i$ ) and quark ( $\phi_i$ ) jets.  $n_f$  is the number of active quark flavors while S refers to supersymmetric (SUSY) QCD.

eqs. (108) and (109) to simplify later notation. Analytic formulas for  $f_i$  and  $\phi_i$  are given in Ref. [85]. Their numerical values for different numbers of active flavors and for SUSY QCD are listed in Table 2. From these values it is seen that the series (108) and (109) change in sign at each term and that higher order terms are more important for the width of a quark jet than for a gluon jet.

The asymptotic values of  $F_2^G$  and  $F_2^F$  are [3]:

$$F_{2,as}^G = \frac{4}{3}, \quad F_{2,as}^F = 1 + \frac{r_0}{3} = \frac{7}{4}. \quad (110)$$

At lower energies the widths are slightly smaller because of the increase of  $\alpha_S$ , leading to larger values of the first corrections (with coefficients  $f_1$  and  $\phi_1$ ) in eqs. (108) and (109).

The MLLA prediction for the energy dependence of the second factorial moments is shown in Fig. 8, using  $n_f=4$  and the values of  $\alpha_S$  in Ref. [80]. The curves demonstrate that the widths are almost Poissonian at low energies, i.e. they approach unity as the scale decreases. The small dots at the ends of the curves show the effects of a change in  $n_f$  to 3 at  $Q=10$  GeV and to 5 at  $Q=90$  GeV: it is seen that the results are almost insensitive to the number of effective flavors. Note that  $n_f$  is the only free parameter in these results. Cutoff of the integration at  $\varepsilon=e^{-y} \approx e^{-2\pi/\beta_0\alpha_S}$  from below and at  $1-\varepsilon$  from above as a consequence of preasymptotic effects is also not particularly important at present energies, as shown by the dashed curves in Fig. 8. The preasymptotic corrections slightly increase the widths and reduce the slope

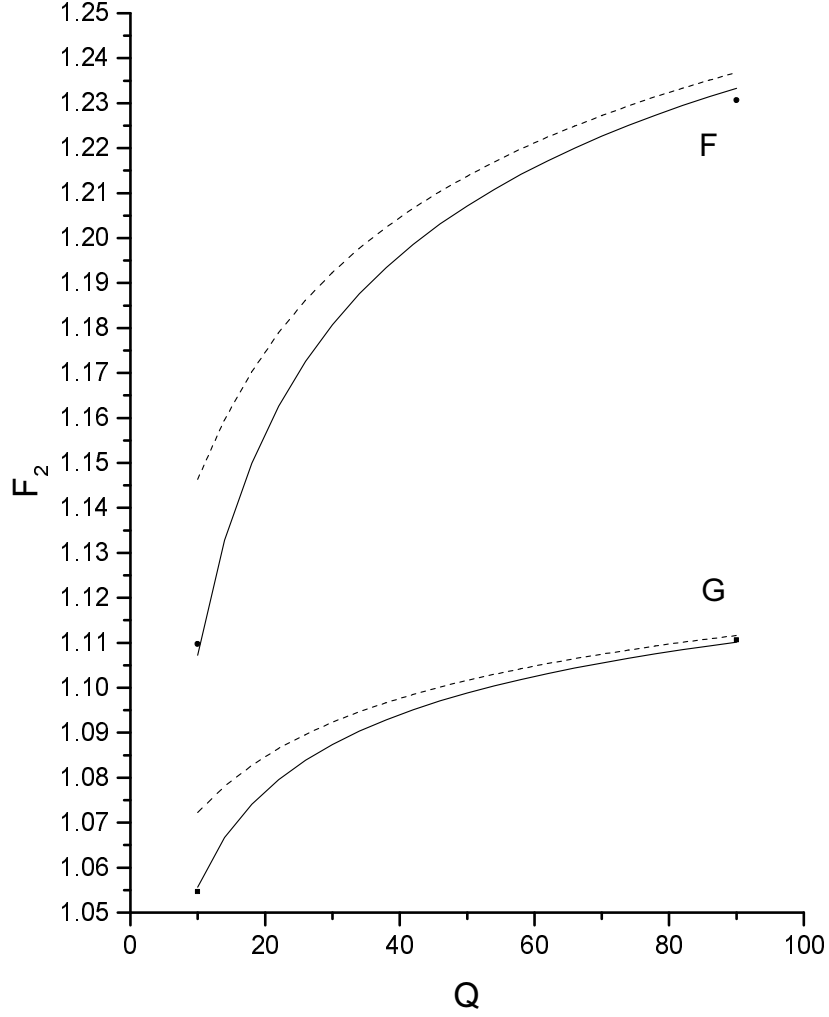


Figure 8: The energy behavior of the second factorial moments of quark (F) and gluon (G) jets [85]. The scale of the energy  $Q$  is GeV. The limits of integration are chosen to be either 0 and 1 (solid curves) or  $\varepsilon$  and  $1 - \varepsilon$  (dashed curves). The dots at the ends of the curves demonstrate that the results are insensitive to variation of the effective number of flavors (see text).

with respect to  $Q$ .

Unfortunately, higher order corrections do not improve the theoretical estimates. The NNLO terms are positive, while the 3NLO corrections are negative and so large they lead to sub-Poissonian widths ( $F_2 < 1$ ) for  $\alpha_S=0.2$ . Indeed, the 3NLO corrections are just as large as those in MLLA. The origin of the large values of  $f_3$  and  $\phi_3$  can be traced to rather large contributions of integrals of the form  $\int_0^1 \ln^n x dx \propto n!$ , i.e. to the region of very soft gluons. Thus the cutoff at  $e^{-y}$  and  $1 - e^{-y}$  should be quite important for the higher order terms. This is analogous to the situation with renormalons (see, e.g., Ref. [111]).

The 3NLO corrections are overestimated in the method of the Taylor series expansion because of the assumption  $y \gg |\ln x|$  which is invalid for soft gluons. For example, the  $k_t$  dependence of the coupling strength is transformed so that

$$\alpha_S \propto \frac{1}{y + \ln x(1-x)} \approx \frac{1}{y} \left( 1 - \frac{\ln x(1-x)}{y} \right). \quad (111)$$

The second term becomes infinitely large for  $x \rightarrow 0$ . The cutoff at  $x=e^{-y}$  yields a factor of 2 only. Thus the above expansion implies a presumption about the behavior of the coupling strength in the non-perturbative region as well as its modification at the limits of the perturbative one.

The slopes of the widths are especially sensitive to higher order terms because each of them is multiplied by the factor  $n$  when differentiating  $\gamma_0^n$ . Thus the 3NLO term in the perturbative expression for the slopes of the widths is about 3 times larger than the MLLA term. This suggests that a precise quantitative estimate of these slopes is not possible. At present energies,  $F_2^{G'}(MLLA) \approx 0.04$  and  $F_2^{F'}(MLLA) \approx 0.092$  for  $\alpha_S=0.2$ . The asymptotic value of the ratio of slopes can be estimated to be

$$\frac{(F_2^G)'_{as}}{(F_2^F)'_{as}} = \frac{16f_1}{21\phi_1} \approx 0.43, \quad (112)$$

which surely coincides with the MLLA prediction for this ratio. Thus the second factorial moment of quark jets approaches its asymptotic value faster than the corresponding quantity for gluon jets.

We stress that all slopes and curvatures in pQCD are related to the running property of the QCD coupling constant since they are proportional to its derivatives which are zero for a fixed coupling strength.



$n_f$	$h_1$	$h_2$	$h_3$	$g_1$	$g_2$	$g_3$
3	0.986	-0.342	2.49	1.61	-1.58	7.74
4	0.972	-0.380	2.36	1.60	-1.59	7.54
5	0.957	-0.417	2.25	1.59	-1.60	7.34
S	0.844	0.722	-1.09	0.844	0.722	-1.09

Table 3: Numerical values of the perturbative corrections up to order  $\gamma_0^3$  for the normalized third factorial moments of gluon ( $h_i$ ) and quark ( $g_i$ ) jets.  $n_f$  is the number of active quark flavors while S refers to supersymmetric (SUSY) QCD.

One can easily check (see Ref. [85]) that the relations of SUSY QCD, where  $n_f=N_c=C_F$ , are valid for the coefficients given above (e.g.,  $F_2^G=F_2^F$  etc.). The asymptotic SUSY values of  $F_2$  equal  $4/3$  for both gluon and quark jets.

Third moments of the multiplicity distributions have been calculated [85] in a manner analogous to that described above for the second moments. The results are

$$F_3^G = h_0(1 - \sum_{i=1}^3 h_i \gamma_0^i); \quad F_3^F = g_0(1 - \sum_{i=1}^3 g_i \gamma_0^i), \quad (113)$$

where  $h_0=9/4$ ,  $g_0=1 + r_0 + r_0^2/4$ , and the values of the coefficients  $h_i$  and  $g_i$  are listed in Table 3. In the asymptotic limit, the third moment of quark jets is about twice as large as the third moment of gluon jets.

Comparing  $f_i$  and  $\phi_i$  to  $h_i$  and  $g_i$ , one concludes that the corrections increase for higher moments, even in MLLA. Moreover, at present values of  $\gamma_0 \approx 0.5$ , the corrections are rather large. Note the similarity in the structure of the corrections for the second and third moments. The corrections alternate in sign, and the third coefficients are larger than the first ones. This is an indication of a sign-alternating asymptotic series, and Borel summation could be effective.

In SUSY QCD the asymptotic values of the third moments equal  $9/4$ . The first correction, given by  $h_1(\text{SUSY})=g_1(\text{SUSY})=0.844$ , is about the same size as for ordinary gluon jets and is similar to the correction for second moments.

However, the NNLO and 3NLO terms for moments in SUSY QCD differ drastically from those for ordinary jets, both in absolute value and sign, as seen from Tables 2 and 3. This demonstrates the sensitivity of the results to the value of  $r_0$ , which is different in the two cases.

A similar procedure can be used to determine yet higher rank moments. However, the series will probably be badly convergent.

## 7 Computer solutions

The analytic approach described in Sections 5 and 6 accounts for energy conservation in an approximate manner. Energy conservation can be included more accurately by solving eqs. (57) and (58) numerically, i.e. by implementing a computer solution. The computer solution also allows the preasymptotic limits of integration to be directly incorporated, i.e. the limits  $e^{-y}$  and  $1 - e^{-y}$  rather than 0 and 1. Thus the non-perturbative region of  $x$  values near 0 and 1 can be avoided.

A computer solution of eqs. (57) and (58) is presented in Refs. [104, 78]. Thresholds for new quark production are approximated using a smoothed function. The coupling constant is considered in the one-loop approximation. A deficiency, shared by the analytic calculations, is the neglect of strict conservation of transverse momentum and a corresponding limitation on the available phase space. This deficiency effectively corresponds to a modification of eqs. (57) and (58).

The principal result of the computer solution is that the value of  $r$  is reduced by more than 10% compared with the 3NLO prediction. The computer solution for  $r$  versus energy scale  $Q$  is shown in Fig. 9. The experimental results shown in this figure are discussed in Section 11.

A perturbative cutoff  $Q_0=507$  MeV is found from a fit to the measured mean particle multiplicity in quark jets [78]. With increasing resolution, more and more jets are resolved, and predictions for the evolution of the subjet multiplicity (see Section 12) can be obtained as well. The subjet multiplicities are found to agree quite well with experiment using this same value of  $Q_0$  [78]. Correlation functions of high ranks up to  $q=18$  in quark and gluon jets were also determined, fully accounting for energy conservation [104]. A quantitative description of the existing data on factorial moments, factorial cumulants, and their ratio  $H_q$  was obtained for single quark and gluon jets

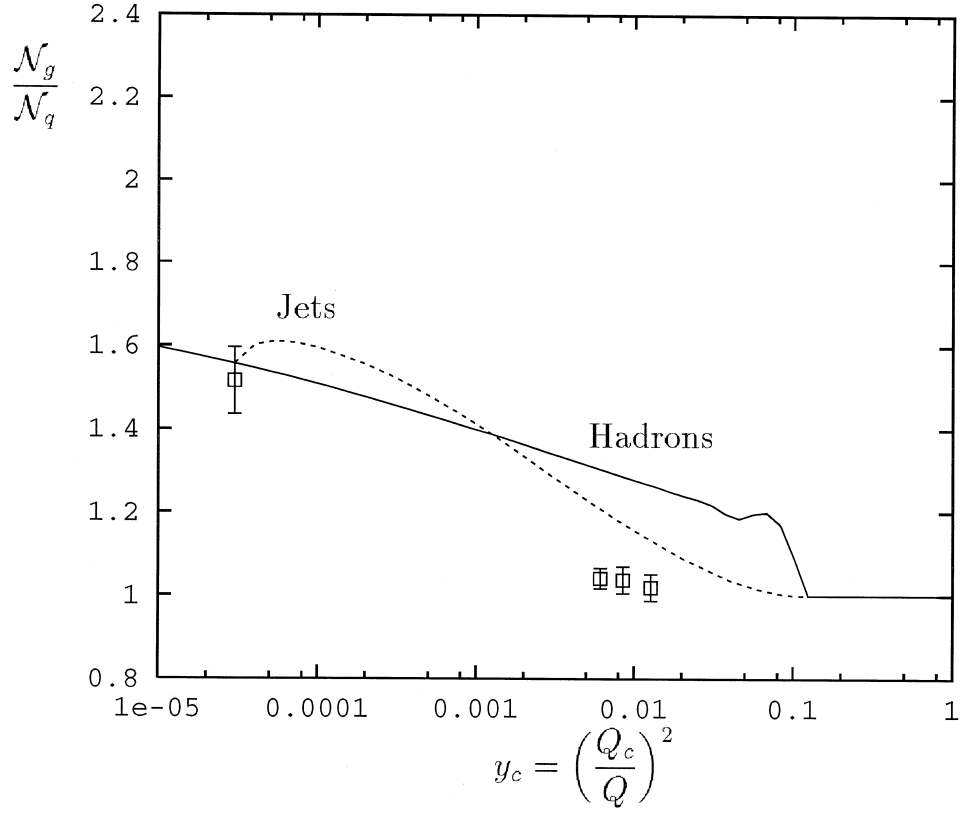


Figure 9: Computer solution [78] for the ratio of mean hadron multiplicities between gluon and quark jets (solid curve) in comparison to data. The experimental result at  $y_c \approx 3 \times 10^{-5}$  is based on  $e^+e^- Z^0$  events from the OPAL Collaboration [112, 113]. The results at  $y_c \approx 0.01$  are from  $\Upsilon$  decays recorded by the CLEO Collaboration [114]. The dashed curve shows the analogous prediction [78] for subjet multiplicities.

and for two-jet  $e^+e^-$  events, using the same parameters determined for the average subjet and particle multiplicities, see Fig. 10 and Section 11.4.

## 8 Exact solutions of QCD equations with a fixed coupling constant

The QCD results described above demonstrate that conservation laws and the non-singular terms of the kernels play a more important role up to MLLA than the running coupling constant, which becomes essential in NNLO only. Thus the running property of the coupling constant does not alter the qualitative predictions of QCD for multiplicity. It is possible to obtain an exact analytic solution of eqs. (57) and (58), i.e. without resorting to a perturbative approximation, if the coupling constant is fixed [36, 117]. No other assumption is necessary. One can obtain the general solution for the moments of any rank in this approximation. The effect of the running coupling constant can be assessed by varying the value chosen for  $\gamma_0$ . This analytic approach provides further insight into the behavior of the solutions.

In the following we first discuss the lowest rank moments obtained in the fixed coupling approximation, and compare them with the results of the previous sections. Following this we discuss the solutions for higher rank moments.

### 8.1 First moments and the ratio of average multiplicities in gluon jets to those in quark jets

The equations for average multiplicities, i.e. unnormalized moments of rank  $q=1$ , are obtained by substituting the series (7) for the generating functions into eqs. (57) and (58) and equating the terms linear in  $z$ , with the conditions  $F_0=F_1=\Phi_0=\Phi_1=1$ . The factorial moments of quark jets are denoted by  $\Phi_q$  and their cumulants by  $\Psi_q$ . If the coupling constant is fixed, the average multiplicities behave like

$$\langle n_G(y) \rangle \propto \exp(\gamma y), \quad \langle n_F(y) \rangle \propto r^{-1} \exp(\gamma y), \quad (114)$$

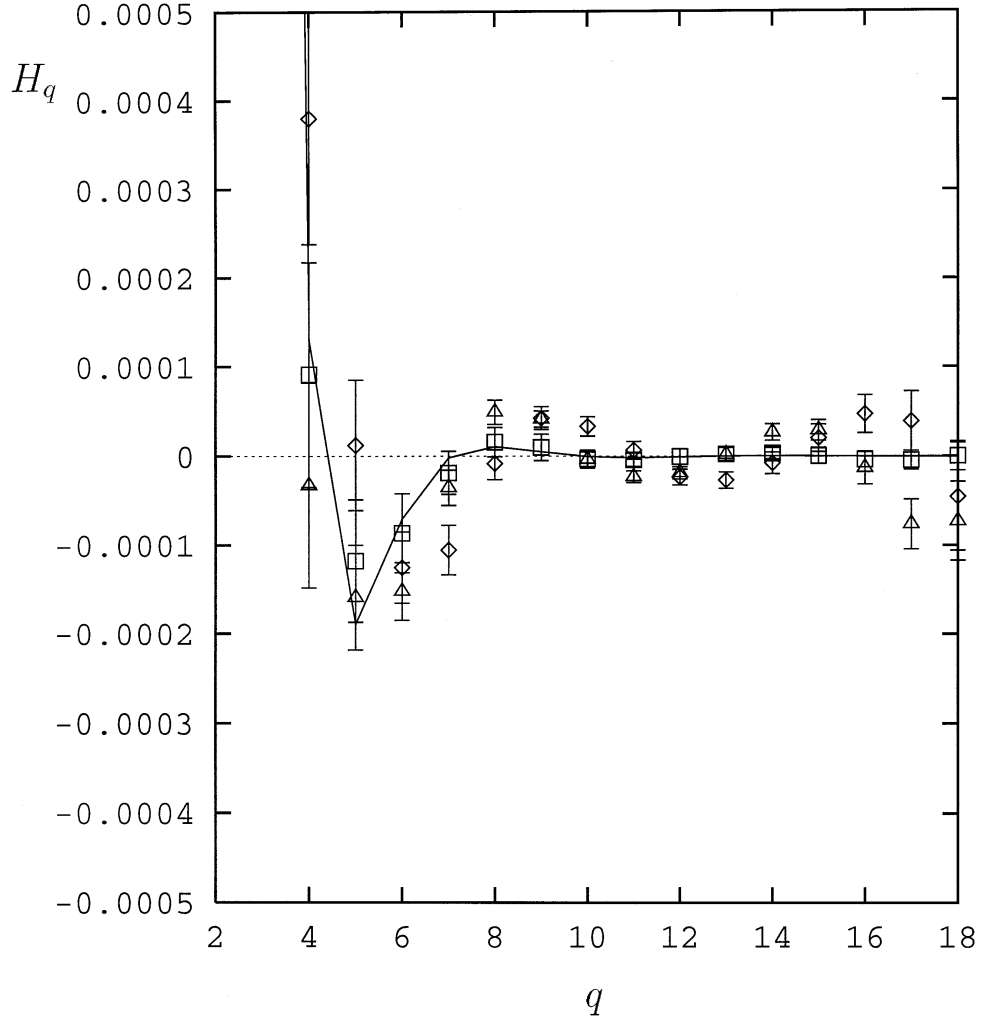


Figure 10: Computer solution for the ratio  $H_q$  of cumulant over factorial moments as a function of rank  $q$  (solid curve) [104] in comparison to experimental results from  $e^+e^- Z^0$  decays from the DELPHI Collaboration [115] as analyzed in [116].

where the anomalous dimension  $\gamma$  and the ratio  $r$  are constants. This behavior follows directly from eqs. (57) and (58) as can be seen using the relations

$$\langle n_{G,F}(y + \ln x) \rangle / \langle n_{G,F}(y) \rangle = x^\gamma, \quad (115)$$

$$\langle n_{G,F}(y) \rangle' = \gamma \langle n_{G,F} \rangle. \quad (116)$$

Then eqs. (57) and (58) can be rewritten as a system of algebraic equations for the variables  $\gamma$  and  $r$ :

$$\gamma = \gamma_0^2 [M_1^G + n_f r (M_1^F - M_0^F)], \quad (117)$$

$$\gamma = \gamma_0^2 [L_2 - L_0 + r L_1], \quad (118)$$

where

$$\begin{aligned} M_1^G &= \int_0^1 dx K_G^G [x^\gamma + (1-x)^\gamma - 1], \\ M_1^F &= \int_0^1 dx K_G^F [x^\gamma + (1-x)^\gamma], \\ M_0^F &= \int_0^1 dx K_G^F = M_1^F(\gamma = 0)/2, \\ L_1 &= \int_0^1 dx K_F^G x^\gamma, \\ L_2 &= \int_0^1 dx K_F^G (1-x)^\gamma, \\ L_0 &= \int_0^1 dx K_F^G = L_1(\gamma = 0). \end{aligned}$$

The coefficients  $M_i$  and  $L_i$  can be expressed in terms of Euler beta functions and psi functions and depend only on  $\gamma$ .

From this, one can estimate the corrections induced by the preasymptotic limits of integration (see e.g. Section 4). For example, the leading term in  $M_1^G$  gives rise to a correction of order  $\mathcal{O}(-\exp(-\gamma y)/\gamma)$ , about 10% of the main term at the  $Z^0$  energy. Computer calculations support this estimate [78]. The corrections decrease with energy in a power-like manner similar to higher twist effects. It is possible that other effects of the same order, e.g. due to instantons, could influence the multiplicity distributions. No definite answer to this question has yet been given.

It should be stressed that  $\gamma$  does not equal  $\gamma_0$  even in gluodynamics ( $n_f=0$ ) because  $M_1^G$  differs from  $\gamma^{-1}$ . An approximate equality between  $\gamma$  and  $\gamma_0$  is valid for  $\gamma_0 \ll 1$  but the perturbative expansion for  $\gamma$  in the fixed coupling approximation,

$$\gamma \approx \gamma_0 - h_1 \gamma_0^2 + \frac{1}{2}(h_1^2 + h_2) \gamma_0^3 + \mathcal{O}(\gamma_0^4), \quad (119)$$

differs from the corresponding formula (81) for the case of the running coupling constant, from which one sees that the first correction is twice as large in the former case as in the latter. This explains why the average multiplicity at low energies increases more slowly for fixed coupling than for running coupling (see Fig. 7), and why the increase in multiplicity for fixed coupling follows a power law at extremely high energies only.

The ratio  $r$  appears linearly in eqs. (117) and (118), allowing these two equations to be written as

$$r(\gamma) = b(\gamma) \left[ \frac{\gamma}{\gamma_0^2} - a(\gamma) \right]^{-1}, \quad (120)$$

$$r(\gamma) = \left[ \frac{\gamma}{\gamma_0^2} - d(\gamma) \right] \frac{1}{c(\gamma)}, \quad (121)$$

where

$$\begin{aligned} a(\gamma) &= \psi(1) - \psi(\gamma + 1) + B(\gamma, 1) - 2B(\gamma + 1, 2) \\ &\quad - 2B(\gamma + 2, 1) + B(\gamma + 2, 3) + B(\gamma + 3, 2) + \frac{11}{12} - \frac{n_f}{6N_c}, \\ b(\gamma) &= \frac{n_f}{2N_c} [B(\gamma + 3, 1) + B(\gamma + 1, 3)], \\ c(\gamma) &= \frac{C_F}{N_c} [B(\gamma, 1) - B(\gamma + 1, 1) + \frac{1}{2}B(\gamma + 2, 1)], \\ d(\gamma) &= \frac{C_F}{N_c} [\psi(1) - \psi(\gamma + 1) - B(\gamma + 1, 1) + \frac{1}{2}B(\gamma + 1, 2) + \frac{3}{4}]. \end{aligned}$$

The beta functions are just inverse polynomials of  $\gamma$  but the above notation is less cumbersome.

Thus the non-linear, integro-differential equations (57) and (58) can be reduced to the algebraic expressions (120) and (121), which yield  $\gamma$  and  $r$  as a function of  $\gamma_0$  and  $n_f$ . The dependence of the solution on  $n_f$  is very small.

The anomalous coupling  $\gamma$  can be related to  $\gamma_0$  by the simple fitted formula

$$\gamma = 0.077 + 0.62\gamma_0, \quad (122)$$

or by a more theoretically motivated one based on eq. (119),

$$\gamma = 0.97\gamma_0 - 0.48\gamma_0^2 + 0.2\gamma_0^3, \quad (123)$$

fitted in the range of  $\gamma_0$  from 0.48 to 0.6. Thus  $\gamma$  changes very slowly with  $\gamma_0$ . The alternating signs of the correction terms correspond to the tendencies observed for the running coupling constant, see Table 1. In itself, the value of  $\gamma$  is not of much interest. Even though it is related to the energy dependence of the average multiplicity, it is known that the power law increase of mean multiplicity for fixed coupling is replaced asymptotically by a slower dependence  $\sim \exp(\ln^{1/2} s)$  for running coupling (see Fig. 7). The more realistic behavior provided by the running coupling constant was discussed in the previous sections.

The ratio  $r$  is of more interest because the energy dependence of the average multiplicities in gluon and quark jets cancels. Thus the fixed coupling prediction for  $r$  can be expected to be rather general. A computer solution of eqs. (120) and (121) yields the results shown in Fig. 11. The dependence on  $n_f$  is seen to be very mild. More important, the dependence of  $r$  on  $\gamma_0$  is even weaker than that of  $\gamma$ , and its average effective value is

$$r = 1.84 \pm 0.02. \quad (124)$$

This value of  $r$  is much lower than the prediction from the double-logarithmic approximation and corresponds well with the estimate of  $r$  from the higher order approximate solution of QCD equations with a running coupling constant, discussed in Section 6. This suggests that yet higher order corrections to eq. (93) will be small. Introduction of the exact (i.e. preasymptotic) limits of integration would reduce the value of  $r$  in eq. (124) yet further, as mentioned in Section 7.

In a realistic process, the virtuality in a jet degrades as the partons evolve toward hadrons, presumably with an associated change in the value of  $n_f$ .



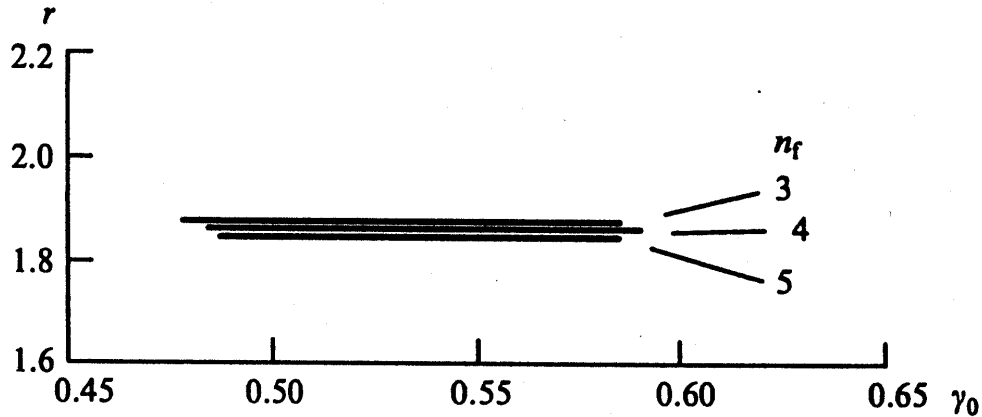


Figure 11:  $r$  versus  $\gamma_0$  in fixed coupling QCD for  $n_f = 3, 4$  and  $5$  [117].

In the framework of the calculations with a fixed coupling strength, the dependence on  $n_f$  can be addressed with the aid of formulas (59) and (75). The dependence on  $n_f$  is found to be very small. Thus, as a jet of partons evolves toward lower  $Q$ , we need not be concerned with a change in the number of active flavors. The parton multiplicity will depend on the evolving virtuality through a mild variation of  $\gamma$ , but not enough to invalidate the fixed coupling approximation. Certainly, in the ratio of the multiplicities, such dependences cancel, yielding a stable result for  $r$ . This conclusion is supported by the perturbative solutions of the equations with the running coupling [93, 98], as has already been discussed (see Table 1).

## 8.2 Widths and higher rank moments of multiplicity distributions in gluon and quark jets

Relations (115) and (116) allow the solution for higher moments of multiplicity to be obtained in the fixed coupling approximation for any rank  $q$ . A system of coupled recurrent equations [36] is obtained by substituting eq. (7) into eqs. (57) and (58) and by comparing the coefficients of  $z^q$  on both sides. These equations can be solved by iteration. The results will not be given here (see [36]). Only the final analytic expressions for the moments of rank  $q$  as they relate to the lower rank moments will be presented. For this purpose,

let us introduce

$$f_q = \frac{F_q}{q!}, \quad \hat{\phi}_q = \frac{\Phi_q}{r^q q!}. \quad (125)$$

The solution of the equations is [36]

$$f_q = [a_q S_q(f, \hat{\phi}) + b_q T_q(f, \hat{\phi})] \Delta_q^{-1}, \quad (126)$$

$$\hat{\phi}_q = [c_q S_q(f, \hat{\phi}) + d_q T_q(f, \hat{\phi})] \Delta_q^{-1}, \quad (127)$$

where

$$S_q = \sum_{l=1}^{q-1} [N_{q,l}^G f_l f_{q-l} + n_f N_{q,l}^F \hat{\phi}_l \hat{\phi}_{q-l}], \quad (128)$$

$$T_q = \sum_{l=1}^{q-1} L_{q,l} \hat{\phi}_l f_{q-l}, \quad (129)$$

$$a_q = \frac{q\gamma}{\gamma_0^2} + L_{0,0} - L_{q,q}, \quad (130)$$

$$b_q = n_f M_q^F, \quad (131)$$

$$c_q = L_{q,0}, \quad (132)$$

$$d_q = \frac{q\gamma}{\gamma_0^2} - M_q^G + n_f N_{0,0}^F, \quad (133)$$

$$\Delta_q = a_q d_q - b_q c_q, \quad (134)$$

$$\begin{aligned} M_q^G &= \psi(1) - \psi(q\gamma + 1) + B(q\gamma, 1) - 2B(q\gamma + 1, 2) \\ &\quad - 2B(q\gamma + 2, 1) + B(q\gamma + 2, 3) + B(q\gamma + 3, 2) + \frac{11}{12}, \\ M_q^F &= \frac{1}{2N_c} [B(q\gamma + 3, 1) + B(q\gamma + 1, 3)], \\ N_{q,l}^G &= B[l\gamma, (q-l)\gamma + 1] - 2B[l\gamma + 1, (q-l)\gamma + 2] \\ &\quad + B[l\gamma + 2, (q-l)\gamma + 3], \\ N_{q,l}^F &= \frac{1}{4N_c} (B[l\gamma + 3, (q-l)\gamma + 1] + B[l\gamma + 1, (q-l)\gamma + 3]), \\ L_{q,l} &= \frac{C_F}{N_c} [B[l\gamma + 1, (q-l)\gamma] - B[l\gamma + 1, (q-l)\gamma + 1] \\ &\quad + \frac{1}{2} B[l\gamma + 1, (q-l)\gamma + 2]]. \end{aligned}$$

The above expressions may seem cumbersome but their structure is simple. They generalize the formulas of the preceding section to any  $q$ . The formulas of gluodynamics are obtained by setting  $n_f=C_F=0$  if one retains, in  $M_q^G$  and  $N_{q,l}^G$ , the leading terms  $B(q\gamma, 1) \equiv 1/q\gamma$  and  $B[l\gamma, (q-l)\gamma + 1]$ , respectively. Using the results for  $\gamma$  and  $r$  from the preceding section at a given value of  $\gamma_0$  and  $n_f$ , one can determine  $F_2$  and  $\Phi_2$ , then increase  $q$  by 1 to determine  $F_3$  and  $\Phi_3$ , etc.

The evolution parameter  $y$  disappears from the formulas. A posteriori, this means that  $F$  scaling, with all dependence on  $y$  hidden in the average multiplicities  $\langle n_{G,F}(y) \rangle$ , is valid for fixed coupling. This leads to a self-consistent system of algebraic equations where all quantities, including  $F_q$  and  $\Phi_q$ , are independent of energy. It should be stressed that  $F$  scaling is only as accurate as the main equations of the fixed coupling approximation. In fact, one should speak about asymptotic  $F$  scaling since the limits of  $x$ -integration in eqs. (57) and (58) are asymptotic.

The results of the calculation, when expressed in terms of  $F_q$  and  $\Phi_q$ , are shown in Fig. 12(a) for  $\gamma_0=0.48$  and  $n_f=5$ . The solutions are seen to increase rapidly with  $q$ , more so for  $\Phi_q$  than for  $F_q$ . Since these are normalized factorial moments, this once again demonstrates that the multiplicity distribution of quark jets is wider than that of gluon jets. The results are insensitive to the value of  $n_f$ . The dependence on the coupling strength is also very mild. Indeed, the results are insensitive to whether the coupling strength is fixed or running. The corresponding results for cumulants are shown in Fig. 12(b).

The ratios of factorial moments to cumulants for gluon and quark jets are defined here as:

$$H_q = \frac{K_q}{F_q}, \quad (135)$$

$$\eta_q = \frac{\Psi_q}{\Phi_q}. \quad (136)$$

The results of the calculations for  $H_q$  and  $\eta_q$  in fixed coupling QCD are presented in Figs. 13 and 14, respectively.

It is of interest to compare the QCD results in Figs. 12-14 to those of the phenomenological models discussed in Section 3. By comparison of Fig. 12 with Figs. 1 and 2, the QCD results are seen to be more similar to the NBD than to fixed multiplicity. In fact,  $F_q$  in Fig. 12(a) can be approximated by the corresponding NBD result with  $k=5$ . While this characterization is

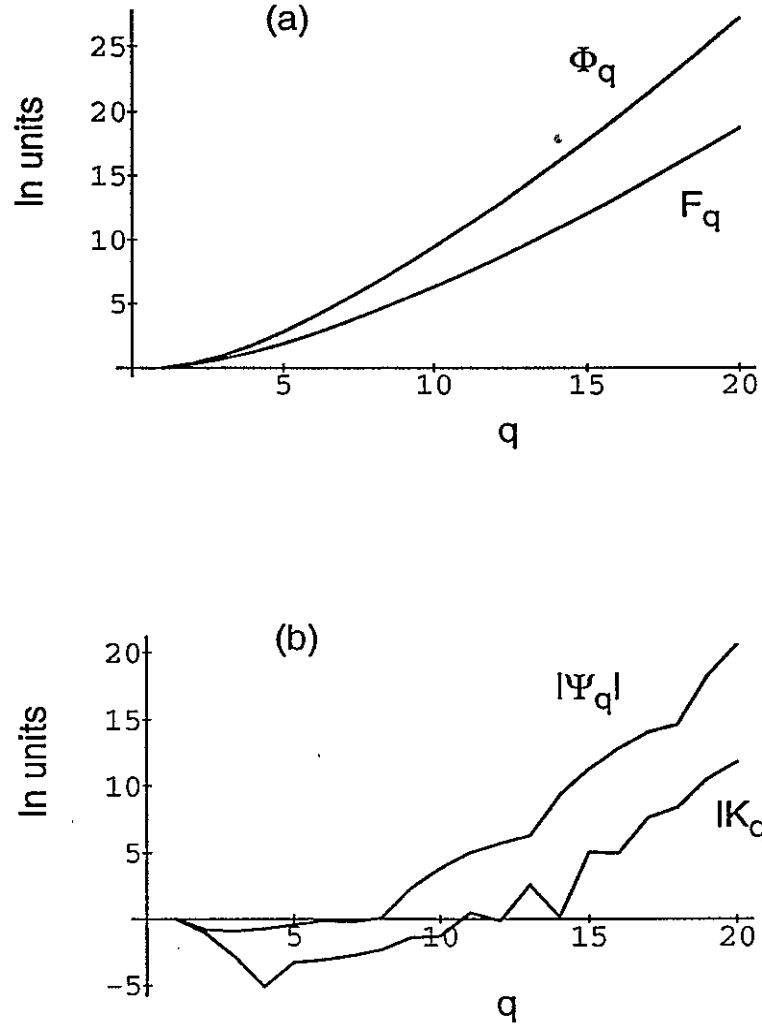


Figure 12: Moments of the multiplicity distribution in fixed coupling QCD for  $\gamma_0=0.48$  and  $n_f=5$  [36]; (a)  $\ln F_q$  and  $\ln \Phi_q$ , (b)  $\ln |K_q|$  and  $\ln |\Psi_q|$ .

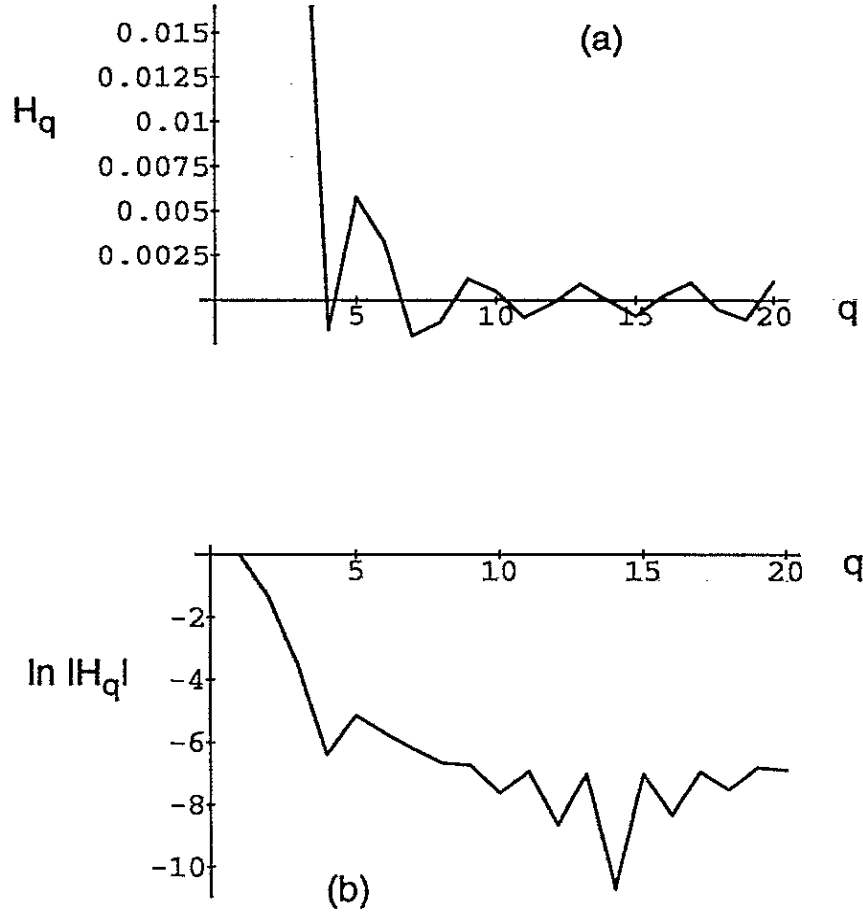


Figure 13: Ratio  $H_q$  of the gluon jet distribution in fixed coupling QCD for  $\gamma_0=0.48$  and  $n_f=5$  [36]; (a)  $H_q$ , (b)  $\ln |H_q|$ .

convenient, fits of higher rank moments by the NBD are not appropriate. For example, the ratio  $H_q$  of the NBD decreases monotonically with  $q$ , as shown in Fig. 1(c). In QCD at present energies, the  $H_q$  moments become negative and then oscillate. These oscillations become even more pronounced if the preasymptotic limits of integration are used. Thus the QCD and NBD predictions for higher moments differ drastically from each other.

The negative binomial distribution fits the second and third moments well and provides a good overall description of experiment. It does not describe features of the data such as the shoulders of the distributions or the oscillations of the  $H_q$  ratios, however. The fixed multiplicity distribution, in contrast to the NBD, *does* yield oscillations. However the  $H_q$  moments change sign at each subsequent integer value of  $q$  in this case, yielding results for the moments and for the period of oscillation in disagreement with experiment (see Section 11.5).

The sensitivity of  $H_q$  to the detailed shape of the multiplicity distribution is clearly demonstrated by its various qualitative forms in the DLA, MLLA, NNLO, and higher order solutions of eqs. (57) and (58). At large ranks the moments behave in radically different manners in these different approximations, as discussed in Section 5.2. Moreover, the behavior of  $H_q$  depends strongly on slight variations of the particular shape of the factorial moments at low values of  $q$ . One can demonstrate how easy it is to obtain oscillations of the fixed multiplicity type imposed on the double-logarithmic behavior from the following exercise. It is known [86, 118] that the large  $q$  behavior of the factorial moments  $F_q$  in the double-logarithmic approximation is (see eq. (66))

$$F_q = \frac{2q\Gamma(q+1)}{C^q}. \quad (137)$$

If one adds a preasymptotic term by replacing the factor  $2q$  by  $2q+1$  in the numerator (which restores the condition  $F_0=1$  but not  $F_1=1$ ), one obtains an additional term in  $H_q$  which imposes oscillations of the fixed multiplicity type on the monotonous decrease of the form  $q^{-2}$ , and the ratio  $H_q$  becomes

$$H_q = \frac{2 + (-1)^{q-1}}{q(2q+1)}, \quad (138)$$

where the second term in the numerator appears because of the newly added preasymptotic term.

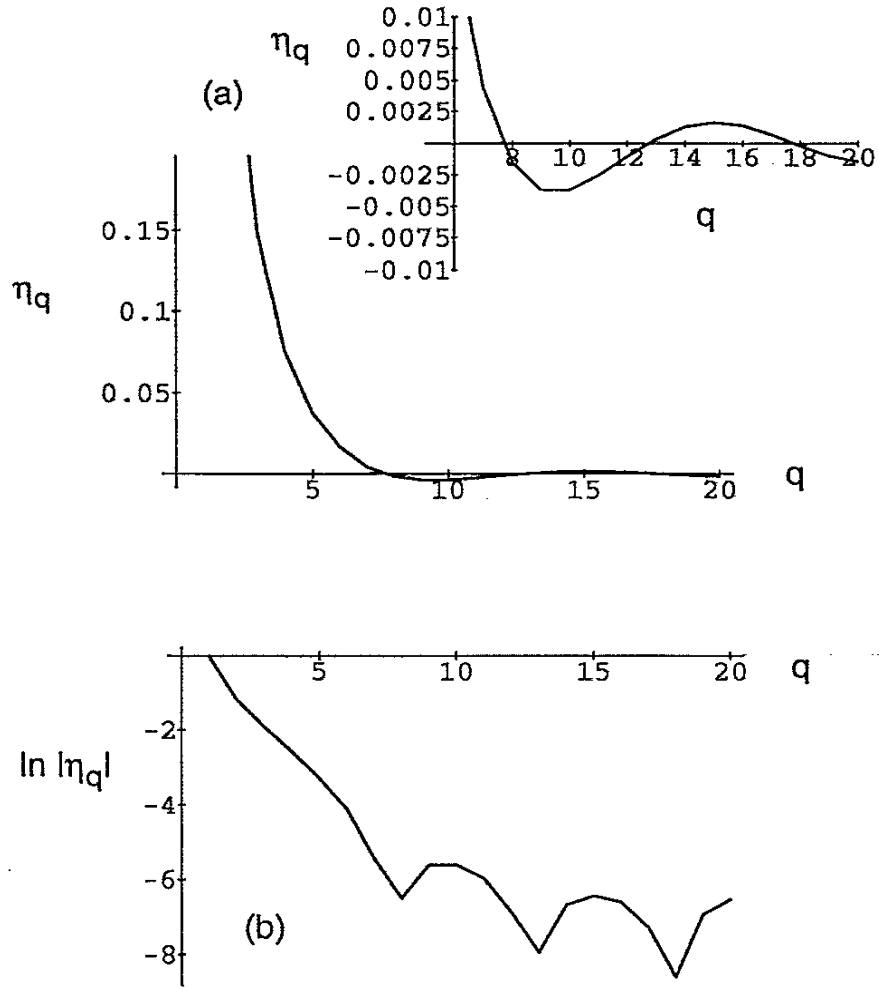


Figure 14: Ratio  $\eta_q$  of the quark jet distribution in fixed coupling QCD for  $\gamma_0=0.48$  and  $n_f=5$  [36]; (a)  $\eta_q$ , (b)  $\ln |\eta_q|$ .

The above examples illustrate the sensitivity of  $H_q$  to the approximations made in solving the set of equations for the generating functions. The different qualitative behavior obtained for different approximations in QCD is illustrated in Figs. 4, 6, 13, and 14, while the difference between QCD and the phenomenological distributions is illustrated by comparing these figures with Figs. 1 and 2. The experimental cutoff of the tail of multiplicity at finite energies induces additional oscillations which have been shown to be rather small [97], as already mentioned in Section 5.2. The numerical solution of equations which incorporate energy conservation both in the generating functions and in the limits of integration yields an extremely good fit of experimental data even for high moments [104] (Section 11.5 and Fig. 10), but also poses some questions about the potential importance of neglected power corrections, as mentioned above.

Unfortunately, there is still no clear understanding of the physical origin of the oscillations, i.e. of their periodicity, amplitude, and dependence on rank  $q$  (it seems that the amplitude increases and the period decreases with increasing  $q$ ). It has been suggested that the oscillations are related to the experimental fact of the shoulder structure of the multiplicity distribution, interpreted as originating from the superposition of jets with different flavors and topologies [53, 119]. However, the insight provided by the solution of fixed coupling QCD suggests otherwise. In QCD, the jet initiated by a single light flavored parton exhibits  $H_q$  oscillations, as long as account is taken of conservation laws. In the NBD framework one needs a superposition of at least two NBDs, interpreted as the contributions of both light- and  $b$ -quark jets, to describe the oscillations [120]. An analysis of the light quark jet data in Ref. [15] demonstrates that the  $H_q$  moments of single light quark jets do oscillate, however, with no admixture of  $b$ -quarks [121]. This supports the QCD prediction but argues against the NBD conjecture.

The fixed coupling solution demonstrates that the running property of the coupling constant is not important for the oscillations. More significant is the vector nature of massless gluons which controls the singularities of the kernels in the QCD equations. This has been demonstrated [122] by comparing the QCD results with those of the  $\lambda\phi_6^3$  theory (i.e. for scalar mesons in six dimensions). This model exhibits asymptotic freedom and contains a non-singular kernel in the evolution equation. There is no minimum at  $q=5$  in this theory. Oscillations appear only at much larger ranks than in QCD. Perhaps the behavior of  $H_q$  will provide some insight into how the equations



for the generating functions can be generalized, including the fine effects of the interaction of “color monsters” [7, 86, 118]. However, this is a difficult problem to solve.

Note that the above oscillations occur for integer values of  $q$  and are not related to oscillations of fractional moments. The latter would impose lower period harmonics on the oscillations from integer ranks.

## 9 Non-perturbative modifications of QCD equations

The non-perturbative aspects of jet evolution are less clear at the moment. They are usually hidden within the hypothesis of local parton-hadron duality or in Monte Carlo hadronization models. The influence of the QCD vacuum condensate on jets cannot be estimated within the perturbative approach. The first proposal to phenomenologically account for its effects within the equations describing QCD jet evolution is given in Refs. [123, 124].

The action of the vacuum condensate on partons in jets was assumed to be similar to the influence of the medium on electron-positron pairs in electromagnetic cascades. As is well known, electromagnetic cascades evolve to a large number of particles, of the order of the ratio of the initial energy to the electron mass, if the ionization processes in the medium are neglected. Because of ionization, low energy electrons stop and exit the cascade. The ionization process is described by a non-scaling term in the evolution equations.

A similar term was added to the QCD equations [123, 124]. Later on, when angular ordering was properly incorporated, it was shown that this non-scaling term could also be included in the equations for the generating functionals [125]. This implies that some energy is spent on the formation of non-perturbative strings, diminishing the number of partons in the cascade. The ratio of partons with and without account of the non-scaling (non-perturbative) term is, in the lowest order approximation [125],

$$\frac{n_{np}}{n_p} = 1 - \gamma_0 \frac{\kappa}{p} - 2\gamma_0^3 \frac{\kappa\Theta}{Q_0}, \quad (139)$$

where  $\kappa$  denotes the typical energy spent for soft non-perturbative interactions, so that  $\kappa/p$  is a small parameter. It is also possible to estimate the

energy distribution of partons in the jet [125] and the behavior of moments of the multiplicity distribution [126]. The most interesting property of eq. (139) is its non-scaling behavior, namely it does not depend on the product  $p\Theta$  (i.e. on  $y$ ), but on  $p$  and  $\Theta$  separately. Also, it depends on the product of the perturbative and non-perturbative scales.

A similar approach is advocated in Refs. [26, 27]. A non-perturbative term is added to the QCD equation for the generating function, and is interpreted as an analogue of an “inactivation process” implying hadronization. This leads to modifications of KNO scaling (see eq. (25)).

A somewhat different approach to the same problem is formulated in Refs. [127, 128] where non-perturbative effects are included in the effective Lagrangian, and a Monte Carlo scheme is developed. The general idea is to construct an effective field theory that embodies both partonic and hadronic degrees of freedom. The effective action is composed of three parts, with quark and gluon fields at small distance scales, an effective low energy Lagrangian with vacuum condensate fields representing hadronic states at large scales, and a term which couples these different degrees of freedom at intermediate scales. The final goal is to describe the transition from the quark-gluon interaction stage to hadrons within a unified scheme of strong interactions.

All such proposals aim at the description of the hadronization stage and, in particular, of the relation between the numbers of partons and final-state hadrons. Unfortunately, it is still necessary to introduce ad hoc phenomenological assumptions to achieve this goal.

## 10 Singularities of the generating functions

To this point, we have considered  $z$  to be a subsidiary variable in the generating function  $G(y, z)$ , which is set to a constant value after calculation of the moments. It is of interest to study the behavior of  $G(y, z)$  in the complex  $z$  plane. This interest stems from the fact that the singularities of the generating function are located close to the point  $z=0$  where the moments are calculated. For example, the singularity of the generating function of the negative binomial distribution is located at  $z=k/\langle n \rangle$ , as mentioned in Section 3.3.2. For  $k=2$  this is just a pole of second order at  $z=2/\langle n \rangle$ , which tends to  $z=0$  at high energies.

In QCD the singularities of the generating function are known in DLA

only (see [7], p. 137). In this approximation, eq. (77) reduces to eq. (65). The leading singularity governing eq. (65) can be written as

$$G(z, y) \propto (z - z_0(y))^{-2} \quad (140)$$

since differentiating  $\ln G$  twice produces a second order pole on the left hand side which must be matched by a singularity of the same order on the right hand side. Since KNO scaling is valid in this approximation, the factorial moments do not depend on  $y$  asymptotically, and the generating function depends on the product of  $z$  and  $\langle n \rangle$ . The singularity is located at

$$z_0^{DLA} \approx \frac{C}{\langle n \rangle}, \quad C \approx 2.552, \quad (141)$$

i.e. close to the singularity of the negative binomial distribution with  $k=2$ , as it should be. This singularity tends to  $z=0$  at high multiplicities as for the NBD.

The overall structure of the singularities is more complicated in DLA QCD than for the NBD, however, because there are poles of second and first orders, logarithmic branch points, etc. A more complete DLA result for  $G(z, y)$  near the singularity is

$$G(z, y) = \frac{2z_0^2}{(z - z_0)^2} + \frac{2z_0}{z - z_0} - \frac{2}{3} \ln \frac{z_0 - z}{z_0} + \mathcal{O}(1). \quad (142)$$

In a certain sense this result is not very helpful since the DLA is a rather crude approximation to reality at present energies. This result shows, however, that  $z=0$  is still quite far from the singularity since the pole contributions cancel at this point. There is no cancelation in the derivatives of  $G$ , however, which increase like factorials because of the leading singularity. It is not yet known how this structure is modified by higher orders. Attempts to go beyond DLA are connected with the Taylor series expansion of  $G$  discussed above. Then eq. (65) acquires additional terms on the right hand side proportional to derivatives of  $G(z, y)$ . Each derivative exhibits a stronger singularity than  $G$  itself. Therefore such an approach cannot be applied near the singular points. This also demonstrates why the DLA has difficulties in practice. However, attempts to employ eq. (77) rather than eq. (65) have not yet been done explicitly.

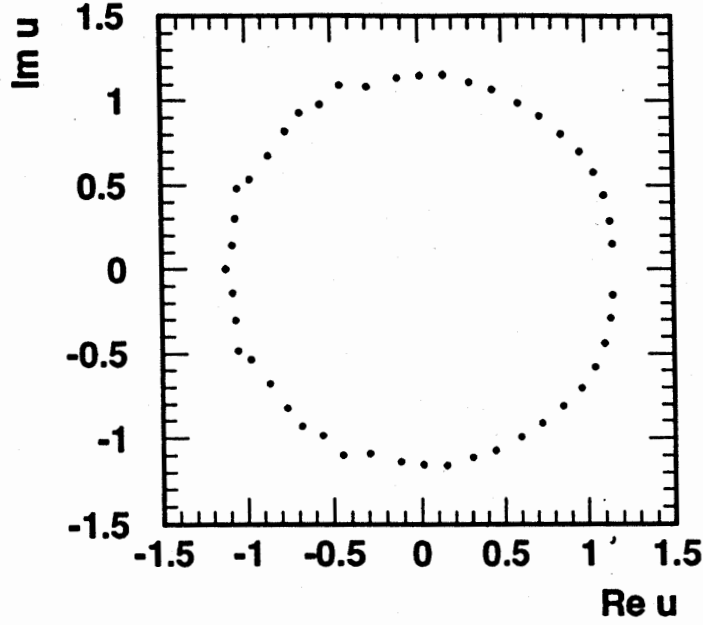


Figure 15: Complex zeros of the charged particle multiplicity distribution, obtained [133] from  $e^+e^-$  Monte Carlo events at  $E_{\text{c.m.}}=1$  TeV, where  $u \equiv z+1$ .

In experiment, only the so-called truncated generating function has been determined

$$G^{\text{tr}}(y, z) = \sum_{n=0}^{n_{\text{max}}} P_n (1+z)^n, \quad (143)$$

where the sum extends up to the maximum multiplicity  $n_{\text{max}}$  available at the energy scale  $y$ . Therefore the truncated generating function is a polynomial in  $z$  and has no singularity at finite  $|z|$ . It possesses  $n_{\text{max}}$  complex conjugated zeros. When  $n_{\text{max}}$  tends to infinity these zeros should converge to the singularity location of  $G(y, z)$ . The properties of zeros (the rate of convergence, etc.) can be used [129] to obtain some knowledge about the singularities of the generating function.

The problem becomes even more intriguing if an analogy with statistical mechanics is invoked (see, e.g. [16, 130]). In this case  $z$  is interpreted as

fugacity, and  $G(y, z)$  and  $G^{tr}(y, z)$  play the roles of the canonical and grand canonical partition functions, respectively. Therefore their properties in the complex  $z$ -plane can be considered to reflect the statistical properties of multiparticle production. In statistical mechanics the motion of zeros to the real  $z$  axis, “pinching it” asymptotically, implies a phase transition [131, 132]. Experiment indicates that such a pinch occurs as the energy increases, for various reactions initiated by particles and nuclei. The zeros tend to lie close to a circle of unit radius in the complex  $z$  plane, as is illustrated in Fig. 15 using  $e^+e^-$  annihilation Monte Carlo events generated at a cms energy of 1 TeV [133]. Similar results have been obtained using simulations of nucleus-nucleus collisions generated according to the dual parton model [134]. Moreover, the quantity analogous to the free energy exhibits its maximum in QCD [94]. This fact is closely related to the minimum of the  $H_q$  ratios at  $q \approx 5$  discussed above. The interpretation in terms of a phase transition is the same here.

Nonetheless, we cannot rely too much on the analogy with statistical mechanics to obtain physics conclusions. The properties of the zeros discussed above have been shown [135] in purely mathematical terms to be a consequence of the falloff of the multiplicity distribution at large  $n$  and its flattening with increasing energy. This behavior forces all zeros to the unit circle in the complex  $z$ -plane, centered at  $z=-1$ , with the point  $z=0$  removed. Experiment favors these tendencies. The physics implications of this behavior are therefore not entirely clear.

## 11 Measurements of mean multiplicity, slopes, and higher moments

We now explicitly turn our attention to experimental results. In this, we concentrate on data which test the QCD predictions discussed in Sections 5-8. We emphasize data from  $e^+e^-$  annihilations. The relative simplicity of hadronic events from  $e^+e^-$  collisions allows a level of precision and conclusiveness difficult to achieve in other types of reactions. For example, ep and pp collisions are characterized by initial-state strong interactions and final-state remnants from the colliding hadrons. These features – absent in  $e^+e^-$  events and the calculations – make a comparison to theory uncertain. The

comparison between experiment and theory is yet more uncertain for nuclear collisions. The available measurements of average multiplicities in ep, pp and  $p\bar{p}$  collisions are compiled in Ref. [80].

To test the predictions in a meaningful manner, the experimental definition of jets should match the theoretical one. The theoretical definition of jets is based on the production of a virtual quark-antiquark  $q\bar{q}$  pair (for quark jets) or gluon-gluon  $gg$  pair (for gluon jets) from a color singlet point source. The inclusive multiplicity of these  $q\bar{q}$  or  $gg$  events defines the multiplicity of “two-jet events.” A single quark or gluon jet corresponds to a hemisphere in these events. Thus there is no selection of a specific event topology, i.e. jets are not selected using a mathematical algorithm such as the  $k_{\perp}$  [136, 137] or JADE [138] jet finders, in contrast to common experimental practice. Jets defined according to the inclusive theoretical prescription are called “unbiased.”

It has proven difficult to measure gluon jet multiplicity in an unbiased manner because  $gg$  production from a color singlet point source is a process which is practically unobserved in nature. This difficulty impeded experimental progress in the field for many years. One channel where the experimental selection criteria match the theoretical definition is the decays of  $b\bar{b}$  bound states to  $\gamma gg$ : events like this have been studied through the selection of  $\Upsilon \rightarrow \gamma gg \rightarrow \gamma + \text{hadrons}$  events. Another possibility is rare  $e^+e^-$  hadronic annihilation events in which the quark jets  $q$  and  $\bar{q}$  from the electroweak decay of the intermediate  $Z^0$  or virtual  $\gamma$  are approximately collinear: the gluon jet hemisphere against which the  $q$  and  $\bar{q}$  recoil in these events corresponds to a nearly unbiased gluon jet [139, 140]. The two photon process  $e^+e^- \rightarrow e^+e^- gg \rightarrow e^+e^- + \text{hadrons}$  has also been suggested as a source for high energy unbiased gluon jets [141]: this possibility has yet to be explored experimentally, however.

In contrast to gluon jets, it is easy to measure quark jet multiplicity in an unbiased manner, using the charged particle multiplicity in hemispheres of  $e^+e^- \rightarrow \text{hadrons}$  events.  $e^+e^-$  hadronic annihilations therefore provide a natural source for quark jets, studied by many experiments.

For the results discussed here, the data have been corrected for detector response and initial-state photon radiation, treating all charged and neutral particles with lifetimes greater than  $3 \times 10^{-10}$  s as stable. Hence charged particles from the decays of  $K_S^0$  and weakly decaying hyperons are included in the definition of multiplicity.

Before proceeding to the main results, presented in Sections 11.1-11.6, it is of interest to recount the original experimental efforts to measure gluon jet multiplicity, and in particular the multiplicity ratio  $r = \langle n_G \rangle / \langle n_F \rangle$  (see also Ref. [140]). The JADE Collaboration selected three-jet  $q\bar{q}g$  events in  $e^+e^-$  annihilations [142]. The gluon jet was identified by assuming it had the lowest energy of the three jets in an event. Quark jets were the higher energy jets in the same events. The UA2 Collaboration studied gluon jets produced in two-jet  $gg$  final states from  $p\bar{p}$  collisions [143]. These gluon jets were compared to lower energy quark jet data from an  $e^+e^-$  experiment [144]. For both studies, qualitative indications were reported that the gluon jet multiplicity was slightly larger. The interpretation of these results was unclear, however, since the gluon and quark jets were not identified using the same criteria in either study.

The HRS Collaboration chose a different strategy, selecting three-fold symmetric  $e^+e^- \rightarrow q\bar{q}g$  events in which the quark and gluon jets were produced with about the same energies and inter-jet angles [145]. Thus in this case the gluon and quark jet identification criteria were equivalent. The probability that the gluon jet had a larger multiplicity was tested by assuming a Poissonian multiplicity distribution and independent production of each of the three jets. A value  $r = 1.29^{+0.29}_{-0.46}$  was derived, the first quoted result for  $r$ . Although the largeness of the uncertainty precluded any definite interpretation, this result was considered at the time to indicate that  $r$  was much smaller than the naïve expectation  $r \approx 2$  (see Section 11.6). The DELPHI Collaboration later applied a similar analysis technique to a much larger data sample and obtained  $r \approx 1$  [115], however, thus demonstrating that the method was not sensitive to gluon and quark jet differences.

The OPAL Collaboration selected quark and gluon jets in one-fold symmetric  $q\bar{q}g$   $e^+e^-$  events in which the angle between the highest energy jet and each of the two lower energy jets was the same, namely  $150^\circ$  [146]. These events later became known as “Y events” since they are shaped like the letter Y. This analysis utilized b-quark tagging to identify a high purity sample of gluon jets which were then compared to a sample of about 50% quark and 50% gluon jets selected using the same criteria. The result  $r = 1.27 \pm 0.07$  was derived from these data, the first positive observation of a larger multiplicity in gluon jets compared to quark jets. This result was later confirmed by other studies [147, 148]. Although the results of this analysis represented a considerable success, establishing a value of  $r$  significantly larger than unity

Experiment	$Q$ (GeV)	$\langle n_{\text{ch.}} \rangle$ , gg events
CLEO [114]	4.5	$4.88 \pm 0.10$
CLEO [114]	5.5	$5.28 \pm 0.10$
CLEO [114]	6.5	$5.65 \pm 0.12$
CLEO [150]	10.3	$9.339 \pm 0.090 \pm 0.045$
OPAL [113]	80.2	$28.56 \pm 0.36 \pm 0.62$

Table 4: The mean charged particle multiplicity,  $\langle n_{\text{ch.}} \rangle$ , of unbiased “two-jet” gg events. For the OPAL data and the CLEO measurement at 10.3 GeV, the first uncertainty is statistical and the second is systematic. For the CLEO measurements below 10 GeV, only the statistical uncertainty is given.

for the first time, the results were found to depend strongly on the jet finding algorithm used to select the events, see Refs. [147, 149]. Since the jets were defined using a jet finder rather than employing a hemisphere definition, they could not be used for a quantitative test of the analytic results presented in Sections 5-8, unlike the unbiased gluon jet measurements discussed below.

### 11.1 Mean multiplicity

Experimental measurements of the inclusive charged particle multiplicity of unbiased gluon jets as a function of energy scale  $Q$  are shown in Fig. 16. The three data points at scale  $Q \approx 5$  GeV are derived from the hadronic component of  $\Upsilon(1S) \rightarrow \gamma gg$  events [114]. The virtuality  $Q$  is given by the invariant mass of the hadronic system. Similarly,  $\Upsilon(3S) \rightarrow \gamma \chi_{b2}(10.27) \rightarrow \gamma gg$  events provide the result at  $Q \approx 10$  GeV [150], with the scale given by the  $\chi_{b2}$  mass. The measurement at  $Q \approx 80$  GeV [112, 113] is based on hadronic  $Z^0$  decays:  $Z^0 \rightarrow q\bar{q}g_{\text{incl.}}$ , in which  $g_{\text{incl.}}$  refers to a gluon jet hemisphere recoiling against two almost collinear quark jets  $q$  and  $\bar{q}$  in the opposite hemisphere. For the results shown here, the  $g_{\text{incl.}}$  hemisphere results in Ref. [113] have been multiplied by a factor of two both for the multiplicity and energy scales so that they correspond to gg “two-jet events” analogous to the  $\Upsilon$  data. Although many studies of gluon jet multiplicity have been performed, only the data in Fig. 16 are based on an unbiased definition of the jets. These data are summarized in Table 4.

The solid curve in Fig. 16 shows the result of a  $\chi^2$  fit of the 3NLO expres-



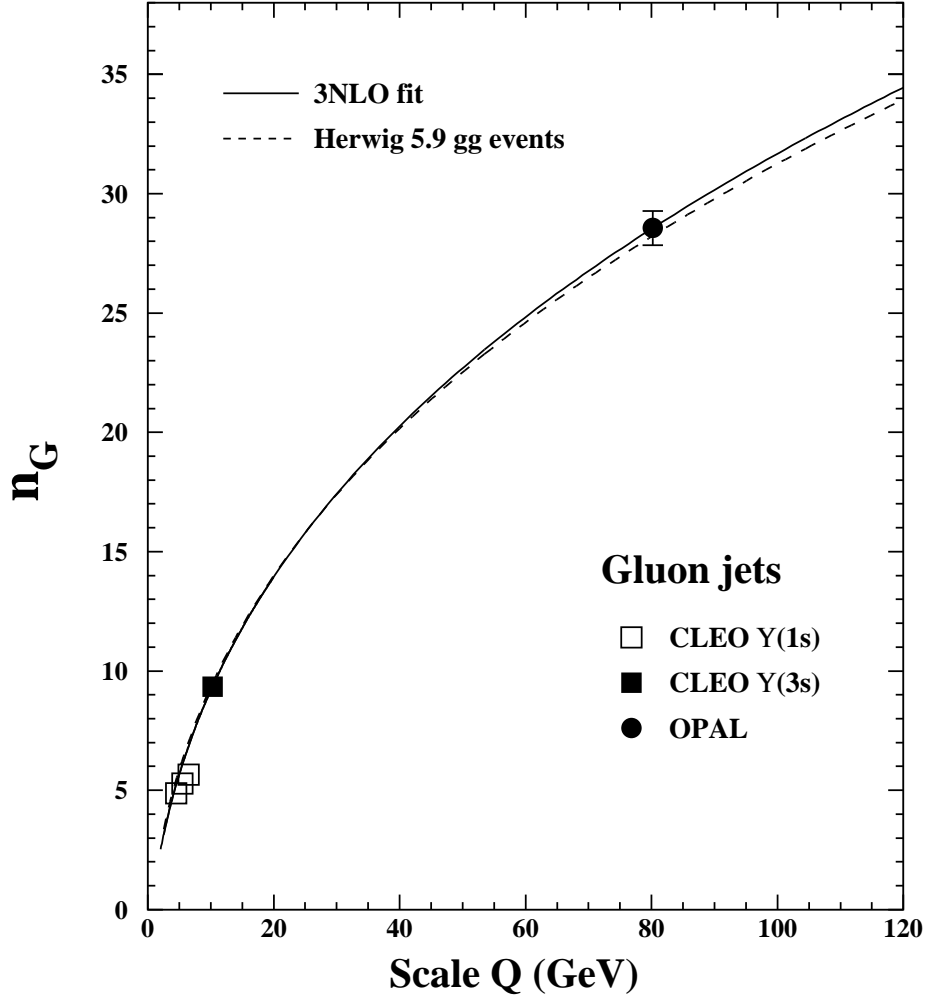


Figure 16: The mean charged particle multiplicity of gg events from a color singlet point source versus energy scale  $Q$ . The solid curve shows a fit of the 3NLO expression, eq. (94), to the data, using  $n_f=3$ , where  $n_f$  is the number of active quark flavors. The dashed curve shows the prediction of the HERWIG Monte Carlo for the mean charged particle multiplicity in gg events.

sion for gluon jet multiplicity, eq. (94), to the data, with  $y=\ln(Q/\Lambda)$ , where  $\Lambda$  is a fitted parameter related to the perturbative cutoff  $Q_0$  by  $\Lambda=Q_0/2$  (see Section 4). The other fitted parameter is the normalization constant  $K$  in eq. (94). For this fit,  $n_f=3$ . The  $\Upsilon(1S)$  measurements [114] are not included in the fit because a systematic uncertainty was not provided for them: the smallness of the statistical uncertainty for these data would unduly bias the fit results. Nonetheless, these data are seen to lie near the fitted curve. The results for the fitted parameters, along with those found using  $n_f=4$  and 5, are given in the top portion of Table 5. The results of the fits with  $n_f=4$  and 5 are virtually indistinguishable from that shown by the solid curve in Fig. 16. The uncertainties given in Table 5 for the gluon jet parameters are defined by the maximum deviations observed when the gluon jet measurements are varied by their one standard deviation uncertainties.

From Fig. 16 and the results in Table 5 it is seen that the 3NLO expression provides a good description of the growth of gluon jet multiplicity with energy using a physically sensible value of the coupling strength, corresponding to a value of  $\Lambda$  in the range from about 100 MeV to 1 GeV. For example the fitted result  $\Lambda = 0.64 \pm 0.17$  GeV obtained for  $n_f = 5$  yields  $\alpha_S(M_Z) = 0.142 \pm 0.008$ , compared to the world average value based on  $\Lambda_{\overline{MS}}$  of  $\alpha_S(M_Z) \approx 0.120 \pm 0.002$  [80]. We remind the reader that  $\Lambda$  is not in general the same as  $\Lambda_{\overline{MS}}$ .

Experimental measurements of unbiased quark jet multiplicity are shown in Fig. 17. These data are the inclusive charged particle multiplicity values of  $e^+e^-$  hadronic annihilation events, corresponding to “two-jet events” as for the data of Fig. 16. The scale is  $Q=E_{c.m.}$ . The results shown for the LEP experiments are combined values of ALEPH, DELPHI, L3 and OPAL. The combined values are obtained using the unconstrained averaging procedure described in [80], for which a common systematic uncertainty is defined by the unweighted mean of the systematic uncertainties quoted by the experiments. LEP-1 refers to data collected at the  $Z^0$  peak, LEP-1.5 to data collected at  $E_{c.m.} \approx 133$  GeV, and LEP-2 to data collected at or above the threshold for  $W^+W^-$  production. The quark jet data are summarized in Table 6.

The vertically striped band in Fig. 17 shows the 3NLO prediction for quark jet multiplicity, eq. (104), for  $n_f=3$ , using the values of  $\Lambda$  and  $K$  found from the fit to the gluon jet measurements (top portion of Table 5). The width of the band corresponds to the uncertainty in the value of  $\Lambda$  presented in the top portion of Table 5. Almost identical results to those shown by the band are obtained using  $n_f=4$  or 5. The band lies 15-20% below the

	$\Lambda$ (GeV)	$K$	$\chi^2/\text{bins of data}$
(a) Gluon jets, eq. (94)			
$n_f=3$	$1.03 \pm 0.24$	$0.288 \pm 0.037$	0.01/2
$n_f=4$	$0.84 \pm 0.21$	$0.244 \pm 0.034$	0.01/2
$n_f=5$	$0.64 \pm 0.17$	$0.205 \pm 0.031$	0.01/2
(b) Quark jets, eq. (104), $K=\text{fixed}$			
$n_f=3$	$0.670 \pm 0.036$	0.288	26.3/18
$n_f=4$	$0.579 \pm 0.034$	0.244	31.3/18
$n_f=5$	$0.469 \pm 0.031$	0.205	38.6/18
(c) Quark jets, eq. (104)			
$n_f=3$	$0.262 \pm 0.072$	$0.198 \pm 0.022$	6.6/18
$n_f=4$	$0.188 \pm 0.063$	$0.156 \pm 0.020$	6.8/18
$n_f=5$	$0.119 \pm 0.048$	$0.118 \pm 0.018$	7.1/18

Table 5: Results of a fit of QCD expressions for the scale evolution of event multiplicity to the measured mean charged particle multiplicities of unbiased (a) gg (top), and (b) and (c)  $q\bar{q}$  (center and bottom) events. For the gluon jets, the fitted expression is the 3NLO result, eq. (94). For the quark jets, the expression is the 3NLO result, eq. (104). In (b) the normalization  $K$  is set equal to the value found from the gluon jet fit; a one parameter fit of the scale parameter  $\Lambda$  is performed. In (c) a two parameter fit of  $\Lambda$  and  $K$  is performed. For the quark jets, the uncertainties are evaluated by varying the fit range as described in the text.

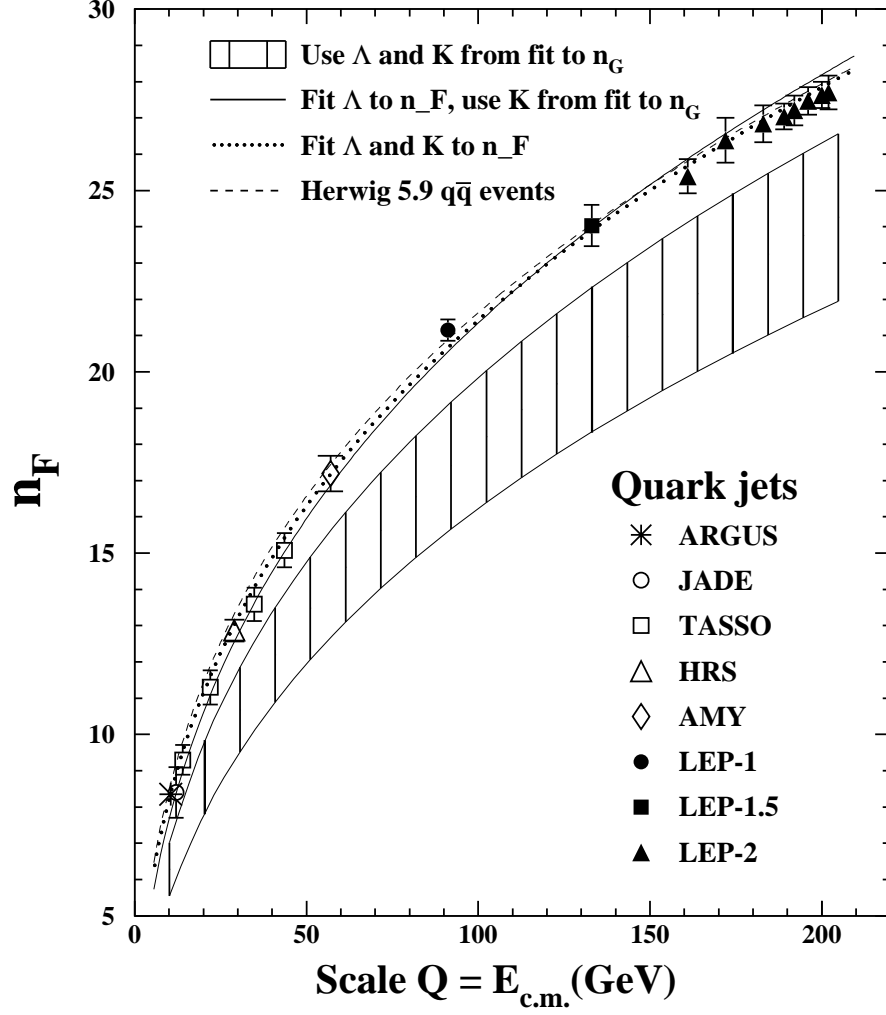


Figure 17: The mean charged particle multiplicity of  $e^+e^-$  hadronic annihilation events versus energy scale  $Q=E_{c.m.}$ . The solid curve shows a fit of the 3NLO expression, eq. (104), to the data, using a one parameter fit of  $\Lambda$  (see text). The dotted curve shows the corresponding result from a two parameter fit of  $\Lambda$  and  $K$ . The hatched band shows the 3NLO result if the parameter values used in the fit of gluon jet multiplicity are used. The width of the band corresponds to the uncertainty in the value of  $\Lambda$ . For the analytic curves,  $n_f=3$ . The dashed curve shows the prediction of the HERWIG Monte Carlo for the mean charged particle multiplicity in  $e^+e^- \rightarrow q\bar{q}$  events.

Experiment	$Q=E_{\text{c.m.}}$ (GeV)	$\langle n_{\text{ch.}} \rangle$
ARGUS [151]	10.5	$8.35 \pm 0.02 \pm 0.20$
JADE [152]	12.0	$8.4 \pm 0.3 \pm 0.6$
TASSO [153]	14.0	$9.30 \pm 0.06 \pm 0.41$
TASSO [153]	22.0	$11.3 \pm 0.08 \pm 0.46$
HRS [154]	29.0	$12.87 \pm 0.03 \pm 0.30$
TASSO [153]	34.8	$13.59 \pm 0.02 \pm 0.46$
TASSO [153]	43.6	$15.08 \pm 0.06 \pm 0.47$
AMY [155]	57.0	$17.19 \pm 0.07 \pm 0.48$
LEP-1 [156]	91.2	$21.15 \pm 0.01 \pm 0.29$
LEP-1.5 [157, 158]	133	$24.03 \pm 0.20 \pm 0.53$
LEP-2 [157, 159, 160]	161	$25.39 \pm 0.23 \pm 0.41$
LEP-2 [157, 159, 161]	172	$26.38 \pm 0.26 \pm 0.56$
LEP-2 [157, 162, 161]	183	$26.84 \pm 0.16 \pm 0.48$
LEP-2 [163, 164, 161]	189	$27.04 \pm 0.11 \pm 0.34$
LEP-2 [165, 164, 166]	192	$27.21 \pm 0.25 \pm 0.32$
LEP-2 [165, 164, 166]	196	$27.47 \pm 0.18 \pm 0.33$
LEP-2 [165, 164, 166]	200	$27.63 \pm 0.17 \pm 0.32$
LEP-2 [165, 164, 166]	202	$27.70 \pm 0.25 \pm 0.38$

Table 6: The mean charged particle multiplicity,  $\langle n_{\text{ch.}} \rangle$ , measured in  $e^+e^-$  annihilations at various c.m. energies. The first uncertainty is statistical and the second is systematic. A more complete compilation for energies below 91 GeV is given in [167]. The results shown for LEP are combined values from ALEPH, DELPHI, L3 and OPAL (see text).

data, representing an inadequacy of the 3NLO calculations to simultaneously describe the gluon and quark jet measurements using precisely the same values of  $\Lambda$  and  $K$ . This problem can mostly be attributed to the analytic prediction for the multiplicity ratio  $r$ , discussed below in Section 11.2.

It is also of interest to *fit* expression (104) to the quark jet data. For this, we use the normalization  $K$  found in the fit of the gluon jet multiplicity (compare eqs. (94) and (104)) and perform a one parameter fit of  $\Lambda$  to the quark jet data using  $n_f=3$ . The result is shown by the solid curve in Fig. 17. The results found using  $n_f=4$  or 5 are almost identical to that shown by

this curve. The fit is seen to provide a reasonable overall description of the measurements. The fitted values of  $\Lambda$  for  $n_f=3, 4$  and  $5$  are given in the central portion of Table 5. The uncertainties of the quark jet parameters in Table 5 are defined by the maximum difference between the results of the standard fit and those found by fitting only data between 29 and 202 GeV, between 10.5 and 161 GeV, or by excluding the LEP-1 data point.

Comparing the parameter values obtained from the fits to the unbiased gluon and quark jet measurements (top and central portions of Table 5), it is seen that the value of  $\Lambda$  from gluon jets is about 40% larger than that from quark jets. For  $n_f=5$ , the quark jet result  $\Lambda=0.469 \pm 0.031$  GeV yields  $\alpha_S(M_Z)=0.135 \pm 0.002$ , to be compared to  $\alpha_S \approx 0.14 \pm 0.01$  found from the gluon jet data as mentioned above. Thus although the gluon and quark jet data are not well described using exactly the same values of  $\Lambda$  and  $K$ , they both yield physically acceptable results for  $\Lambda$ , leading to similar values of the coupling strength. In this sense, the analytic description of multiplicity in single gluon and quark jets is quite consistent.

For completeness, we include in Fig. 17 the result of a two parameter fit of  $\Lambda$  and  $K$  to the quark jet data, using  $n_f=3$ . The result of this fit is shown by the dotted curve in Fig. 17. The corresponding parameter values are given in the bottom portion of Table 5, with systematic uncertainties defined as for the quark jet parameters in the central portion of that table. The results for  $\Lambda$  are seen to be about 3 times smaller than if the normalization factor  $K$  is required to be the same for quark and gluon jets as described above. For  $n_f=5$ , the quark jet result  $\Lambda=0.119 \pm 0.048$  GeV yields  $\alpha_S(M_Z)=0.109 \pm 0.005$ .

The dashed curves in Figs. 16 and 17 show the prediction of the HERWIG Monte Carlo [70] for the mean inclusive charged particle multiplicity of  $gg$  and  $e^+e^-$  annihilation events, respectively. The prediction of HERWIG is generally similar to the fitted analytic results.

## 11.2 Multiplicity ratio

A test of the QCD prediction for the ratio  $r$  of mean multiplicities between gluon and quark jets is possible using the data in Table 4. Such a test is in principle limited to these data since they are the only unbiased measurements of gluon jet multiplicity currently available. See also Refs. [98, 168], however, where results for  $r$  based on gluon jets from  $e^+e^-$  three-jet events are also discussed.

Experiment	$Q$ (GeV)	$E_{\text{jet}}$ (GeV)	$r$
CLEO [114]	5.5	2.75	$1.04 \pm 0.02 \pm 0.04$
CLEO [150], ARGUS [151]	10.3	5.15	$1.118 \pm 0.011 \pm 0.032$
OPAL [113]	80.2	40.1	$1.514 \pm 0.019 \pm 0.034$

Table 7: Measurements of the multiplicity ratio  $r$  between unbiased gluon and quark jets. The first uncertainty is statistical and the second is systematic.

To obtain a result for  $r$  from their measurements of gluon jet multiplicity in  $\Upsilon(1S)$  decays, CLEO [114] divided the gluon jet multiplicity given in the top three rows of Table 4 by the charged particle multiplicity in radiative  $q\bar{q}\gamma$  events with similar hadronic recoil mass values. The three  $\Upsilon(1S)$ -based data points are shown with their statistical uncertainties at  $y_c \approx 0.01$  in Fig. 9. CLEO combined the three data points into a single value at an effective scale of about 5.5 GeV [114]. The resulting value for  $r$  is given in the top row of Table 7.

OPAL [113] divided their result for the multiplicity in gluon jet hemispheres at 40 GeV by the multiplicity in hemispheres of light quark (uds flavored) events with about the same energy. The reason for selecting light quark jets is that it provides closer correspondence with the massless quark assumption of the calculations. The OPAL result for  $r$  is shown at  $y_c \approx 3 \times 10^{-5}$  in Fig. 9 and is listed in the bottom row of Table 7.

CLEO did not report a result for  $r$  based on their measurement [150] of gluon jet multiplicity in  $\Upsilon(3S)$  decays. The effective scale of this result, 10.3 GeV, is not too different from the scale of the lowest energy quark jet result in Table 6, however, viz. 10.5 GeV. Dividing the 10.3 GeV gluon jet result from CLEO by the 10.5 GeV quark jet result from ARGUS yields the result for  $r$  given in the central row of Table 7.

The experimental results for  $r$  are shown in Fig. 18. The results are presented as a function of the jet energy  $E_{\text{jet}}$  rather than the “two-jet event” scale  $Q$  to correspond to the analytic results. Fig. 18 includes the QCD analytic predictions for  $r$  at various orders of perturbation theory. The data are seen to lie substantially below the predictions (Section 6.1). The theoretical predictions approach the experimental results more closely, however, as higher order terms are included. At the scale of the  $Z^0$ , the 3NLO expression,

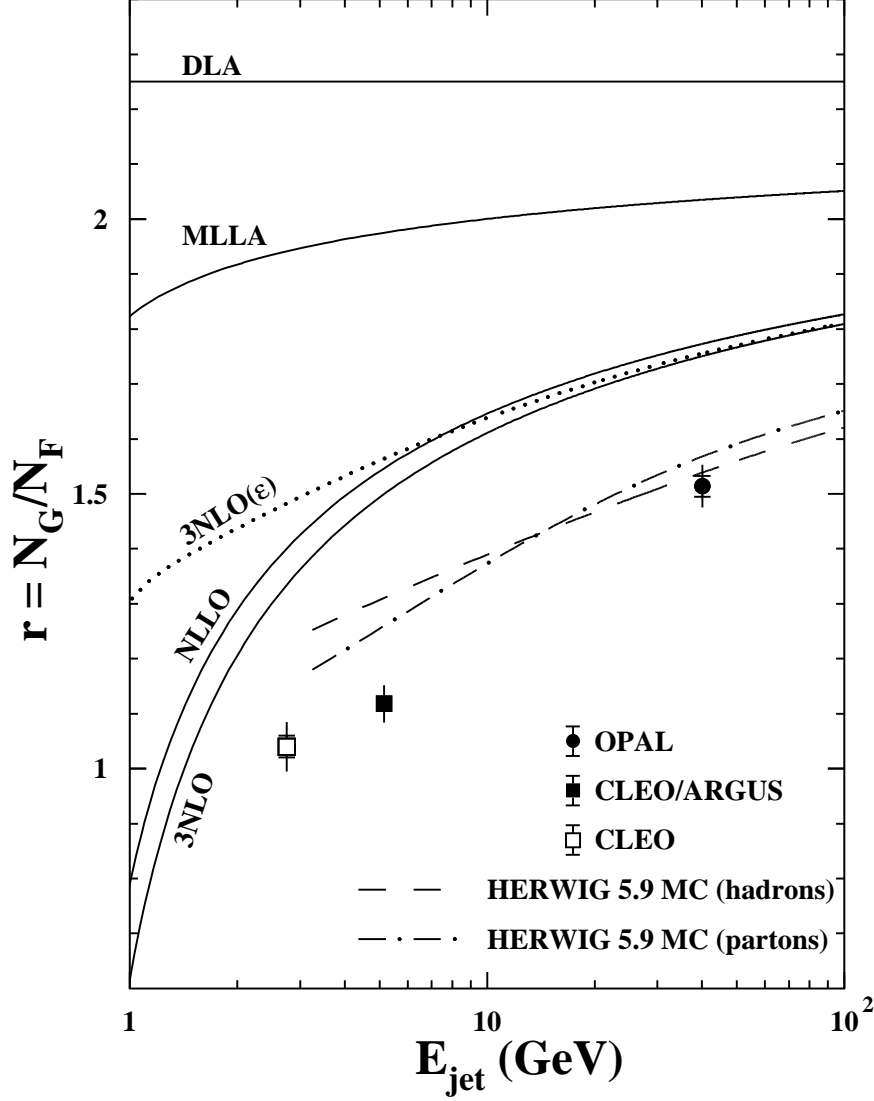


Figure 18: Experimental results for the multiplicity ratio of unbiased gluon and quark jets, in comparison to QCD analytic predictions. The curve marked  $3\text{NLO}(\epsilon)$  shows the analytic prediction at order 3NLO with an approximate accounting for truncation of the limits of integration at  $e^{-y}$  and  $1 - e^{-y}$ , see Ref. [98]. The dashed and dash-dotted curves show the prediction of the HERWIG Monte Carlo at the hadron and parton levels. The experimental and HERWIG results at the hadron level are based on charged particles only.



eq. (93), predicts  $r \approx 1.7$ , about 13% larger than the OPAL result  $r_{exp.} \approx 1.51$ . At the scale of the  $\Upsilon$ , the difference between theory and data is larger. It is likely that uncalculated non-perturbative terms play an important role at this low scale, however. By itself, it is perhaps surprising to obtain any level of agreement between theory and data at all given the large value of the expansion parameter  $\gamma_0 \approx 0.5$ .

The dashed and dash-dotted curves in Fig. 18 show the predictions of the HERWIG Monte Carlo for the ratio  $r$  at the hadron and parton levels. The HERWIG prediction is obtained by dividing the results for hemispheres of gg events by those for light quark  $q\bar{q}$  events. The HERWIG results at the hadron level are based on charged particles only. HERWIG is seen to represent the OPAL measurement quite well at both the hadron and parton levels, implying a modest correction for hadronization at the  $Z^0$  energy.

The computer solution of the QCD equations, discussed in Section 7, leads to near perfect agreement with the OPAL result for  $r$ , as shown in Fig. 9. The computer solution differs from the analytic estimates by use of the explicit multiplicities in the integrals, with no Taylor series expansion, leading to a more accurate accounting of energy conservation, as mentioned in Section 7. This fact becomes especially important for higher order terms because of the large value of  $\gamma_0$ . The computer solution also implements the exact preasymptotic limits of integration, in contrast to the analytic solutions, as was also mentioned in Section 7. This agreement between the experimental and theoretical (computer) results for  $r$  at the scale of the  $Z^0$  is an impressive success for the QCD approach to multiplicity in jets.

In contrast to the result at the scale of the  $Z^0$ , the computer prediction for  $r$  at the scale of the  $\Upsilon$  exceeds the data by about 25% (see Fig. 9). For such low scales, neglected non-perturbative effects are likely to be important, as noted above.

Recently, results on the charged particle multiplicity of jets in dijet events produced in  $p\bar{p}$  collisions have been reported by CDF Collaboration [169]. The dijet masses range from 80 to 630 GeV. This substantially increases the range of accessible jet energies compared with  $e^+e^-$  collisions. The multiplicity ratio  $r$  has been estimated to be  $1.7 \pm 0.3$  from these data. It should be noted that this result is obtained using a fit of an MLLA expression to the data. Since in MLLA quark and gluon jets differ only by the constant factor  $r=9/4$ , it is unclear how the experimental result  $r \approx 1.7$  should be interpreted. Also, the large uncertainty precludes a precise differentiation

between the different theoretical predictions in this region.

### 11.3 Slopes

According to eq. (93), the ratio  $r$  becomes smaller as the scale decreases since  $\gamma_0$  increases. The same trend is observed experimentally (see Fig. 9 or 18). Thus the data and theory are in qualitative agreement. From Figs. 9 and 18 it is seen that the theoretical predictions decrease with scale more slowly than the data, however. For example, the computer solution for  $r$  [78] agrees perfectly with the data at the scale of the  $Z^0$ , but it exceeds the experimental result by about 25% at the scale of the  $\Upsilon$  (Fig. 9), as discussed in Section 11.2. Thus there is a significant difference between the theoretical and experimental results for the slope  $r'$  (see eq. (95)), at least for energies below the  $Z^0$ . From Fig. 2 in [78], the slope predicted by the computer solution can be estimated to be about 0.096 at the  $Z^0$ . Using the data in Fig. 9, the corresponding result is about 0.174. Both these values differ from the analytic prediction of 0.06 given in Section 6.1 (cf. eq. (95)). This implies a strong influence of higher order perturbative corrections, even at the  $Z^0$ , and of non-perturbative terms at lower energies.

The ratio of slopes  $r^{(1)}$ , eq. (96), is less sensitive to higher order corrections than  $r'$  and is better approximated by the MLLA expression than  $r$ , as discussed in Section 6.1. Experimental results for  $r^{(1)}$  are available from the DELPHI [168] and OPAL [170] Collaborations. These data are based on three-jet events selected using a jet finder and thus – unlike the other  $e^+e^-$  data presented in Section 11 – do not employ the unbiased (hemisphere) definition of a jet utilized by the calculations. This makes a quantitative test of the QCD prediction uncertain. Nonetheless we proceed to a comparison of experiment with theory with an eye towards qualitative agreement.

The energy scale of the experimental results [168, 170] for  $r^{(1)}$  is presented in terms of the so-called jet hardness  $\kappa=2E \sin(\Theta/2)$  (see e.g. [7]), where  $\Theta$  is the opening angle between the two lowest energy jets. For small  $\Theta$ ,  $y \approx \ln(\kappa/Q_0)$ . The jet hardness has been shown [168] to be a more appropriate scale than the jet energy when comparing jets embedded in a three-jet environment.

Both DELPHI and OPAL observe the experimental value of  $r_{exp}^{(1)}$  to depend very little on scale. The OPAL measurement  $r_{exp}^{(1)}=2.27 \pm 0.09$  (stat.)  $\pm 0.27$  (syst.) is about one standard deviation higher than the DELPHI result

$1.97 \pm 0.10$  (stat.). Note that the systematic uncertainty quoted by OPAL is mostly due to the jet selection bias. The experimental results agree with the MLLA prediction  $r_{MLLA}^{(1)} \approx 2.01$ -2.03. The expressions (93), (97) and (101) yield  $r_{3NLO}^{(1)} \approx 1.86$ -1.92 in the energy range from the  $\Upsilon$  to the  $Z^0$ , in agreement with DELPHI but about 1.3 standard deviations of the total uncertainty below OPAL. Fig. 19 displays the values of  $r^{(1)}$  in the MLLA and 3NLO approximations for  $n_f=4$  in comparison to the experimental limits from DELPHI.

A recent study [171] attempts to correct for the jet bias introduced by the three-jet event selection by subtracting the biased quark jet component from the multiplicity of the  $q\bar{q}g$  events. The result,  $r^{(1)} = 1.77 \pm 0.03$  (stat.) is substantially smaller than the DELPHI and OPAL results presented above. There are a number theoretical and phenomenological assumptions which enter this analysis, however.

From the DELPHI result [168] for  $r_{exp}^{(1)}$ , the measured values of  $\rho_{1,exp} \approx r_{exp}/2$  can be determined to range from 0.53 at the  $\Upsilon$  to 0.75 at the  $Z^0$ . Its perturbative values according to eq. (101) vary from 0.85 to 0.9. Either the next order perturbative or else non-perturbative terms are needed [172] to reproduce the large difference  $d_1 = r_{exp}^{(1)} - r_{exp} \approx 2(1 - \rho_{1,exp})$  observed in experiment. The simplest Padé expression (102) improves the situation only slightly.

## 11.4 Higher moments

Measurements of higher moments of the multiplicity distribution in unbiased gluon and quark jets are presented in Ref. [15]. The data are collected at the  $Z^0$ . The experimental results are given for factorial and cumulant moments with ranks 2-5. These data are shown in Figs. 20(a) and 20(b) in comparison to the predictions of QCD Monte Carlo programs, and are listed in Table 8. The quark jet moments are observed to be larger than those of gluon jets in accordance with theoretical expectation (Section 6), i.e. event-to-event fluctuations are larger for quark jets than for gluon jets. Note that factorial moments of different rank are highly correlated with each other statistically. In contrast, cumulant moments of different rank are not (see e.g. Ref. [15]). Thus there is a high degree of bin-to-bin correlation in Fig. 20(a) but not in Fig. 20(b). It is worth noting that cumulants of ranks 2, 3 and 4 are directly correlated to dispersion, skew and kurtosis, respectively, i.e. to

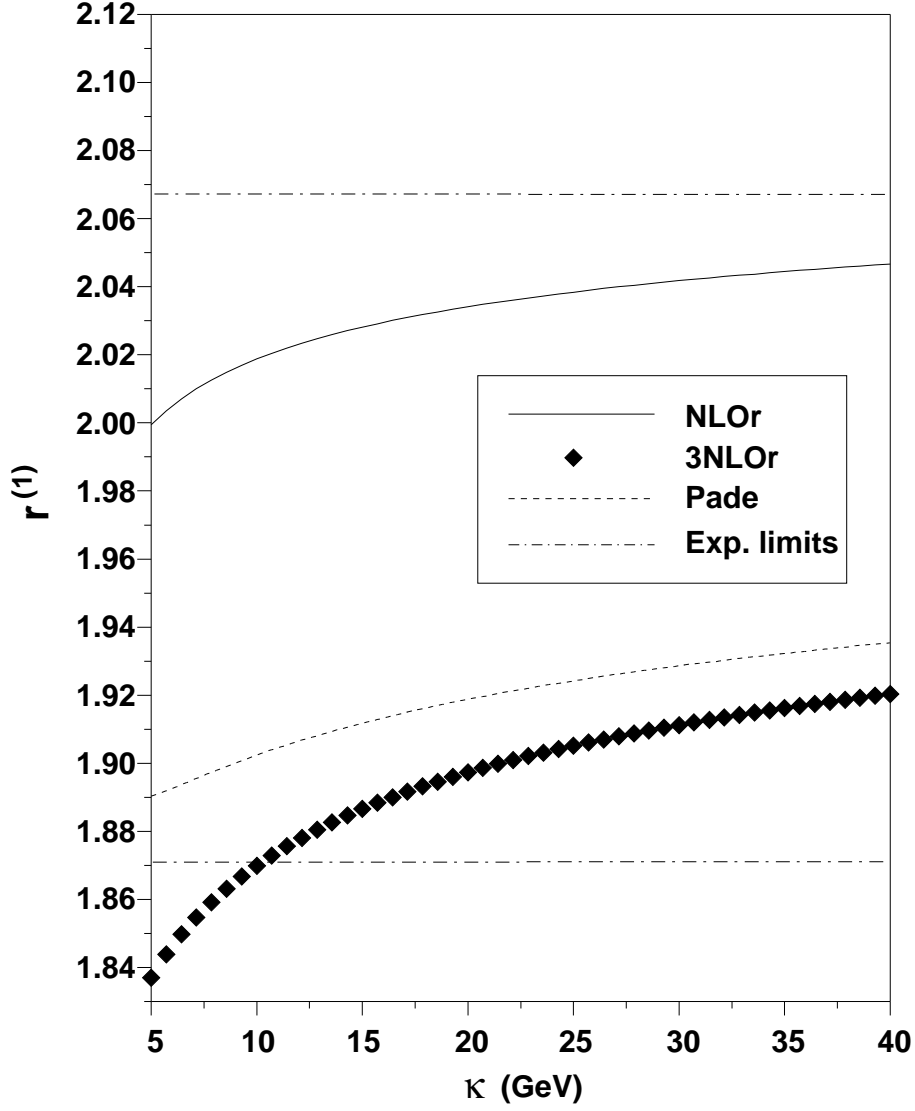


Figure 19: The ratio of slopes of the average multiplicities in gluon and quark jets,  $r^{(1)}$ , in the MLLA and 3NLO (with its Padé expression) approximations. The theoretical results are obtained using  $n_f=4$ . Experimental limits (statistical uncertainties only) from Ref. [168] are shown by the dash-dotted lines.

the ordinary moments, cf. Ref. [15].

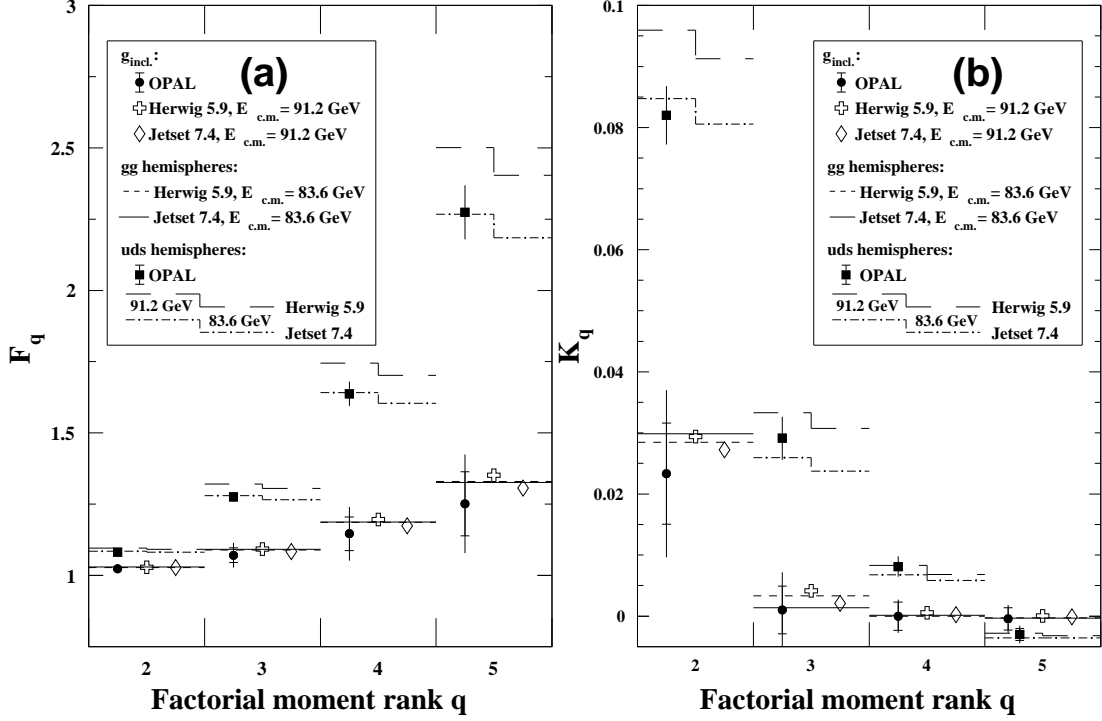


Figure 20: The (a) factorial ( $F_q$ ) and (b) cumulant ( $K_q$ ) moments of the charged particle multiplicity distributions of unbiased single gluon and quark jets, for 41.8 GeV  $g_{\text{incl.}}$  gluon jets and 45.6 GeV  $uds$  quark jets [15], as a function of the rank  $q$ . The predictions of the HERWIG and JETSET parton shower Monte Carlo event generators are also shown.

The experimental results for 41.8 GeV gluon jets,  $F_2^G = 1.023$ , and for 45.6 GeV  $uds$  quark jets,  $F_2^F = 1.082$ , are much smaller than the DLA predictions, viz. 1.33 and 1.75, respectively (see eq. (110)). The analytic results in MLLA,  $F_2^G(MLLA) \approx 1.11$  and  $F_2^F(MLLA) \approx 1.22$  (for  $n_f=4$ ), agree much better with the data. This is analogous to the situation described in Section 11.2 for the multiplicity ratio  $r$ , i.e. the inclusion of higher orders results in a marked improvement in the description of the data compared to leading order. If one accepts the effective value of  $\alpha_S$  averaged over all the

$q$	$F_q$ , gluon jets	$F_q$ , quark jets
2	$1.023 \pm 0.008 \pm 0.011$	$1.0820 \pm 0.0006 \pm 0.0046$
3	$1.071 \pm 0.026 \pm 0.034$	$1.275 \pm 0.002 \pm 0.017$
4	$1.146 \pm 0.059 \pm 0.074$	$1.637 \pm 0.005 \pm 0.042$
5	$1.25 \pm 0.11 \pm 0.13$	$2.274 \pm 0.014 \pm 0.093$

$q$	$K_q$ , gluon jets	$K_q$ , quark jets
2	$0.0233 \pm 0.0083 \pm 0.0109$	$0.0820 \pm 0.0006 \pm 0.0048$
3	$0.0010 \pm 0.0039 \pm 0.0048$	$0.0291 \pm 0.0006 \pm 0.0035$
4	$0.0000 \pm 0.0023 \pm 0.0015$	$0.0081 \pm 0.0007 \pm 0.0015$
5	$-0.0005 \pm 0.0018 \pm 0.0014$	$-0.00300 \pm 0.00096 \pm 0.00095$

Table 8: The factorial ( $F_q$ ) and cumulant ( $K_q$ ) moments of the charged particle multiplicity distribution of unbiased 41.8 GeV  $g_{\text{incl}}$  gluon jets and 45.6 GeV uds quark jets [15] as a function of the rank  $q$ . The first uncertainty is statistical and the second is systematic.

energies of the partons during the jet evolution to be  $\alpha_s \approx 0.2$ , one obtains  $F_2^G(MLLA) \approx 1.039$  and  $F_2^F(MLLA) \approx 1.068$ , which are quite close to the experimental results. In this sense the MLLA prediction can be said to describe the widths of the gluon and quark jet multiplicity distributions at the  $Z^0$  energy to within 10% accuracy.

Unfortunately the NNLO and 3NLO terms worsen the agreement with data compared to MLLA (but not compared to DLA), as was already mentioned in Section 6.2. The analogy with  $r$ , for which each subsequent correction brings the theory closer to data, does not hold here. The NNLO calculation yields slightly larger values for  $F_2^G$  and  $F_2^F$  than in MLLA, resulting in a slight worsening of the description of experiment. The 3NLO corrections are large and negative, yielding  $F_2^G(3NLO) \approx 1.01$  and  $F_2^F(3NLO) \approx 0.94$  for  $n_f=4$ . These latter results are in qualitative conflict with the data in that they imply  $F_2^F < F_2^G$ . The problem in the analytic description of higher moments can be traced to an inappropriate treatment of soft particles, as discussed in Section 6.2.

Given this problem with the analytic approach, it is remarkable that the computer solution of the QCD equations provides a near perfect description

of the higher moments. This is shown in Fig. 21, which displays the computer solutions for the factorial moments of single gluon and quark jets [104] in comparison to the corresponding data from Table 8. Overall, excellent agreement is observed between experiment and theory for ranks up to  $q \approx 5$ . This suggests that the failure of the analytic approach to describe the widths of single quark and gluon jets is mainly a technical issue. The success of the computer solution again emphasizes the importance of an exact treatment of energy conservation and the limits of integration.

Further insight into this issue can be gained by examining the predictions of the ARIADNE Monte Carlo [71] at the parton level, as was done in [173] using Monte Carlo parameter values consistent with LPHD.<sup>7</sup> At the parton level, ARIADNE is roughly equivalent to a DLA analytic calculation except that it includes exact conservation of both energy and momentum. The parton level predictions of ARIADNE for the factorial moments of uds quark jet hemispheres [173] are listed in the rightmost column of Table 9. These values are remarkably similar to the corresponding measurements in Table 8. This suggests that an exact treatment of energy-momentum conservation is essential for an accurate prediction of the higher moments. The corresponding ARIADNE results for hemispheres of gg events are also listed in Table 9. The agreement with the corresponding data in Table 8 is not as good as for quark jets. Nonetheless, the ARIADNE results are much more similar to the data than either the LO or 3NLO analytic results discussed above, for both quark and gluon jets.

$q$	$F_q$ , gluon jets	$F_q$ , quark jets
2	1.044	1.092
3	1.132	1.310
4	1.271	1.720
5	1.474	2.444

Table 9: The factorial ( $F_q$ ) moments of the parton level multiplicity distributions of hemispheres of gg and uds  $q\bar{q}$  events generated using the ARIADNE multihadronic Monte Carlo event generator, as a function of the rank  $q$ .

Qualitatively, the results shown in Fig. 8 for the energy dependence of

---

<sup>7</sup>Essentially this means using a small value of the cutoff parameter,  $Q_0 \approx 0.2$  GeV [173].

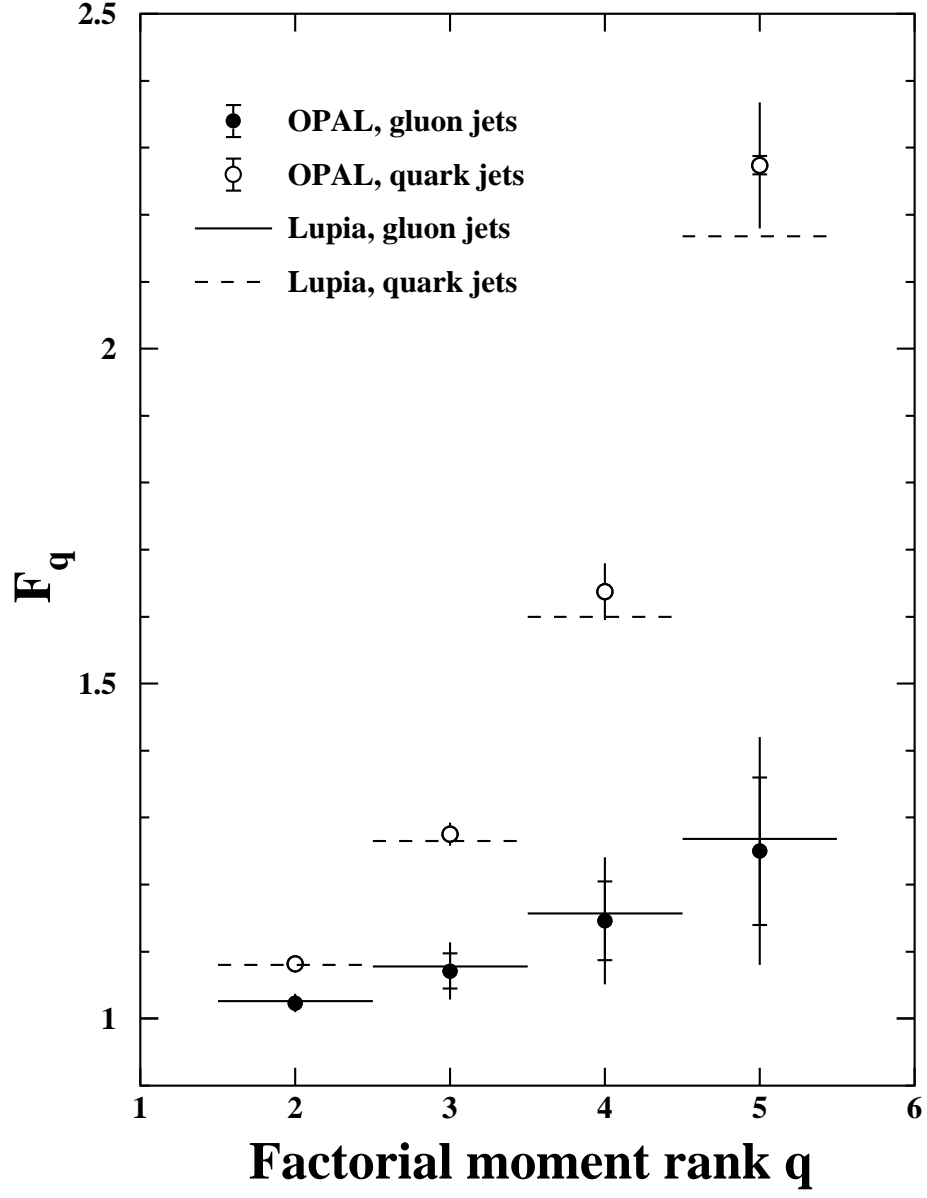


Figure 21: The measured, normalized factorial moments of the charged particle multiplicity distributions of unbiased, separated gluon and quark jets [15], in comparison to the corresponding QCD predictions obtained from a computer solution of the equations for the generating functions [104].



the second factorial moments are similar to experimental trends reported at LEP [147]. The NNLO terms tend to slightly violate the level of agreement with experiment while the agreement is even worse if the 3NLO terms are included, analogous to the situation discussed above in connection with the data of Table 8.

## 11.5 Oscillating $H_q$ moments

The  $H_q$  moments of quark jets, eq. (15), have been experimentally studied up to rank  $q \approx 17$  in  $e^+e^-$  annihilations [174, 175]. Results from the SLD Collaboration based on the charged particle multiplicity distribution from hadronic  $Z^0$  decays are shown in Fig. 22 [174]. Note that these results employ full inclusive  $e^+e^-$  hadronic annihilation events and thus correspond to unbiased “two-jet”  $q\bar{q}$  configurations, unlike the data in Table 8 and Fig. 20 which are based on event hemispheres, i.e. single jets.

The results in Fig. 22 are strikingly similar to the QCD analytic predictions discussed in Sections 5.2 and 8.2, viz. the  $H_q$  moments oscillate with increasing rank, with the occurrence of the first minimum at rank  $q \approx 5$ . We again note the essential role that energy conservation plays for the theoretical prediction. Similar oscillations also have been observed in ep,  $p\bar{p}$ , and heavy ion collisions [178, 179], see Fig. 23. From Fig. 23 it is seen that the amplitude of the oscillations increases as the structure of the colliding particle becomes more complicated. The large positive values for ranks less than about 3 are due to strong correlations between particles from resonance decays. The positive values for  $q \approx 7$  or 8 imply the production of clusters (or mini-jets) at this multiplicity scale. The negative cumulants at  $q \approx 5$  suggest anti-correlations between resonances (and particles) inside these mini-jets. The behavior at larger ranks arises from a complicated mixture of attractive and repulsive forces inside higher multiplicity groups (jets). It is interesting that these features are rather universal in nature.

In a study by the L3 Collaboration [175], it is noted that Monte Carlo simulations provide a good representation of the oscillations in the data. This is found to be true even for simulations based on the MLLA approximation, despite the fact that analytic calculations predict oscillations only at order NNLO and above (Section 5.2). This situation can easily be understood to be a consequence of energy conservation. Unlike the MLLA analytic results, Monte Carlo results based on MLLA formulas incorporate

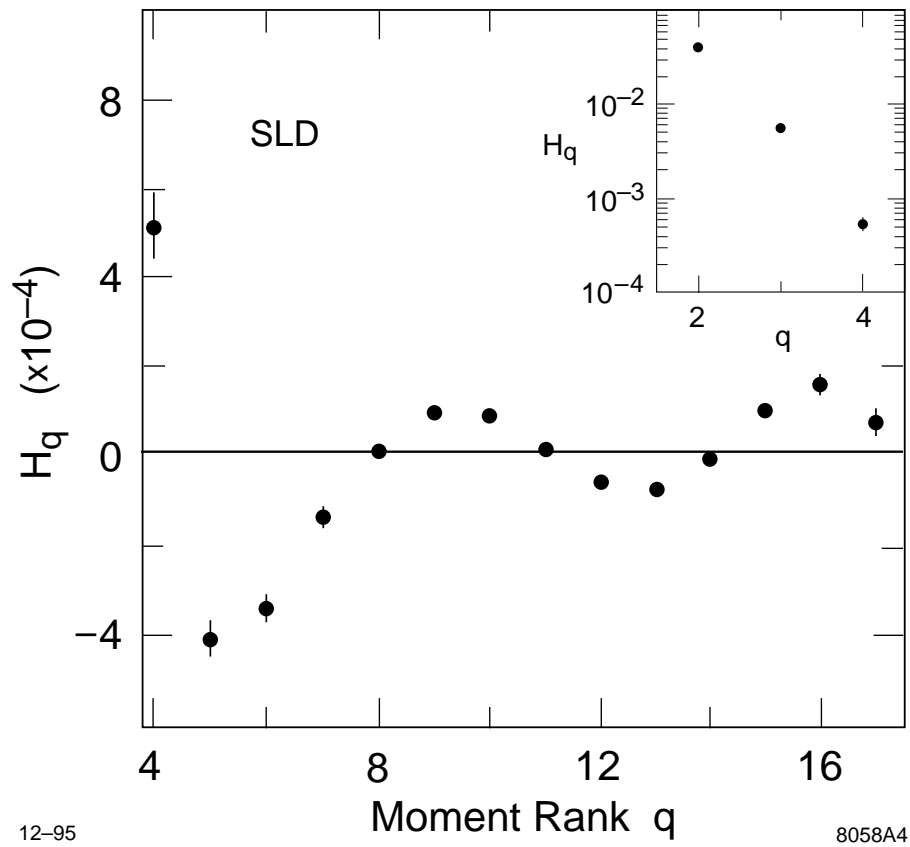


Figure 22: Measured ratio of cumulant to factorial moments,  $H_q$ , as a function of the rank  $q$ , for the charged particle multiplicity distribution in  $e^+e^-$  hadronic  $Z^0$  decays [174]. The uncertainties are statistical only.

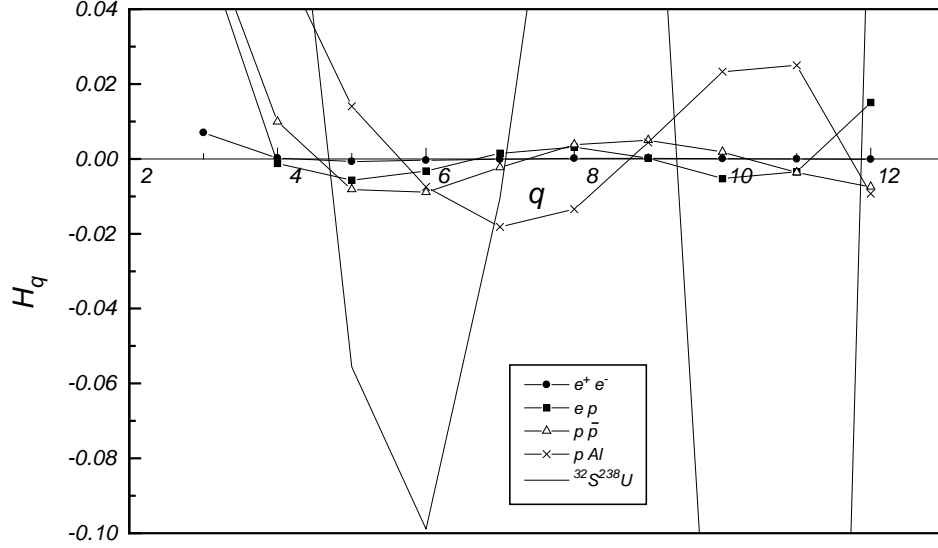


Figure 23: The ratio  $H_q$  for  $e^+e^-$ ,  $ep$ ,  $p\bar{p}$ ,  $pA$  and  $AA$  collisions [179], where  $A$  denotes a heavy ion.

exact energy-momentum conservation. However, one of the principal differences between analytic results at NNLO compared to lower orders is that energy conservation is included. Thus Monte Carlo results based on the MLLA effectively incorporate terms at NNLO and above. This provides an explanation of why MLLA based Monte Carlo event generators exhibit oscillations of  $H_q$  in agreement with the data.

## 11.6 Soft particles

So far, our discussion has focused exclusively on multiplicity in full phase space, i.e. within an entire jet. It is of considerable interest to also consider multiplicity within a limited region of phase space. In this section, we consider the limited phase space volume defined by soft particles, i.e. particles with an energy or momentum below some cutoff. See also Section 14 where multiplicity in limited phase space is discussed in the context of intermittency.

Particle multiplicity in limited phase space is not described by the ana-

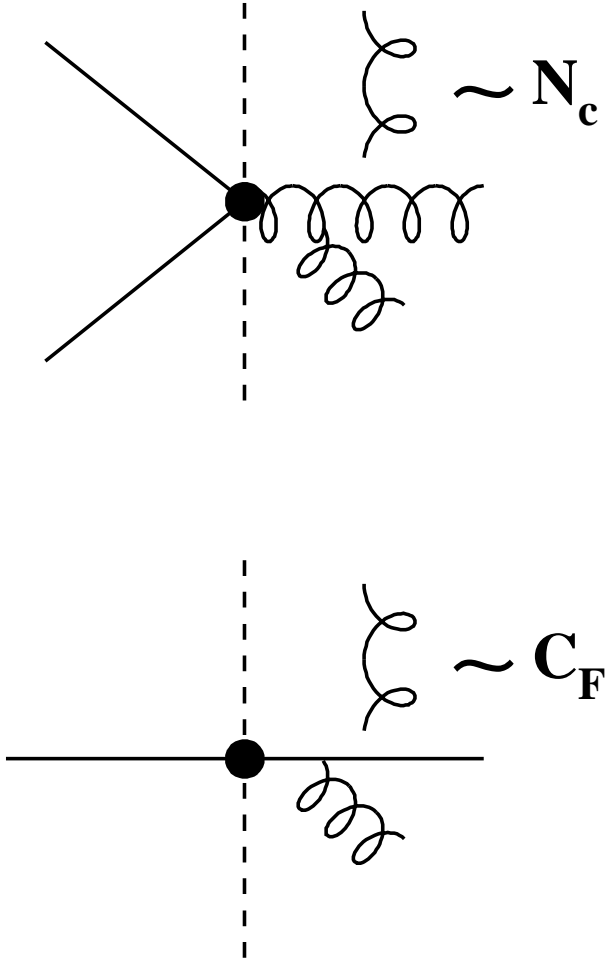


Figure 24: Soft gluons radiated from a gluon (top) or quark (bottom) jet cannot resolve the color substructure of the jet because of their long wavelength. They therefore couple to gluon and quark jets with relative strengths given by the respective color factors  $N_c=3$  and  $C_F=4/3$ , see Refs. [77, 113, 176].

lytic approach based on generating functions presented above in Sections 4-8. Nonetheless soft particle multiplicity possesses a simple theoretical interpretation when considered in terms of the ratio between unbiased gluon and quark jets (see below). Recent theoretical and experimental progress in this area merits discussion in our review.

In QCD, the ratio of mean multiplicities between gluon and quark jets,  $r$ , equals  $r_0 = N_c/C_F = 2.25$  in the asymptotic limit  $E_{\text{jet}} \rightarrow \infty$ , as discussed in Section 6.1. The approach to this limit is very slow, however. For finite energies such as  $E_{\text{jet}} \approx M_Z$ , preasymptotic corrections from higher order terms and conservation laws limit  $r$  to values of approximately 1.5–1.7 (Sections 6.1 and 7). Energy and momentum conservation only apply to full phase space, however. In limited phase space, conservation laws are not a constraint. Furthermore, the asymptotic condition  $E_{\text{jet}} \rightarrow \infty$  may effectively be replaced by the condition that the energy of the particles being considered,  $E$ , satisfy  $Q_0 < E \ll E_{\text{jet}}$ . By selecting *soft* particles, one therefore fulfils the asymptotic condition in at least an approximate manner, opening the possibility of observing  $r \rightarrow r_0 = 2.25$  even for finite energies.

These ideas are developed in Refs. [77, 176]. Because of color coherence in the radiation of soft gluons, the low energy end of the particle spectrum is found to be nearly independent of the energy scale  $E_{\text{jet}}$ . Qualitatively, this arises because soft gluons have long wavelengths and cannot resolve individual partons within a jet. Instead, they couple to the jet with a strength proportional to the color charge of the parton which initiated it, given by  $N_c$  for gluon jets and  $C_F$  for quark jets, see Fig. 24. Thus for *soft* particles, the ratio of mean multiplicities between gluon and quark jets,  $r_{\text{soft}}$ , is predicted to approach  $r_{\text{soft}} \rightarrow N_c/C_F$  as  $E \rightarrow Q_0$  irrespective of the energy scale.

Using their samples of unbiased gluon (“g<sub>incl.</sub>”) and quark jets (see Section 11.1), the OPAL Collaboration tested this prediction by measuring  $r$  as a function of particle momenta  $p$  [113]. The results are shown in Fig. 25. As  $p$  becomes small,  $r$  is seen to saturate at a value of approximately 1.8. This result is larger than the result  $r \approx 1.5$  obtained in full phase space (Table 7). However it is considerably smaller than the theoretical prediction  $r_{\text{soft}} \approx 2.25$  discussed in the previous paragraph.

Insight into this difference between the measured and theoretical values of  $r_{\text{soft}}$  can be obtained by examining the predictions of the HERWIG Monte Carlo. The predictions of HERWIG for  $r$  versus  $p$  at the hadron and parton levels are shown in Fig. 26. For small momenta, the hadron level result

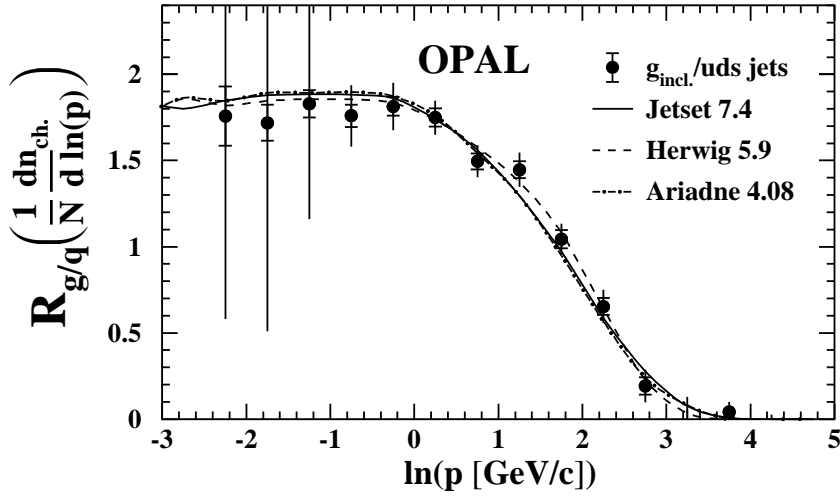


Figure 25: The ratio of mean charged particle multiplicities between unbiased gluon and quark jets as a function of  $\ln p$ , with  $p$  particle momentum [113]. The results are shown in comparison to the predictions of QCD Monte Carlo programs.

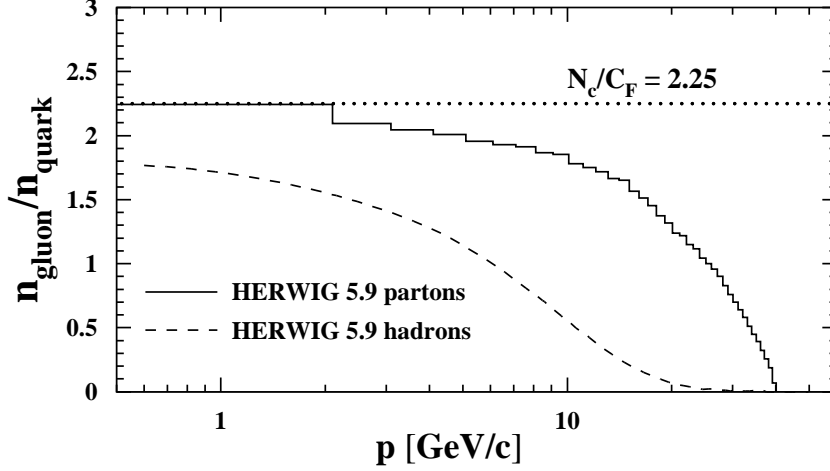


Figure 26: Predictions of the HERWIG Monte Carlo [70] for the ratio of mean particle multiplicities between unbiased gluon and quark jets as a function of particle momentum  $p$ , for partons and charged hadrons.

(dashed curve) converges to  $r_{soft} \approx 1.8$ , in agreement with OPAL (see also the Monte Carlo curves in Fig. 25). The parton level prediction (solid histogram) converges to  $r_{soft} \approx 2.25$ , in agreement with the theoretical expectation [77]. Thus the difference between the measured and theoretical values of  $r_{soft}$  can be attributed to the effects of hadronization.

For soft particles, hadronization is most important within the core of a jet, corresponding to small transverse momenta  $p_{\perp}$  with respect to the jet axis. For example, Fig. 27 shows the predictions of HERWIG for the  $p_{\perp}$  distributions of particles in quark jets, for partons (solid histogram) and charged hadrons (dashed curve). Partons are overwhelmingly produced with  $p_{\perp}$  values larger than 0.8 GeV/ $c$  (because of the cutoff  $Q_0$  in the Monte Carlo) in contrast to hadrons which predominantly appear at smaller  $p_{\perp}$ . On the basis of this information, OPAL repeated their analysis selecting particles with  $p_{\perp} > 0.8$  GeV/ $c$  only, i.e. they restricted their analysis to the perturbative region of phase space as predicted by HERWIG.

The results are shown in Fig. 28. The charged particle multiplicity ratio  $r$  is shown as a function of the softness of the particles. The softness of particles is defined by the maximum particle momentum  $p_{max}$  considered

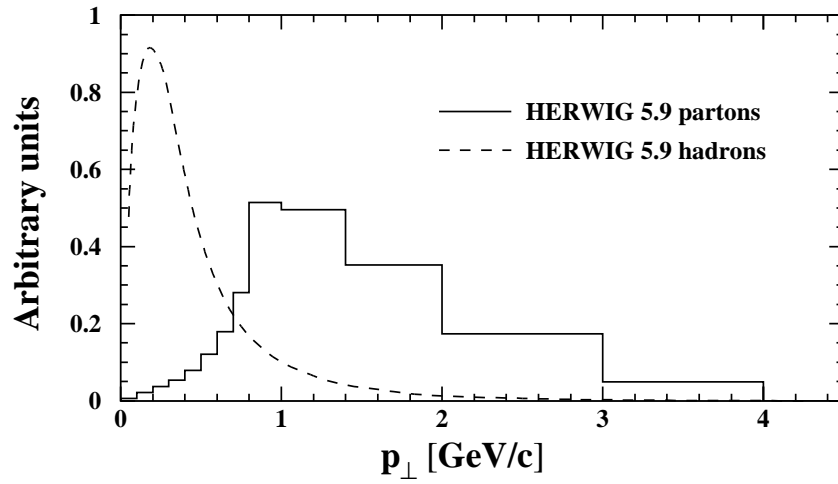


Figure 27: Predictions of the HERWIG Monte Carlo [70] for the transverse momentum distributions of partons and charged hadrons in unbiased uds quark jets. The transverse momentum  $p_{\perp}$  is defined with respect to the jet axis. The ordinate units are arbitrary.



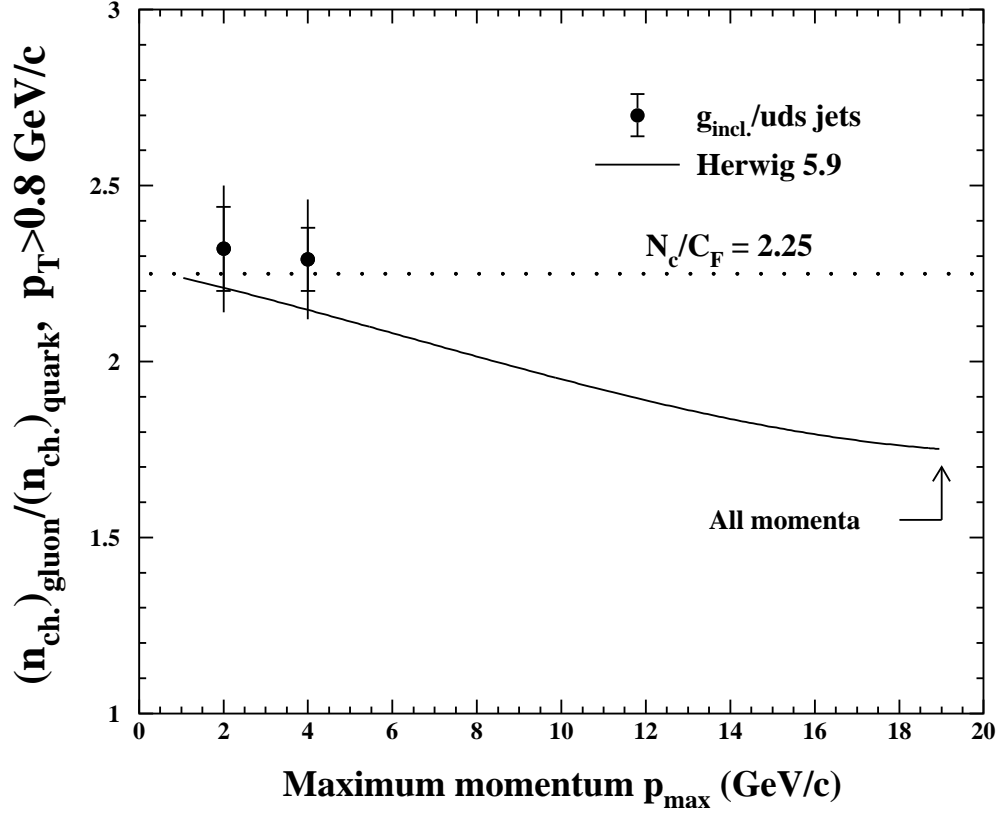


Figure 28: Ratio of charged particle multiplicities between unbiased gluon and quark jets for particles with large transverse momenta to the jet axis defined by  $p_{\perp} > 0.8$  GeV/c. The results are shown as a function of the softness of the the particles, defined by the maximum particle momentum  $p_{\text{max}}$ , used to determine  $r$ .

when determining  $r$ . Unlike the results in Fig. 25, particles are required to have  $p_{\perp} > 0.8$  GeV/ $c$  as explained in the previous paragraph. The solid curve shows the prediction of HERWIG.

With no explicit cut on  $p_{\text{max.}}$  (“All momenta”), the multiplicity ratio is predicted to be about 1.8. As softer and softer particles are selected ( $p_{\text{max.}}$  is decreased), the HERWIG prediction approaches the QCD result  $r_{\text{soft}} \approx 2.25$  in conformity with theory [77]. Thus a measurement of  $r_{\text{soft}}$  for particles with  $p_{\perp} > 0.8$  GeV/ $c$  effectively yields a measurement of the color factor ratio  $N_c/C_F$ . OPAL results are shown for  $p_{\text{max.}}=2$  GeV/ $c$  and 4 GeV/ $c$ . The result using  $p_{\text{max.}}=4$  GeV/ $c$  is  $r=2.29 \pm 0.017$  (stat. + syst.) [113] which provides one of the most accurate experimental determinations of  $N_c/C_F$  currently available. Note that unlike all other measurements of  $N_c/C_F$ , this result is not based on a fit of a QCD motivated expression – in which  $N_c/C_F$  is extracted as a fitted parameter – but is the ratio of directly measured quantities. This OPAL result confirms one of the oldest, previously unverified predictions for multiplicities in gluon and quark jets, that the particle multiplicity ratio between gluon and quark jets should equal the color factor difference (in an appropriate region of phase space), dating back to Refs. [105, 177].

## 12 Jet and subjet multiplicities

To this point, we have considered only the final result of well developed cascades, namely hadron multiplicities. It is also of interest to study the intermediate stages of the cascade evolution, i.e. the jet substructure. Recalling the phrase about “whorls inside whorls inside whorls” from the field of turbulence, one can ask what is predicted by pQCD for the structure of “jets inside jets inside jets” in  $e^+e^-$  events. The ordering of emissions by transverse momentum ( $k_t$ ) is at the heart of this issue. Thus one can ask about the number of jets or subjets (the “jets inside jets”) as the angular ( $k_t$ ) resolution scale is varied. With very low resolution one obtains two jets, corresponding to the condition eq. (88) imposed on the equations for the generating functions, eqs. (57) and (58), which requires that a single quark-antiquark pair be initially created in an  $e^+e^-$  annihilation. A three-jet structure appears when a gluon with large transverse momentum is emitted by the quark or antiquark. Three-jet event production is suppressed by an additional factor

of  $\alpha_S$ , which is small for large transferred momenta. Therefore, this process can be calculated perturbatively. The well known exact three-jet matrix element [180] can then be directly compared with the results of the generating function approach described above. At relatively low transferred momenta, the jet evolves to angular (or  $k_t$ ) ordered subjets. By increasing the resolution, more and more subjets are observed. In the ideal case, each subjet is an individual final-state hadron in the limit of very small resolution scales. The resolution criteria must be chosen in a manner to provide infrared safe results. Then the perturbative expansion gives rise to finite answers which can be confronted to experimental data, so long as the hadronization stage does not significantly alter the situation as is assumed by local parton-hadron duality.

Details of the resolution criteria are not too important if ratios are considered. In particular, one can form the ratio of subjet multiplicities in three- and two-jet events. Naïvely, this ratio should equal the corresponding ratio of Casimir factors:

$$\frac{\langle n_3^{sj} \rangle}{\langle n_2^{sj} \rangle} = \frac{2C_F + C_A}{2C_F} = \frac{17}{8}. \quad (144)$$

However soft gluon coherence suppresses this ratio to a value below 1.5 (see Ref. [90]), demonstrating the importance of correlations when dealing with interfering jets.

The first proposal to eliminate collinear and mass singularities when resolving subjets was formulated in Ref. [181]. According to this proposal, one should consider the relative angles between any two partons  $\theta_{kl}$  and their fractional energies  $x_k$  and  $x_l$  which exceed some finite values:  $\theta_{kl} > \delta$  and  $x_{k,l} > \epsilon$ . The algorithm can be simplified by replacing these two conditions by a single one, as is accomplished by the JADE and Durham proposals. In the JADE algorithm [138], the relative invariant mass of two partons  $M_{kl}/s^{1/2}$  is required to exceed some value ( $M_{kl}^2/s > \xi_c$ ). In the Durham (or  $k_t$ ) algorithm [136, 137], a similar inequality is imposed on the relative transverse momentum, or, more precisely,

$$\xi_{kl} = 2(1 - \cos \theta_{kl}) \min \frac{(E_k^2, E_l^2)}{s} > \xi_c, \quad (145)$$

where  $E_{k,l}$  are the energies of partons  $k$  and  $l$ . For small relative angles  $\theta_{kl}$ , the parameter  $\xi_c$  approximates the rescaled transverse momentum  $k_{t,kl}^2/Q^2$  of the jet of lower momentum with respect to that of higher momentum.

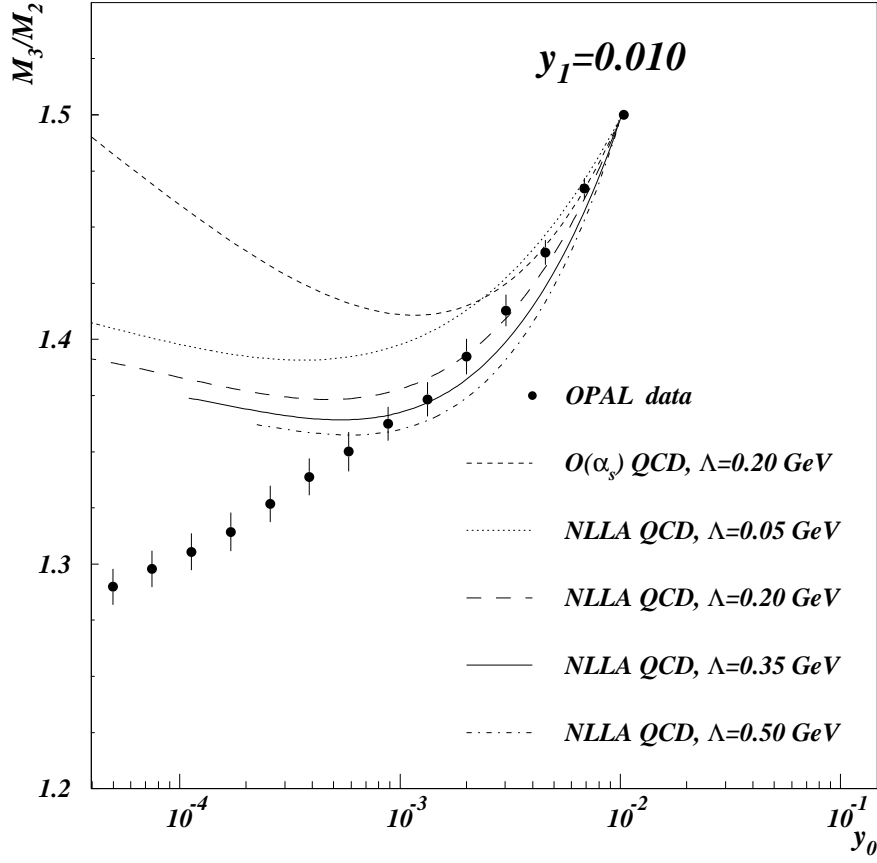


Figure 29: The measured ratio of subjet multiplicities between three- and two-jet events as a function of the subjet resolution scale  $y_0$  [184], in comparison to analytic calculations [90]. The results are obtained from  $e^+e^- Z^0$  data using the Durham jet finder with an initial clustering scale  $y_1=0.010$ .

The Durham algorithm is well suited for analytic calculations and gives rise to small hadronization corrections according to Monte Carlo schemes. Therefore it is widely used for comparison of theory with experiment. The two limiting cases of  $\xi_c \rightarrow 1$  and  $\xi_c \rightarrow 0$  correspond to low resolution, for which the minimum number of jets are resolved<sup>8</sup>, and to the final parton (or particle) limit of the highest available resolution, discussed in detail in the previous sections. In terms of virtualities,  $\xi_c = Q_c^2/Q^2$ . Thus for  $Q_c = Q$  one deals with the initial stage of the process, while ever smaller values of  $Q_c$  correspond to its later subjet stages, and final hadrons appear at values of  $Q_c$  approaching the non-perturbative scale  $Q_0$  of a few hundred MeV. The number of jets increases as  $\xi_c$  decreases, as calculated in Ref. [83].

Jet multiplicities in  $e^+e^-$  processes are usually fitted by the formula

$$\langle n_{e^+e^-}^{jet}(Q_c, Q) \rangle = 2 \langle n_F \left( \frac{Q}{Q_c}, \frac{Q_c}{\Lambda} \right) \rangle, \quad (146)$$

whereas the multiplicity of charged hadrons has been approximated by a formula with two additional constants:

$$\langle n_{e^+e^-}^{ch}(Q_0, Q) \rangle = 2K_{ch} \langle n_F \left( \frac{Q}{Q_0}, \frac{Q_0}{\Lambda} \right) \rangle + constant \quad (147)$$

It is interesting to determine if eqs. (57) and (58) can describe jet, subjet and hadron multiplicities in  $e^+e^-$  annihilations in a unified manner. The answer is yes [104, 78], so long as the equations are solved numerically using the proper limits of integration. By proper limits of integration, we mean a lower limit  $x_c$  and an upper limit  $1 - x_c$  instead of 0 and 1, with  $x_c = Q_c \sqrt{2}/Q$  as has been suggested in Refs. [104, 78]. The numerical solutions presented in Refs. [104, 78] describe the average multiplicities of jets, subjets and hadrons using a common normalization corresponding to “one parton=one hadron” without additional constants, over a wide energy interval from the threshold region to the  $Z^0$  energy. This result is especially remarkable given that only two hard partons are present at the initial stage, whereas up to 60 charged particles appear in the final stage at the  $Z^0$  energy, some of which originate from the decays of intermediate resonances. The most common approach consists of inserting a so-called  $K$ -factor,  $K_{ch}$  (see eq. (147)), i.e. some constant relating the parton and hadron distributions which usually differs from

---

<sup>8</sup> $\langle n_{e^+e^-}^{jet}(\xi_c=1) \rangle$  corresponds to two initial quark jets in  $e^+e^-$  collisions.

unity (typically,  $K_{ch} \approx 1.2$ ). This difference from unity is ascribed to the confinement process. In Monte Carlo models, this stage is fitted by some phenomenological formulas which are not yet explained in the framework of the more theoretical approaches discussed above.

The ratio of hadron multiplicities in gluon and quark jets is found [78] to be even smaller than in the analytic solutions of the evolution equations, bringing it into closer agreement with experiment, see Fig. 9 and the discussion in Section 11.2. The running property of the coupling constant is a crucial consideration for this result. Even more astonishing is that high moments of the multiplicity distributions and their oscillations fit the experimental data using the same normalization as used for  $r$  [104], see Figs. 10 and 21. This implies that power corrections due to energy conservation, obtained by using the correct integration limits, are essential, raising questions about the potential importance of other possible power corrections, due to instantons, etc., as discussed above.

We have briefly described the latest theoretical developments in the problem, leaving aside the corresponding formulas which can be found in Refs. [17, 90, 92, 104, 78, 137, 139, 90, 182].

Subjet multiplicities have been studied experimentally by a number of groups [183]-[185]. Measured results for the ratio (144) as a function of the subjet resolution scale  $y_0 \equiv \xi_c$  are shown in Fig. 29. These results are obtained using the Durham jet finder with an initial clustering scale  $\xi_c \equiv y_1 = 0.010$  to select the two- and three-jet events. The ratio has a value of 1.5 for  $y_0 = y_1$ , as required from its construction, and decreases rapidly at smaller resolution scales  $y_0$ . The results are far below the naïve prediction of  $17/8$  for all values of  $y_0$ . Fig. 29 also shows the perturbative predictions of Ref. [90], both for fixed order  $\mathcal{O}(\alpha_S)$  calculations and including resummed terms in the MLLA approximation. The MLLA results are shown for different choices of the scale parameter  $\Lambda$ . Both the fixed order and MLLA results reproduce the qualitative behavior of the data for  $y_0 \approx y_1$ , i.e. they exhibit a falloff from the value of 1.5 with about the same slope as the data as  $y_0$  decreases.

Subjet multiplicities have also been studied in separated gluon and quark jets, both experimentally [185] and theoretically [186]. An example is shown in Fig. 30. The jets in this example are defined using the Durham algorithm. The analytic results [186] are seen to represent the data fairly well for large values of the subjet resolution scale  $y_0$ .

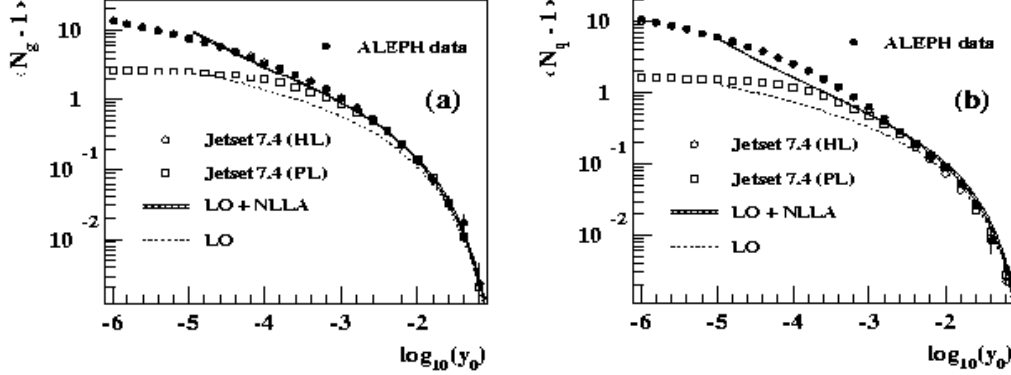


Figure 30: The subjet multiplicities of separated (a) gluon and (b) quark jets [185] in comparison to analytic results from Ref. [186] and to Monte Carlo predictions.

### 13 Multiplicity of three-jet events

The multiplicity of two-jet events was defined from the product of the generating functions for single jets, eq. (88), implying their independence. The assumption of independence is valid because the angular separation of the jets is large, i.e. about  $180^\circ$ . For three-jet events, various angular combinations are possible. Mutual interference between the jets cannot be neglected. Thus the particle multiplicity in three-jet events depends on the angular topology of the events.

To describe this effect it is necessary to go beyond the equations presented in this work, to consider angular correlations between jets in the framework of the equations for the generating functionals or directly in terms of Feynman graphs. Therefore we refer to Refs. [17, 139] where this problem is treated in detail. Up to further correction terms of order  $\mathcal{O}(\alpha_s)$ , the multiplicity of three-jet events can be approximately written as the sum of the multiplicities of independent jets at properly defined energy scales:

$$\langle n_{F\overline{F}G} \rangle \approx 2\langle n_F(y_F) \rangle + \langle n_G(y_G) \rangle, \quad (148)$$

where  $y_F = \ln(E^*/\Lambda)$  and  $y_G = \ln(p_t/2\Lambda)$ , with  $E^*$  the quark energy in the quark-antiquark cms and  $p_t$  the gluon transverse momentum in this system.

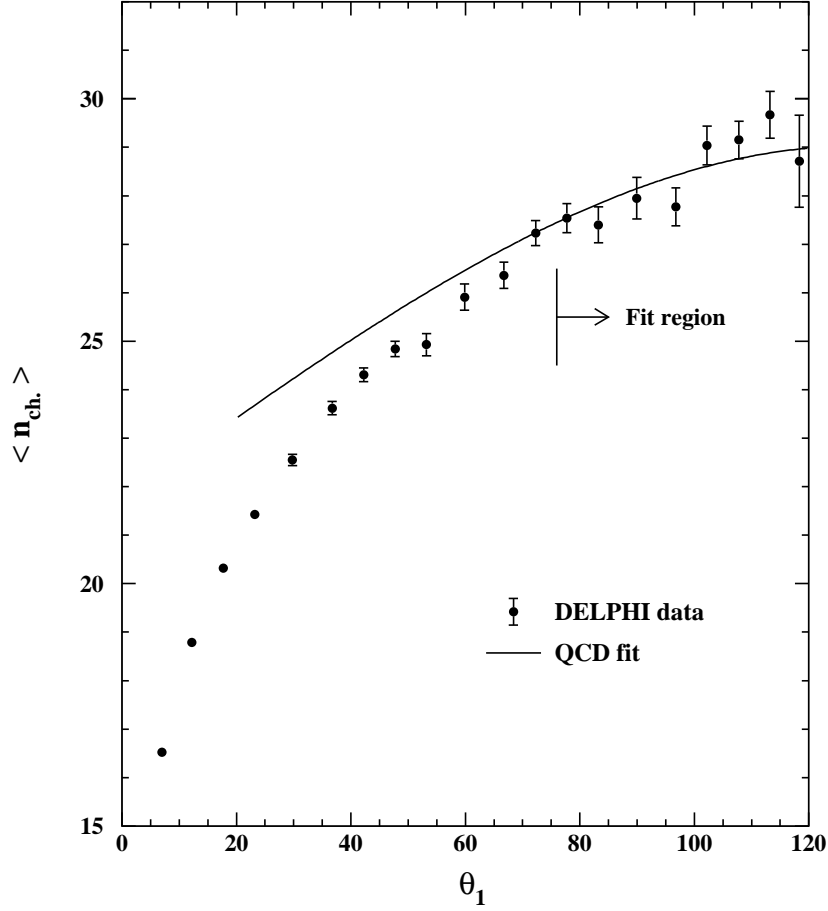


Figure 31: Measurements [115] of the mean charged particle multiplicity of three-jet Y events [187] as a function of the opening angle  $\theta_1$  between the two lower energy jets, for  $E_{\text{c.m.}}=91$  GeV. The events are selected using the  $k_{\perp}$  jet finder. The solid curve shows the result of a one parameter fit [188] of eq. (149) to the data within the fit region shown.



This expression has the correct limit when  $p_t \rightarrow 0$  and the two jet configuration is restored.

Eq. (148) can be re-expressed using directly observable quantities such as the multiplicity of  $e^+e^-$  events and the ratio  $r$  of multiplicities between gluon and quark jets:

$$\langle n_{F\overline{F}G} \rangle \approx \langle n_{e^+e^-}(2E^*) \rangle + \frac{1}{2}r(p_t)\langle n_{e^+e^-}(p_t) \rangle. \quad (149)$$

These formulas also can be written in forms suitable for studies of gluon jets or to relate multiplicities at different scales (see Ref. [17]).

Expression (149) has been tested in several experimental studies [115, 188]. As an example, the data in Fig. 31 show the charged particle multiplicity of so-called “Y events”<sup>9</sup>, namely three-jet events for which the angle between the highest energy jet and each of the two other jets is about the same, versus the opening angle  $\theta_1$  between the two lower energy jets. In Ref. [188] it is found that eq. (149) describes this data accurately only if the angular separation between the jets is about  $80^\circ$  or larger, as shown by the solid curve in Fig. 31. In Ref. [189], this effect is explained to arise as a consequence of the bias in quark jet multiplicity introduced by the three-jet event selection procedure. A modified version of eq. (149) is suggested [189] based on the dipole model of QCD (see Ref.[190] and references therein), which implicitly includes non-perturbative string effects. The modified prediction is found to yield a better description of the experimental measurements, see Ref. [171].

## 14 Evolution of distributions with decreasing phase space: intermittency and fractality

Multiplicity distributions can be studied not only in total phase space (as discussed in the previous sections for very large phase space volumes) but within any subset of it. For a homogeneous distribution of particles, the average multiplicity decreases in proportion to the considered volume, whereas the fluctuations increase. The most interesting problem here is the law governing the growth of the fluctuations and its possible deviation from a purely

---

<sup>9</sup>Y events were first studied in [187].

statistical law related to the decrease of the average multiplicity. Such a deviation necessarily would be a consequence of the dynamics of the underlying interaction. In particular, it has been proposed [191] to search for a power law behavior of the factorial moments in small rapidity intervals  $\delta y$ :

$$F_q \sim (\delta y)^{-\phi(q)} \quad (\delta y \rightarrow 0), \quad (150)$$

where  $\phi(q) > 0$ . This proposal is motivated by an analogy to turbulence in hydrodynamics, where a similar behavior is known as intermittency and the  $\phi(q)$  are called intermittency exponents.

The power-like dependence in eq. (150) can be related to fractal properties of particle distributions in the available phase space, as was first discussed in Ref. [192]. Earlier, the fractal properties of branching processes and, in particular, of QCD jets in  $e^+e^-$  annihilation were considered in Refs. [193]-[195]. From the point of view of multiplicity, intermittency implies a rather strong increase of the distribution's width, and a longer tail at high multiplicities.

Experimental data from various processes over a wide energy range reveal a power law dependence in agreement with eq. (150) and thus suggest the relevance of intermittency to high energy multiparticle processes. Simple branching models have been proposed to explain this phenomenon [196]-[199]. Calculations based on perturbative QCD provide more specific predictions than these models, however. The current state of affairs is reviewed in Ref. [16]. In the following we show how Quantum Chromodynamics produces intermittency [94], [200]-[204] and then compare the theoretical predictions to recent experimental results.

We again stress that QCD deals with partons (quarks and gluons), in contrast to experiment which provides results based on hadrons. Local parton-hadron duality implies the proportionality of inclusive distributions. The validity of LPHD is not obvious for correlations, however, and is sometimes not fulfilled in Monte Carlo schemes. For phenomena such as intermittency, one can therefore anticipate a qualitative agreement between theory and data, at best.

In contrast to the previous sections, here we rely on the diagrammatic approach rather than on the equations for the generating functions. This is because we must now deal with a small part of the parton content of a well developed jet, namely with those partons which are present in a small phase space volume. The pre-history of the jet as a whole is significant for

the subjet under consideration. This is most readily addressed using the diagrammatic technique, viz.:

1. the primary quark emits a hard gluon with energy  $E$  in the direction of the angular interval  $\theta$ , but not necessarily hitting the window;
2. the emitted gluon produces a jet of partons with parton splitting angles larger than the window size;
3. among those partons there exists a parton with energy  $k$  which initiates a subjet which hits the window;
4. all decay products of the subjet exactly cover the angle  $\theta$ .

This picture dictates the rules of calculation of the  $q$ th correlator of the whole jet. The  $q$ th correlator of the subjet  $\Delta N^{(q)}(k\theta)$  should be averaged over all possible ways it can be produced, i.e. convoluted with the inclusive spectra of partons  $D^\theta$  in the whole jet and with the probability of creation of the jet ( $\alpha_S K_F^G$ ). Analytically, this is represented by

$$\Delta N^{(q)}\left(Q\theta_0, \frac{\theta_0}{\theta}\right) \propto \int^Q \frac{dE}{E} \frac{\alpha_S}{2\pi} K_F^G\left(\frac{E}{Q}\right) \int^E \frac{dk}{k} D^\theta\left(\frac{E}{k}; E\theta_0, k\theta\right) \Delta N^{(q)}(k\theta), \quad (151)$$

where  $\Delta N^{(q)} \equiv F_q \langle n \rangle^q$  is the unnormalized factorial moment (on the left hand side for the whole jet, and on the right hand side for the parton subjet with momentum  $k$  within the angle  $\theta$ ). Since the unnormalized moments increase with energy, whereas the parton energy spectrum decreases, the product  $D^\theta \Delta N^{(q)}(k\theta)$  has a maximum at some energy, and the integral over momenta can be calculated using the method of steepest descent. Leaving aside the details (see Ref. [94]), we describe the general structure of the correlator in the case of a fixed coupling constant,  $\gamma_0 = \text{constant}$ :

$$\Delta N^{(q)} \propto \Delta\Omega \left(\frac{\theta_0}{\theta}\right)^{\frac{\gamma_0}{q}} \left(\frac{E\theta}{\mu}\right)^{q\gamma_0}, \quad (\mu = \text{constant}), \quad (152)$$

where the three factors represent the phase space, the energy spectrum factor, and the  $q$ th power of the average multiplicity. To obtain the normalized moment, expression (152) should be divided by the  $q$ th power of that part of the mean multiplicity of the whole jet which appears inside the window  $\theta$ ,

i.e. by the proportion of the total average multiplicity corresponding to the phase space volume  $\Delta\Omega$ :

$$\Delta N(\theta) \sim \Delta\Omega \Delta N(\theta_0). \quad (153)$$

If the analysis is performed in  $D$ -dimensional space, the phase space volume obeys

$$\Delta\Omega \sim \theta^D, \quad (154)$$

where  $\theta$  corresponds to the minimum linear size of the  $D$ -dimensional window which stems from the singular behavior of parton propagators in Quantum Chromodynamics (see Ref. [94]). This allows the factorial moments to be represented as the product of a purely kinematic factor depending on the dimension of the analyzed space, and of a dynamic factor not related to that dimension which depends on the coupling constant, i.e.

$$F_q \sim \theta^{-D(q-1)} \theta^{\frac{q^2-1}{q}\gamma_0}. \quad (155)$$

For small angular windows,  $\theta \sim \delta y$ . The intermittency indices defined by eq. (150) are then

$$\phi(q) = D(q-1) - \frac{q^2-1}{q}\gamma_0. \quad (156)$$

Expression (156) is valid for moderately small windows, for which the condition  $\alpha_S \ln \theta_0/\theta < 1$  is fulfilled. For extremely small windows it is necessary to account for the running property of the coupling constant. In this case the constant  $\gamma_0$  should be replaced by an effective value  $\langle\gamma\rangle$ , which depends logarithmically on the width of the window  $\theta$  and may be approximated by [94]

$$\langle\gamma\rangle \approx \gamma_0 \left(1 + \frac{q^2+1}{4q^2}\epsilon\right), \quad (157)$$

where

$$\epsilon = \frac{\ln \theta_0/\theta}{\ln(E\theta_0/\mu)} \leq 1. \quad (158)$$

Thus intermittency indices for very small windows are markedly smaller than for intermediate sized windows (fixed coupling regime), especially for low rank moments. Moreover, the simple power law, eq. (150), becomes modified by logarithmic corrections, and the intermittency indices depend on the size

of the chosen interval. The resulting curve of  $\ln F_q$  versus  $-\ln \theta$  is characterized by two distinct regions with different slopes. A rather steep linear increase is predicted for moderately small windows  $\theta$ , with a slope given by eq. (156). For smaller window sizes, this behavior is replaced by a much slower quasi-linear increase given by eqs. (157) and (158). It is easy to determine the location of the transition point between the two regimes and to show that this point shifts to smaller window sizes at larger values of  $q$ . In any case, the factorial moments of any rank increase as the size of the interval decreases. This demonstrates that the fluctuations of the multiplicity distribution become stronger for smaller intervals and, more importantly, that they significantly exceed Poisson fluctuations.

Above, we have described the results of the double-logarithmic approximation, with corrections from the running coupling constant, eq. (157). Corrections from the modified-leading logarithm approximation (see eq. (164) below) are comparatively small, i.e. about 10%. The MLLA terms move the transition point between the power law and quasi-power law regimes to slightly smaller windows for all moments except the second one, which moves to somewhat larger windows. This tendency can be attributed to the mutual influence of the energy spectrum and the average multiplicity.

Of greater interest are qualitative effects introduced in MLLA which yield a functional dependence on the rank  $q$  from terms proportional to  $q\gamma$ . Consider an analogy to statistical mechanics, presented in Ref. [94], where the quantity

$$\Phi = 1 - \frac{\phi(q) + 1}{q} \quad (159)$$

is interpreted as the free energy and the rank  $q$  as the inverse temperature  $\beta = 1/kT$ . In the lowest order approximation,  $\Phi$  increases monotonically with  $q$ . Higher order corrections produce a maximum in  $\Phi$  at values of  $q$  where  $H_q$  exhibits its first minimum (see eq. (86)), i.e. at

$$q_{cr} \approx \frac{1}{h_1 \gamma_0} + \frac{1}{2} \approx 5. \quad (160)$$

In statistical mechanics, this corresponds to zero entropy, i.e. to a phase transition. In Quantum Chromodynamics it just indicates the role of the new parameter  $q\gamma$ . This feature is related to the singularities of the generating function and to the pinching behavior of the zeros of the truncated generating function discussed in Section 10.

The above results can be restated in terms of fractals. The power-like behavior of factorial moments suggests fractal properties of particle (parton) distributions in phase space. According to the general theory of fractals (see Ref. [16] and references therein), intermittency indices are related to fractal (Rényi) dimensions  $D_q$  by the formula

$$\phi(q) = (q-1)(D - D_q). \quad (161)$$

In the double-logarithmic approximation taking into account eqs. (156) and (157), one obtains

$$D_q = \frac{q+1}{q} \langle \gamma \rangle = (\gamma_0 + \frac{\gamma_0}{q})(1 + \frac{q^2+1}{4q^2} \epsilon). \quad (162)$$

The first term in the first bracket corresponds to mono-fractal behavior in the case of fixed coupling and is due to the increase in average multiplicity. The second term in the first bracket corresponds to multi-fractal properties and is related to the falloff of the energy spectrum. One can easily obtain the multi-fractal spectral function in this case (see Ref. [94]). It is found that the fractality in Quantum Chromodynamics has a purely dynamical origin ( $D_q \sim \gamma_0$ ) related to the cascade nature of the process, and that the kinematic factor in relation (155) has an integer dimension. The term with  $\epsilon$  in eq. (162) accounts for the running property of the coupling constant. This term slightly violates pure multi-fractal behavior, giving rise to a slower increase of factorial moments at small angles. The fixed coupling regime corresponds to  $\epsilon=0$ , yielding

$$D_q = \gamma_0 \frac{q+1}{q}. \quad (163)$$

Further corrections to eq. (162) appear in MLLA [94]. The general form of eq. (162) remains valid, but  $\gamma_0(Q)$  is replaced by an effective  $\gamma_0^{eff}(Q)$  which depends on  $q$ :

$$\gamma_0^{eff}(Q) = \gamma_0(Q) + \gamma_0^2(Q) \frac{\beta_0}{4N_c} \left[ -B_0 \frac{q-1}{2(q+1)} + \frac{q-1}{2(q+1)(q^2+1)} + \frac{1}{4} \right], \quad (164)$$

where

$$B_0 = \frac{1}{\beta_0} \left[ \frac{11N_c}{3} + \frac{2n_f}{3N_c^2} \right]. \quad (165)$$

For large ranks  $q$  one obtains a negative shift:

$$\gamma_0^{eff} = \gamma_0 - \gamma_0^2 \frac{\beta_0(2B_0 - 1)}{16N_c}. \quad (166)$$

This corresponds to the general tendency of negative shifts from MLLA corrections. However, this represents only a partial accounting for higher order effects. Other corrections stemming from energy conservation are more difficult to include and are not incorporated into the above equations.

An alternative approximation for the  $\epsilon$  dependence of  $D_q$  in DLA has been suggested in Ref. [203]:

$$D_q = 2\gamma_0(Q) \frac{q+1}{q} \cdot \frac{1 - \sqrt{1-\epsilon}}{\epsilon}. \quad (167)$$

A somewhat different expression for  $D_q$  was derived in Refs. [201, 202] starting from the expression for cumulant moments, supposing that they converge to factorial moments at high energies up to a factor of  $q^{-2}$  as discussed above:

$$D_q = 2\gamma_0(Q) \frac{q}{q-1} \cdot \frac{1 - \sqrt{1-\epsilon} \left(1 - \frac{\ln(1-\epsilon)}{2q^2}\right)}{\epsilon}. \quad (168)$$

The variety of proposed forms for  $D_q$  suggests that there are neglected effects which are important for a proper analytic treatment. In particular, energy conservation constraints are just as severe in small phase space windows as in total phase space (see [205]). This problem has not yet been solved. Thus the above formulas should be compared to experiment on a qualitative level only. In addition, variables such as rapidity or pseudo-rapidity should be used. Other variables, such as the invariant mass  $Q^2$ , are more suitable for studies of Bose-Einstein correlations than of intermittency (for more details, see [206]).

In general, the qualitative trends predicted by the QCD equations are observed in experiment. Intermittency is observed to be stronger in  $e^+e^-$  annihilations than in reactions with initial hadrons, and weaker yet in nucleus-initiated processes [16]. This is related to the increasing number of competing subprocesses (sources) in reactions with complicated structure, which smoothes out the intermittent behavior of individual sources. Due to the stronger effect and higher statistics, intermittency studies in  $e^+e^-$  collisions

are more conclusive. Recent studies from LEP [66, 207, 208] represent considerable improvements upon earlier results (summarized in Ref. [16]). In the new studies, the experimental data are compared with QCD predictions for local multiplicity fluctuations in 1-, 2- and 3-dimensional intervals at LEP-1 and LEP-2 energies. The general predictions of QCD are confirmed by the data. The factorial moments rise in an approximately linear manner for large bins and level off for smaller ones. The dependence on the bin dimension, the order of the factorial moments, and on energy are qualitatively reproduced, i.e. the moments increase as the bin dimension increases, become larger for higher orders, and increase with energy. The analytic predictions depend sensitively on the QCD parameter  $Q_0$ , as is also true for the predictions of the QCD Monte Carlo models.

On a quantitative level, significant differences are observed between theory and data, however. The factorial moments increase faster in experiment than in the calculations as the phase space interval decreases, and generally level off at larger bin sizes than the theory as the intervals continue to decrease. An example is shown in Fig. 32 [207], for which  $z \propto \ln(\Theta_0/\Theta)$  measures the size of the phase space window  $\Theta \leq \Theta_0$ . Thus  $z=0$  corresponds to the maximum phase space region  $\Theta=\Theta_0$  (where  $\Theta_0=25^\circ$  in this example), while  $z$  increases as the window size decreases. Variation of the QCD parameters, e.g.  $Q_0$ , does not improve the level of agreement between theory and data.

Given the quantitative discrepancies between theory and data, an evaluation of QCD parameters using intermittency is not possible at present. The discrepancies are not surprising given the crucial role played by energy conservation in total phase space, see Sections 5-8, and the absence of energy conservation from the analytic description here. Energy conservation is included in Monte Carlo studies, and they provide a reasonably good description of the data as is shown in Refs. [66, 207, 208].

The increase of correlations for smaller bin sizes, as described by the behavior of the cumulants, reveals the important role of genuine four- and five-particle correlations in  $e^+e^-$  annihilations [66]. This is in contrast to nucleus collisions where it has not yet proved possible to observe correlations for groups of more than two particles. The fractal nature of the particle distributions in  $e^+e^-$  events has been also demonstrated [209] using the so-called bunching parameters [210, 211].

The fractality of particle distributions in limited phase space volumes



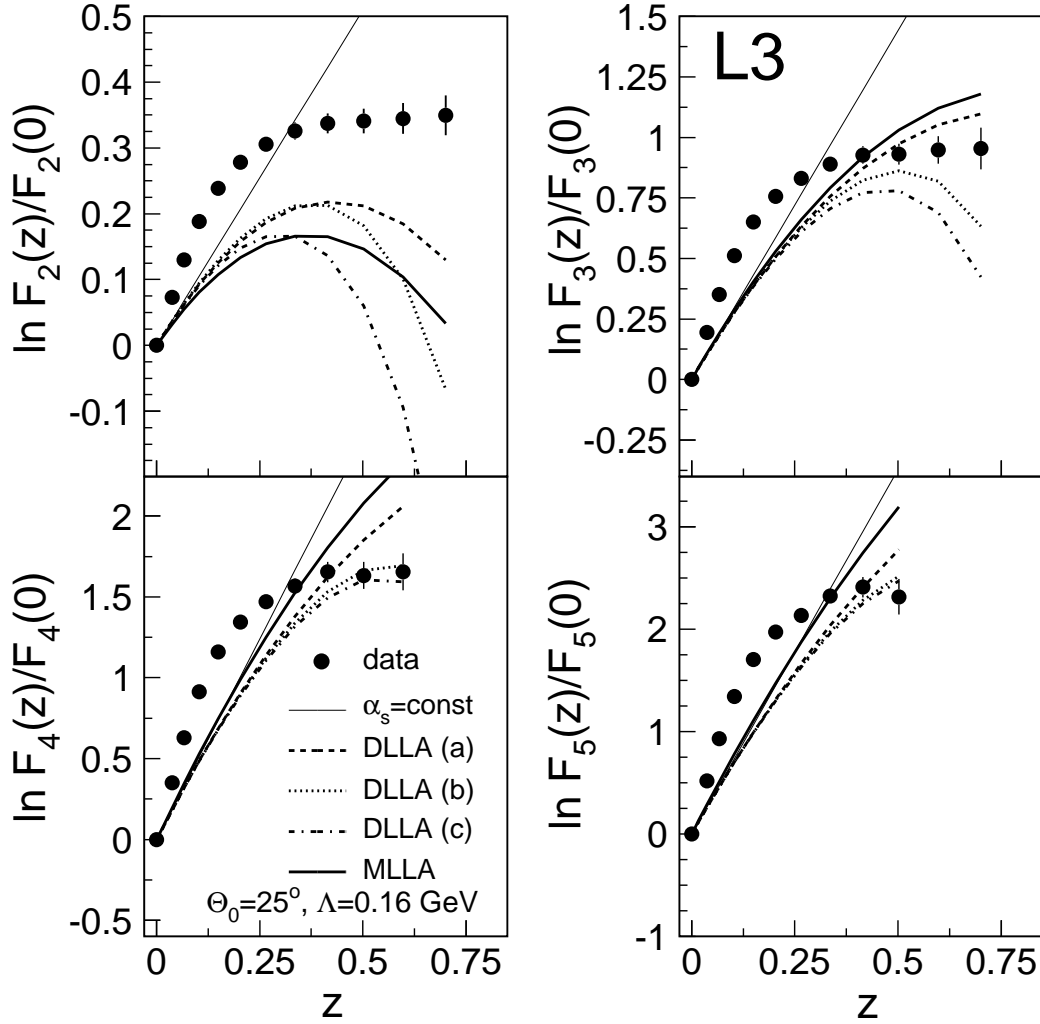


Figure 32: Measurements of the ratio  $F_q(z)/F_q(0)$  from  $e^+e^- Z^0$  data for  $q=2-5$ , as a function of the scaling variable  $z \equiv \epsilon$  [207]. The data are compared to QCD analytic calculations with fixed coupling strength  $\alpha_S$  (eq. (163)): DLA (a) (eq. (162)), DLA (b) (eq. (167)), DLA (c) (eq. (168)), and MLLA (eq. (164)). Note that DLA is referred to as “DLLA” in the figure legend.

suggests fractal properties for colliding objects in ordinary space. Surely, owing to its dynamical origin, such a structure would itself be dynamical, i.e. rapidly evolving in space and time. There are two reasons to favor this interpretation. First, the evolution of the parton shower in ordinary space must give rise to a tree-like structure of a fractal type which should evolve due to the cascade evolution. Second, lattice computations in  $SU(2)$  gluodynamics [212] have shown that the system of gluons in the vicinity of the phase transition is fractal in the sense that it fills a volume  $V$  bounded by a surface  $S$  which are related by the formula  $V \sim S^{1.12}$ . This is typical of fractal objects: the exponent would equal 1.5 for ordinary three-dimensional objects.

The geometric fractality of macroscopic bodies has been revealed by measurements of the power-like shape of their structure functions when point-like particles (photons, electrons, neutrons, etc.) are scattered from them. Using this example, one might try to measure [213] structure functions in deep inelastic processes, in order to determine the fractal dimensions of the scattered partners. Theoretically, this has been considered only at the level of models. Experimental difficulties have prevented direct tests of these models. The question of the fractal geometry of particles in ordinary space-time therefore remains open.

## 15 Heavy quark jets

The multiplicity of heavy quark jets is of special interest because it exhibits two peculiar effects with analogues in QED. It is well known from QED that photon emission from muons is strongly suppressed compared to emission from electrons (as the ratio of corresponding masses squared). This suppression is related to the different masses in the propagators and to the vector nature of the emitted photons. The second effect, known from cosmic ray studies and named after Chudakov, is that two opposite charges in an electron-positron pair screen each other if they are not well separated, i.e. until the distance between them becomes larger than the inverse transverse momentum of the resolving quanta.

In QCD, the emission of gluons by heavy quarks is suppressed in a similar manner. At relatively small angles ( $\theta \ll 1$ ), gluons are emitted according to

the formula

$$\frac{\theta^2}{(\theta^2 + \theta_M^2)^2}, \quad (169)$$

where  $\theta_M = M/E_Q$ , with  $M$  and  $E_Q$  the mass and energy of a heavy quark. The form of the numerator in eq. (169) is due to the vector nature of the radiated quanta. The denominator equals the quark propagator squared. The larger the value of  $M$ , the stronger the suppression of forward ( $\theta < \theta_M$ ) emissions. This gives rise to “ring-like” events as advocated in Refs. [214]–[216] using somewhat different but similar arguments, or to the “dead cone” phenomenon [217, 218]. Note that the suppression of gluon emission at small angles does not necessarily imply a suppression of emissions with low transverse momenta. The origin of the ring-like events is the large mass of heavy quarks, which is not the same as  $k_t$  ordering.

There is a difference between QED and QCD with respect to the properties of the emitted quanta, however. While photons do not have electric charge, gluons carry color. Radiated photons do not multiply, in contrast to gluons which produce jets. Gluons emitted at rather large angles ( $\theta \geq \theta_M$ ) multiply in the usual manner. For gluons emitted at smaller angles, it is necessary to account for interference between the secondary emissions and possible emission by the quark. This situation is analogous to the Chudakov effect. In QCD, the analogous effect for partons moving close to one another is called color transparency.

However, there is a substantial difference for heavy quarks (for a more detailed discussion, see Ref. [17]). Because its mass is large, the heavy quark moves more slowly than the emitted gluon, and the two become separated more quickly than is the case when the quark is light. Therefore color charge screening is not as effective for heavy quarks as it is for light quarks and interference effects are less important. It can be shown that the primary gluon can be treated as an incoherent state with respect to the quark, and that, as a consequence, gluon emission by massive quarks is suppressed for angles  $\theta < \theta_M$  compared to light quarks.

To obtain an expression for the multiplicity of partons accompanying a heavy quark pair in  $e^+e^-$  annihilations, the distribution of gluons emitted by the quark, eq. (169), should be convoluted with the multiplicity of a gluon subjet. According to the above discussion, this expression can be integrated

over all transverse momenta exceeding a fixed value  $Q_0$  to obtain

$$\langle n_{Q\bar{Q}}(W) \rangle = 2 \int_{M^2}^{W^2} \frac{d\kappa^2}{\kappa^2} \left( 1 - \frac{M^2}{\kappa^2} \right) \int_{Q_0}^{\kappa} \frac{dk_t}{k_t} K_F^G(x) \frac{\alpha_S(k_t)}{4\pi} \langle n_G(k_t) \rangle, \quad (170)$$

with  $K_F^G(x)$  given by eq. (62),  $k_t = x\kappa$ , and  $\kappa^2 = W^2[\sin^2(\theta/2) + \theta_M^2/4]$ . Eq. (170) yields the relation between the multiplicities accompanying quark-antiquark pairs with heavy and light components produced in  $e^+e^-$  processes [217]:

$$\langle n_{Q\bar{Q}}(W) \rangle = \langle n_{q\bar{q}}(W) \rangle - \langle n_{q\bar{q}}(\sqrt{e}M) \rangle, \quad (171)$$

which is valid up to terms of order  $\mathcal{O}(\alpha_S)$ . Therefore the difference between the total multiplicities of events with heavy and light quarks is

$$\langle n_{Q\bar{Q}}^{tot}(W) \rangle - \langle n_{q\bar{q}}^{tot}(W) \rangle = \langle n_{Q\bar{Q}}^{dc}(M) \rangle - \langle n_{q\bar{q}}^{tot}(\sqrt{e}M) \rangle, \quad (172)$$

where  $\langle n^{dc} \rangle$  denotes the decay multiplicity of a heavy quark with mass  $M$ . The difference does not depend on the primary energy  $W$  but only on the heavy quark mass.

In contrast to eq. (172), the so-called naïve model [219]-[221] considers the difference between heavy and light quark event multiplicities to be the consequence of energy rescaling only:

$$\langle n_{Q\bar{Q}}(W) \rangle = \langle n_{q\bar{q}}[(1 - \langle x_Q \rangle)W] \rangle, \quad (173)$$

where  $\langle x_Q \rangle$  denotes the mean energy fraction of the heavy quark,  $\langle x_Q \rangle \equiv 2\langle E_Q \rangle/W$ . In this case the difference in total multiplicities between heavy and light quark events is energy dependent, decreasing towards zero as  $W$  becomes larger.

Measurements of the difference  $\delta_{Q\ell} \equiv \langle n_{Q\bar{Q}}^{tot}(W) \rangle - \langle n_{q\bar{q}}^{tot}(W) \rangle$  between heavy and light quark event multiplicities in  $e^+e^-$  annihilations are shown as a function of the center-of-mass energy in Fig. 33 [222]. The heavy and light quark jet samples consist of b and uds flavored events, respectively. The data support the QCD hypothesis that  $\delta_{Q\ell}$  is independent of energy, eq. (172), over the energy dependent hypothesis of the naïve model. Note the essential contribution that the highest energy points (from LEP-2) provide for this conclusion. The initial QCD estimates [217] predicted a rather large value  $\delta_{Q\ell} \approx 5.5$ . Later this prediction was reduced to  $\delta_{Q\ell} \approx 3.7$  [221].

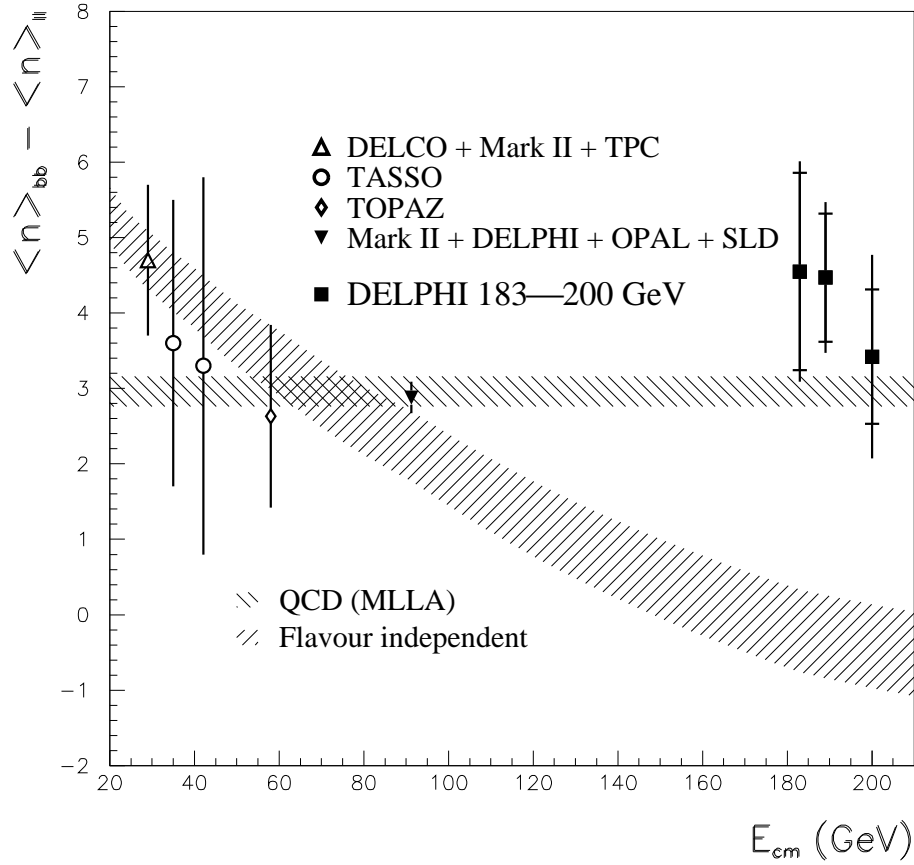


Figure 33: Measurements of the difference  $\delta_{Q\ell}$  between the total event multiplicities of heavy and light quark events in  $e^+e^-$  annihilations, versus the center-of-mass energy, compared to a prediction motivated by MLLA QCD and the prediction of the so-called naïve model of energy rescaling (the naïve model is referred to as “Flavour independent” in the figure legend). The figure is taken from Ref. [222].

The horizontal band in Fig. 33 at  $\delta_{Q\ell} \approx 3$  [222] is not, strictly speaking, a theoretical estimate, but an admixture of the the MLLA statement that  $\delta_{Q\ell}$  is constant together with the experimental measurement from the  $Z^0$  pole.

We will also briefly mention an interesting feature of heavy quark fragmentation. Because of their large masses, heavy quark hadrons tend to retain a substantial portion of the primary quark energy, which can be described in the framework of perturbative QCD (for more details, see Ref. [17]). The comparatively long lifetime of heavy quark hadrons plays an important role at extremely high energies in the spatial multiplicity distribution of cosmic ray showers [223]. Because of relativistic effects and smaller interaction cross sections, high energy heavy hadrons created in cosmic ray showers penetrate more deeply into detectors on average than light quark hadrons, giving rise to so-called long flying cascades. The multiplicity of the main cascade in these events is somewhat reduced, while particles appear at longer distances from the primary interaction point, compared to cascades without heavy quarks. Thus the mean length of the cascade is larger than normal, from which term “long flying” is derived.

## 16 Conclusions

The distribution of particle multiplicity in high energy inelastic processes provides essential information on the dynamics of strong interactions. Its importance stems from the fact that it contains all the correlations between final-state hadrons in an integrated form. It is comparatively easy to measure, in contrast to differential correlation functions which require much more detailed analysis.

Higher order perturbative solutions of the equations for the generating functions based on the running coupling constant, or the exact solution based on a fixed coupling, exhibit qualitative features which are absent in lowest order. Features predicted for partons, such as the oscillations of the  $H_q$  ratios or the larger factorial moments of quark jets compared to gluon jets, are experimentally observed for hadrons. The shape of the multiplicity distribution is mostly defined by soft particles created during the final stages of development of the cascade. The success of the theoretical methods implies the applicability of higher order perturbative techniques to the soft stages of evolution, and the suitability of local parton-hadron duality to multiplicity

ity based measurements. The principal features of multiplicity predicted by QCD are observed qualitatively both in  $e^+e^-$  and hadron-initiated processes. This prompts speculation about the similarity of the production mechanisms in the two cases. This similarity probably occurs because the parton wave functions of the colliding particles in hadron collisions are prepared long before the scattering, and are described by a space-like bremsstrahlung cascade with angular ordering similar to  $e^+e^-$  case.

The historical development of the perturbative approach to multiplicity is summarized in the introduction. The initial excitement created by the first applications of QCD to multiplicity gave way to disappointment over the extremely wide multiplicity distribution predicted by the theory at lowest order, although it was soon realized that the corrections were rather large. Now the importance of higher orders, up to NNLO and beyond, is well recognized, and it is possible to account for them in a consistent manner. The results reveal approximate  $F$  (or KNO) scaling, with some dependence on the coupling constant in the preasymptotic regime.

The long standing discrepancy between theory and experiment for the value of the ratio of the average multiplicities in gluon and quark jets has now been effectively resolved. Measurements of the higher moments of the multiplicity distribution are found to be in excellent agreement with the computer solutions of the QCD equations. The rise in average multiplicity with energy is described in a satisfactory manner, using a sensible value of the strong coupling strength  $\alpha_S$  for both quark and gluon jets. The evolution of the distributions in smaller phase space regions has also been successfully described, at least at a qualitative level. Energy conservation in the calculations and a proper unbiased definition of jets in the experiments are crucial for the quantitative tests of the QCD results, and are the principal developments which allowed recent progress in the field. The astonishing success of the computer solutions also demonstrates the importance of using the correct limits of integration over the parton energy splitting variables, i.e. the importance of the treatment of the boundary between the perturbative and non-perturbative regions.

In combination with predictions for inclusive spectra and various correlation functions, the above results suggest that Quantum Chromodynamics can be successfully applied to predict qualitative features of soft processes. Angular ordering inside each jet and the collective nature of the inter-jet flows are essential considerations for multiplicity and its energy evolution in

individual events. Analytic approaches provide a means to predict qualitative new effects and to gain insight into the behavior of the solutions (dependence on energy scale, the number of active quark flavors, etc.). Recent progress in that direction, described at some length above, gives hope for further success.

## 17 Acknowledgments

We are very much indebted to A. Capella, Yu.L. Dokshitzer, G. Gianini, R.C. Hwa, C.S. Lam, B.B. Levtchenko, V.A. Nechitailo and J. Tran Thanh Van for collaboration and discussions.

This work was supported by the Russian Fund for Basic Research, by INTAS, and by the US Department of Energy under grant DE-FG03-94ER40837.



## References

- [1] I.M. Dremin, *Physics-Uspekhi*, 37 (1994) 715.
- [2] A Giovannini and L Van Hove, *Z. Phys.* C30 (1986) 391; *Acta Phys. Pol.* B19 (1988) 495; 917; 931.
- [3] I.V. Andreev, *Chromodynamics and hard processes at high energies* (Moscow, Nauka, 1981) (in Russian).
- [4] B.L. Ioffe, L.N. Lipatov and V.A. Khoze, *Deep inelastic processes* (Moscow, Energoatomizdat, 1983) (in Russian).
- [5] F.J. Yndurain, *Quantum Chromodynamics* (N.-Y.-Berlin-Heidelberg-Tokyo, Springer Verlag, 1983).
- [6] M.B. Voloshin and K.A. Ter-Martirosyan, *Theory of gauge interactions of elementary particles* (Moscow, Energoatomizdat, 1984) (in Russian).
- [7] Yu.L. Dokshitzer, V.A. Khoze, A.H. Mueller and S.I. Troyan, *Basics of perturbative QCD* (Gif-sur-Yvette, Editions Frontieres, 1991).
- [8] Ya.I. Azimov, Yu.L. Dokshitzer, V.A. Khoze and S.I. Troyan, *Z. Phys.* C27 (1985) 65.
- [9] D. Amati and G. Veneziano, *Phys. Lett.* B83 (1979) 87.
- [10] A. Bassetto, M. Ciafaloni and G. Marchesini, *Phys. Rep.* C100 (1983) 201.
- [11] A. Bassetto, M. Ciafaloni and G. Marchesini, *Nucl. Phys.* B163 (1980) 477.
- [12] Z. Koba, H.B. Nielsen and P. Olesen, *Nucl. Phys.* B40 (1972) 317.
- [13] Yu.L. Dokshitzer, *Phys. Lett.* B305 (1993) 295.
- [14] I.M. Dremin, *Phys. Lett.* B313 (1993) 209.
- [15] OPAL Collaboration, K. Ackerstaff et al., *Eur. Phys. J.* C1 (1998) 479.
- [16] E.A. DeWolf, I.M. Dremin and W. Kittel, *Phys. Rep.* 270 (1996) 1.

- [17] V.A. Khoze and W. Ochs, Int. J. Mod. Phys. A12 (1997) 2949.
- [18] S.K. Kaufmann and M. Gyulassi, J. Phys. A11 (1978) 1715.
- [19] S. Hegyi, Phys. Lett. B309 (1993) 443; B318 (1993) 642; B463 (1999) 126.
- [20] E.M. Friedländer and I. Stern, LBL-31354, 1991.
- [21] K. Oldham, The fractional calculus (Orlando, Academic Press, 1974) p.60.
- [22] B. Ross, Fractional calculus and its applications, in Lecture Notes in Mathematics (Berlin, Springer Verlag, 1975) v.457, p.1.
- [23] I.M. Dremin, JETP Lett. 59 (1994) 585.
- [24] A.M. Polyakov, Sov. Phys. JETP 32 (1971) 296; 33 (1971) 850; 34 (1972) 1177.
- [25] S. Hegyi, Proc. 8th Int. Conf. on Correlations and Fluctuations, Matrahaza, Hungary, 1998 (World Scientific, Singapore, to be published).
- [26] M. Ploszajczak, Proc. 8th Int. Conf. on Correlations and Fluctuations, Matrahaza, Hungary, 1998 (World Scientific, Singapore, to be published).
- [27] R. Botet and M. Ploszajczak, Z. Phys. C76 (1997) 257.
- [28] S. Hegyi, Phys. Lett. B467 (1999) 126.
- [29] A.I. Golokhvastov, Sov. J. Nucl. Phys. 27 (1978) 430; 30 (1979) 253.
- [30] A. Wehrl, Rev. Mod. Phys. 50 (1978) 221.
- [31] V. Šimák, M. Šumbera and I. Zborovský, Proc. XVIII Int. Symp. on Multiparticle Dynamics, Tashkent, USSR, 1987, eds. I. Dremin and K. Gulamov (World Scientific, Singapore, 1988) p. 205.
- [32] V. Šimák, M. Šumbera and I. Zborovský, Phys. Lett. B206 (1988) 159.

- [33] M. Pachr, V. Šimák, M. Šumbera and I. Zborovský, *Mod. Phys. Lett.* A7 (1992) 2333.
- [34] F. Takagi, *Proc. XXI Int. Symp. on Multiparticle Dynamics*, Wuhan, China, 1991, ed. C.S. Liu et al. (World Scientific, Singapore, 1992) p. 346.
- [35] I.M. Dremin, *Mod. Phys. Lett.* A8 (1993) 2747.
- [36] I.M. Dremin and R.C. Hwa, *Phys. Rev.* D49 (1994) 5805.
- [37] A. Giovannini, *Nuovo Cim.* A15 (1973) 543.
- [38] S. Hegyi, *Phys. Lett.* B387 (1996) 642; B417 (1998) 186.
- [39] M. Biyajima, *Phys. Lett.* B137 (1984) 225.
- [40] P.V. Chliapnikov, O.G. Tchikilev and V.A. Uvarov, *Phys. Lett.* B352 (1995) 461.
- [41] V.D. Rusov, T.N. Zelenzova and S.J. Kosenko, OPU-98-1-ENIN, 1998.
- [42] S. Carius and G. Ingelmann, *Phys. Lett.* B252 (1990) 647.
- [43] R. Szwed and G. Wrochna, *Z. Phys.* C47 (1990) 447;  
R. Szwed, G. Wrochna and A.K. Wroblewski, *Mod. Phys. Lett.* A5 (1990) 981.
- [44] I.M. Dremin and A.M. Dunaevskii, *Phys. Rep.* 18 (1975) 159.
- [45] B. Andersson, G. Gustafson and T. Sjöstrand, *Phys. Lett.* B94 (1980) 211.
- [46] B. Andersson, G. Gustafson, G. Ingelman and T. Sjöstrand, *Phys. Rep.* 97 (1983) 33.
- [47] A. Capella, U. Sukhatme, C.I. Tan and J. Tran Thanh Van, *Phys. Lett.* B81 (1979) 68.
- [48] A. Capella and J. Tran Thanh Van, *Phys. Lett.* B93 (1980) 146; *Z. Phys.* C10 (1981) 249.

- [49] A.B. Kaidalov, Phys. Lett. B116 (1982) 459.
- [50] A.B. Kaidalov and K.A. Ter-Martirosyan, Phys. Lett. B117 (1982) 247; Sov. J. Nucl. Phys. 39 (1984) 979; 40 (1984) 135.
- [51] R. Ugoccioni, A. Giovannini and S. Lupia, Proc. XXIII Int. Symp. on Multiparticle Dynamics, Aspen, USA, 1993, eds. M.M. Block and A.R. White (World Scientific, Singapore, 1994) p. 297.
- [52] B.B. Levchenko, Proc. VIII Workshop on High Energy Physics and Quantum Field Theory and III Workshop on Physics at VLEPP, Zvenigorod, Russia, 1993, ed. B.B. Levchenko (Moscow State Univ., Moscow, 1994) p. 68.
- [53] R. Ugoccioni and A. Giovannini, Nucl. Phys. Proc. Suppl. 71 (1999) 201.
- [54] F. Bianchi, A. Giovannini, S. Lupia and R. Ugoccioni, Z. Phys. C58 (1993) 71.
- [55] I.M. Dremin and D.S. Chernavsky, Zh. Exper. Teor. Fiz. 38 (1960) 229.
- [56] L. McLerran and R. Venugopalan, Phys. Rev. D49 (1994) 2233; D49 (1994) 3352; D50 (1994) 2225.
- [57] Yu.V. Kovchegov, E.M. Levin and L. McLerran, BNL-NT-99/7, TAUP-2613-99.
- [58] E. Fermi, Progr. Theor. Phys. 5 (1950) 570.
- [59] I.Ya. Pomeranchuk, Doklady AN SSSR 78 (1951) 78.
- [60] L.D. Landau, Izvestia AN SSSR 17 (1953) 51.
- [61] E.A. Kuraev, J. Manjavidze, A.N. Sisakian, hep-ph/9909287; hep-ph/0003093.
- [62] UA5 Collaboration, G.J. Alner et al., Phys. Lett. B160 (1985) 193; 199.
- [63] A. Zichichi, M. Basile, G. Bonvicini et al, Proc. Erice 1982, p.701.
- [64] M. Basile et al, Lett. Nuovo Cim. 41 (1984) 293; 298.

- [65] ALEPH Collaboration, D. Buskulic et al., Z. Phys. C69 (1995) 15.
- [66] OPAL Collaboration, G. Abbiendi et al., Eur. Phys. J. C11 (1999) 239.
- [67] E.K.G. Sarkisyan, Phys. Lett. B477 (2000) 1.
- [68] M. Biyajima, T. Kawabe and N. Suzuki, Phys. Lett. B189 (1987) 466.
- [69] T. Sjöstrand, Comp. Phys. Comm. 82 (1994) 74; CERN-TH.7112/93 (revised August 1995).
- [70] G. Marchesini, B.R. Webber et al., Comp. Phys. Comm. 67 (1992) 465.
- [71] L. Lönnblad, Comp. Phys. Comm. 71 (1992) 15.
- [72] B. Bambah et al., Z Physics at LEP, CERN 89-08, eds. G. Altarelli, R. Kleiss and C. Verzegnassi, (Geneva, 1989) vol.3, p.143.
- [73] K. Goulianos, Phys. Lett. B193 (1987) 151.
- [74] X.N. Wang, M. Gyulassy and M. Plümer, Phys. Rev. D51 (1995) 3436.
- [75] B.I. Ermolaev and V.S. Fadin, JETP Lett. 33 (1981) 269;  
A.H. Mueller, Phys. Lett. B104 (1981) 161.
- [76] K. Konishi, A. Ukawa and G. Veneziano, Nucl. Phys. B157 (1979) 45.
- [77] V.A. Khoze, S. Lupia and W. Ochs, Eur. Phys. J. C5 (1998) 77.
- [78] S. Lupia and W. Ochs, Phys. Lett. B418 (1998) 214; Nucl. Phys. Proc. Suppl. 64 (1998) 74.
- [79] W. A. Bardeen, A.J. Buras, D.W. Duke and T. Muta, Phys. Rev. D18 (1978) 3998.
- [80] PDG, R.M. Barnett et al, Phys. Rev. D 54 (1996) 1.
- [81] Yu.L. Dokshitzer, V.A. Khoze and S.I. Troyan, Phys. Rev. D53 (1996) 89.

- [82] V.N.Gribov and L.N. Lipatov, Sov. J. Nucl. Phys. 15 (1972) 438;  
L.N. Lipatov, Sov. J. Nucl. Phys 20 (1975) 95;  
G. Altarelli and G. Parisi, Nucl. Phys. B126 (1977) 298;  
Yu.L. Dokshitzer, Sov. Phys. JETP 46 (1977) 641.
- [83] Yu.L. Dokshitzer and M. Olsson, Nucl. Phys. B396 (1993) 137.
- [84] F. Cuypers and K. Tesima, Z. Phys. C54 (1992) 87.
- [85] I.M. Dremin, C.S. Lam, V.A. Nechitailo, Phys. Rev. D61 (2000) 074020.
- [86] Yu.L. Dokshitzer, V.A. Khoze and S.I. Troyan, Perturbative QCD, ed. A.H. Mueller (World Scientific, Singapore, 1989).
- [87] E.D. Malaza and B.R. Webber, Nucl. Phys. B267 (1986) 702.
- [88] J.B. Gaffney and A.H. Mueller, Nucl. Phys. B250 (1985) 109.
- [89] F. Cuypers and K. Tesima, Z. Phys. C52 (1991) 69.
- [90] S. Catani, Yu.L. Dokshitzer, F. Fiorani and B.R. Webber, Nucl. Phys. B383 (1992) 419.
- [91] M. Olsson and G. Gustafson, Nucl. Phys. B406 (1993) 293.
- [92] S. Catani, Yu.L. Dokshitzer, F. Fiorani and B.R. Webber, Nucl. Phys. B377 (1992) 445.
- [93] I.M. Dremin and V.A. Nechitailo, Mod. Phys. Lett. A9 (1994) 1471.
- [94] Yu.L. Dokshitzer and I.M. Dremin, Nucl. Phys. B402 (1993) 139.
- [95] I.M. Dremin, Phys. Lett. B341 (1994) 95.
- [96] I.M. Dremin and V.A. Nechitailo, JETP Lett. 58 (1993) 881.
- [97] R. Ugoccioni, A. Giovannini and S. Lupia, Phys. Lett. B342 (1995) 387.
- [98] A. Capella, I.M. Dremin, J.W. Gary, V.A. Nechitailo and J. Tran Thanh Van, Phys. Rev. D61 (2000) 074009.

- [99] I.M. Dremin, B.B. Levtchenko and V.A. Nechitailo, Phys. Atom. Nucl. 57 (1994) 1029.
- [100] I.M. Dremin and J.W. Gary, Phys. Lett. B459 (1999) 341.
- [101] K. Shizuya and S.-H. H. Tye, Phys. Rev. Lett. 41 (1978) 787.
- [102] M.B. Einhorn and B.G. Weeks, Nucl. Phys. B146 (1978) 445.
- [103] Ya.I. Azimov, Yu.L. Dokshitzer and V.A. Khoze, Sov. Phys. Uspekhi 23 (1980) 732.
- [104] S. Lupia, Phys. Lett. B439 (1998) 150.
- [105] S.J. Brodsky and J.F. Gunion, Phys. Rev. Lett. 37 (1976) 402.
- [106] A.H. Mueller, Nucl. Phys. B241 (1984) 141.
- [107] P. Eden and G. Gustafson, JHEP 09 (1998) 015.
- [108] B.R. Webber, Phys. Lett. B143 (1984) 501.
- [109] Yu.L. Dokshitzer, V.A. Khoze and S.I. Troyan, Int. J. Mod. Phys. A7 (1992) 1875.
- [110] W.J. Marciano, Phys. Rev. D29 (1984) 580.
- [111] V.I. Zakharov, Progr. Theor. Phys. Suppl. 131 (1998) 107.
- [112] OPAL Collaboration, G. Alexander et al., Phys. Lett. B388 (1996) 659.
- [113] OPAL Collaboration, G. Abbiendi et al., Eur. Phys. J. C11 (1999) 217.
- [114] CLEO Collaboration, M.S. Alam et al., Phys. Rev. D56 (1997) 17.
- [115] DELPHI Collaboration, P. Abreu et al., Z. Phys. C56 (1992) 63.
- [116] A. Giovannini, S. Lupia and R. Ugoccioni, Phys. Lett. B374 (1996) 231.
- [117] I.M. Dremin and R.C. Hwa, Phys. Lett. B324 (1994) 477.
- [118] Yu.L. Dokshitzer, V.A. Khoze, A.H. Mueller and S.I. Troyan, Rev. Mod. Phys. 60 (1988) 373.

- [119] A. Giovannini and R. Ugoccioni, Proc. XXVIII Int. Symp. on Multiparticle Dynamics, Delphi, Greece, 1998 (World Scientific, Singapore, to be published).
- [120] A. Giovannini, S. Lupia and R. Ugoccioni, Phys. Lett. B388 (1996) 639.
- [121] J.W. Gary, unpublished.
- [122] I.M. Dremin, V.A. Nechitailo and M. Biyajima, J. Atom. Nucl. 59 (1996) 2264.
- [123] I.M. Dremin, JETP Lett. 31 (1980) 185.
- [124] I.M. Dremin and A.V. Leonidov, Sov. J. Nucl. Phys. 35 (1982) 247.
- [125] A.V. Leonidov and D.M. Ostrovskii, Phys. Atom. Nucl. 60 (1997) 119.
- [126] A.V. Leonidov and D.M. Ostrovskii, Lebedev Physical Institute reports, 1-2 (1997) 36.
- [127] J. Ellis and K. Geiger, Phys. Rev. D52 (1995) 1500.
- [128] J. Ellis and K. Geiger, Nucl. Phys. A590 (1995) 609c.
- [129] I.M. Dremin, JETP Lett. 60 (1994) 764.
- [130] R. Blankenbecler, Phys. Rev. D8 (1973) 1611.
- [131] C.N. Yang and T.D. Lee, Phys. Rev. 87 (1952) 404.
- [132] T.D. Lee and C.N. Yang, Phys. Rev. 87 (1952) 410.
- [133] E.A. De Wolf, Proc. XXIV Int. Symp. on Multiparticle Dynamics, Vietri sul Mare, Italy, 1994, eds. A. Giovannini, S. Lupia and R. Ugoccioni (World Scientific, Singapore, 1995) p. 15.
- [134] A. Capella, I.M. Dremin, V.A. Nechitailo and J. Tran Thanh Van, Z. Phys. C75 (1996) 89.
- [135] T.C. Brooks, K.L. Kowalski and C.C. Taylor, Phys. Rev. D56 (1997) 5857.



- [136] N. Brown and W.J. Stirling, Phys. Lett. B252 (1990) 657; Z. Phys. C53 (1992) 629.
- [137] S. Catani, Yu.L. Dokshitzer, M. Olsson, G. Turnock and B.R. Webber, Phys. Lett. B269 (1991) 432.
- [138] JADE Collaboration, W. Bartel et al., Z. Phys. C33 (1986) 23; S. Bethke et al., Phys. Lett. B213 (1988) 235.
- [139] Yu.L. Dokshitzer, V.A. Khoze and S.I. Troyan, Sov. J. Nucl. Phys. 47 (1988) 881.
- [140] J.W. Gary, Phys. Rev. D49 (1994) 4503.
- [141] V.A. Khoze, Proc. Workshop on Physics with Linear Colliders, Saariselkä, Finland, 1991, eds. R. Orava, E. Eerola and M. Nordberg (World Scientific, Singapore, 1992) p. 547.
- [142] JADE Collaboration, W. Bartel et al., Z. Phys. C21 (1983) 37.
- [143] UA2 Collaboration, P. Bagnaia et al., Phys. Lett. B144 (1984) 291.
- [144] TASSO Collaboration, M. Althoff et al., Z. Phys. C22 (1984) 307.
- [145] HRS Collaboration, M. Derrick et al., Phys. Lett. B165 (1985) 449.
- [146] OPAL Collaboration, P.D. Acton et al., Z. Phys. C58 (1993) 387.
- [147] DELPHI Collaboration, P. Abreu et al, Z. Phys. C70 (1996) 179.
- [148] ALEPH Collaboration, D. Buskulic et al., Phys. Lett. B384 (1996) 353.
- [149] OPAL Collaboration, R. Akers et al., Z. Phys. C68 (1995) 179.
- [150] CLEO Collaboration, M.S. Alam et al., Phys. Rev. D46 (1992) 4822.
- [151] ARGUS Collaboration, H. Albrecht et al., Z. Phys. C54 (1992) 13.
- [152] JADE Collaboration, W. Bartel et al., Z. Phys. C20 (1983) 187.
- [153] TASSO Collaboration, W. Braunschweig et al., Z. Phys. C45 (1989) 193.

- [154] HRS Collaboration, M. Derrick et al., Phys. Rev. D34 (1986) 3304.
- [155] AMY Collaboration, H.W. Zheng et al., Phys. Rev. D42 (1990) 737.
- [156] ALEPH Collaboration, R. Barate et al., Phys. Rep. 294 (1998) 1;  
 DELPHI Collaboration, P. Abreu et al., Eur. Phys. J. C6 (1999) 19;  
 L3 Collaboration, B. Adeva et al., Z. Phys. C55 (1992) 39;  
 OPAL Collaboration, K. Ackerstaff et al., Eur. Phys. J. C7 (1999) 369.
- [157] ALEPH Collaboration Note 98-025, CONF 98-014.
- [158] DELPHI Collaboration, P. Abreu et al., Phys. Lett. B372 (1996) 172;  
 L3 Collaboration, M. Acciarri et al., Phys. Lett. B371 (1996) 137;  
 OPAL Collaboration, G. Alexander et al., Z. Phys. C72 (1996) 191.
- [159] DELPHI Collaboration, P. Abreu et al., Phys. Lett. B416 (1998) 233;  
 L3 Collaboration, M. Acciarri et al., Phys. Lett. B404 (1997) 390.
- [160] OPAL Collaboration, K. Ackerstaff et al., Z. Phys. C75 (1997) 193.
- [161] OPAL Collaboration, G. Abbiendi et al., Eur. Phys. J. C16 (2000) 185.
- [162] L3 Collaboration, M. Acciarri et al., Phys. Lett. B444 (1998) 569.
- [163] ALEPH Collaboration Note 99-023, CONF 99-018.
- [164] L3 Collaboration Note 2505.
- [165] ALEPH Collaboration Note 2000-017, CONF 2000-014.
- [166] OPAL Collaboration, Physics Note PN420.
- [167] G. D. Lafferty, P. I. Reeves, and M. R. Whalley, Journal of Physics G,  
 Nucl. Part. Phys. 21 (1995) A1-A151;  
 The Durham RAL Databases, <http://durpdg.dur.ac.uk/HEPDATA>.
- [168] DELPHI Collaboration, P. Abreu et al., Phys. Lett. B449 (1999) 383.
- [169] A.N. Safonov, Nucl. Phys. Proc. Suppl. 86 (2000) 55.
- [170] OPAL Collaboration, G. Abbiendi et al., CERN-EP-2000-070.

- [171] DELPHI Collaboration, CERN-OPEN-2000-134.
- [172] I.M. Dremin, JETP Lett. 68 (1998) 559.
- [173] S. Lupia, W. Ochs and J. Wosiek, Nucl. Phys. B540 (1999) 405.
- [174] SLD Collaboration, K. Abe et al., Phys. Lett. B371 (1996) 149.
- [175] L3 Collaboration, L3 Note 2407; W. Metzger, Proc. XXIX Int. Symp. on Multiparticle Dynamics, Providence, USA, 1999 (World Scientific, Singapore, to be published).
- [176] V.A. Khoze, S. Lupia and W. Ochs, Phys. Lett. B394 (1997) 179.
- [177] K. Konishi, A. Ukawa and G. Veneziano, Phys. Lett. B78 (1978) 243.
- [178] I.M. Dremin, V. Arena, G. Boca, G. Gianini et al., Phys. Lett. B336 (1994) 119.
- [179] I.M. Dremin, V.A. Nechitailo, M. Biyajima and N. Suzuki, Phys. Lett. B403 (1997) 149.
- [180] R.K. Ellis, D.A. Ross and A.E. Terrano, Nucl. Phys. B178 (1981) 421.
- [181] G. Sterman and S. Weinberg, Phys. Rev. Lett. 39 (1977) 1436.
- [182] S. Bethke, Z. Kunszt, D.E. Soper and W.J. Stirling, Nucl. Phys. B370 (1992) 310.
- [183] L3 Collaboration, O. Adriani et al., Phys. Rep. 236 (1993) 1.
- [184] OPAL Collaboration, R. Akers et al., Z. Phys. C63 (1994) 363.
- [185] ALEPH Collaboration, D. Buskulic et al., Phys. Lett. B346 (1995) 389; ALEPH Collaboration, D. Barate et al., CERN-EP/98-016.
- [186] M.H. Seymour, Phys. Lett. B378 (1996) 279.
- [187] OPAL Collaboration, M.Z. Akrawy et al. Phys. Lett. B263 (1991) 311; OPAL Collaboration., G. Alexander et al., Phys. Lett. B265 (1991) 462.
- [188] J.W. Gary, Phys. Rev. D61 (2000) 114007.

- [189] P. Edén, G. Gustafson and V. Khoze, Eur. Phys. J. C11 (1999) 345.
- [190] P. Edén and G. Gustafson, JHEP 9809 (1998) 015.
- [191] A. Bialas and R. Peschanski, Nucl. Phys. B273 (1986) 703.
- [192] I.M. Dremin, JETP Lett. 45 (1987) 643.
- [193] R.P. Feynman, Proc. III Workshop on Current Problems in High Energy Particle Theory, Florence, Italy, 1979, eds. Casalbuoni et al. (John Hopkins University Press, Baltimore).
- [194] A. Giovannini, Nucl. Phys. B161 (1979) 429.
- [195] G. Veneziano, Proc. III Workshop on Current Problems in High Energy Particle Theory, Florence, Italy, 1979, eds. Casalbuoni et al. (John Hopkins University Press, Baltimore).
- [196] A. Bialas and R. Peschanski, Nucl. Phys. B308 (1988) 857.
- [197] W. Ochs and J. Wosiek, Phys. Lett. B214 (1988) 617.
- [198] I.M. Dremin, Mod. Phys. Lett. A4 (1989) 1027.
- [199] C.B. Chiu and R. Hwa, Phys. Lett. B236 (1990) 446.
- [200] G. Gustafson and A. Nilsson, Z. Phys. C52 (1991) 533; Nucl. Phys. B355 (1991) 106.
- [201] W. Ochs and J. Wosiek, Phys. Lett. B289 (1992) 159; B304 (1993) 144.
- [202] W. Ochs and J. Wosiek, Z. Phys. C68 (1995) 269.
- [203] Ph. Brax, J.L. Meunier and R. Peschanski, Z. Phys. C62 (1994) 649.
- [204] Yu.L. Dokshitzer, G. Marchesini and G. Orian, Nucl. Phys. B387 (1992) 675.
- [205] J.L. Meunier and R. Peschanski, Z. Phys. C72 (1996) 647.
- [206] I.V. Andreev, M. Biyajima, I.M. Dremin and N. Suzuki, Int. J. Mod. Phys. A10 (1995) 3951.

- [207] L3 Collaboration, M. Acciarri et al., Phys. Lett. B428 (1998) 186.
- [208] DELPHI Collaboration, P. Abreu et al., Phys. Lett. B457 (1999) 368.
- [209] L3 Collaboration, M. Acciarri et al., Phys. Lett. B429 (1998) 375.
- [210] S.V. Chekanov and V.I. Kuvshinov, Acta Phys. Polonica B25 (1994) 1189.
- [211] S.V. Chekanov, W. Kittel and V.I. Kuvshinov, Z. Phys. C74 (1997) 517.
- [212] M.I. Polikarpov, Phys. Lett. B236 (1990) 61.
- [213] I.M. Dremin and B.B. Levchenko, Phys. Lett. B292 (1992) 155.
- [214] I.M. Dremin, JETP Lett. 34 (1981) 594.
- [215] I.M. Dremin, JETP Lett. 30 (1979) 140; Sov. J. Nucl. Phys. 33 (1981) 726.
- [216] A.V. Apanasenko, N.A. Dobrotin, I.M. Dremin and K.A. Kotelnikov, JETP Lett. 30 (1979) 145.
- [217] B.A. Schumm, Yu.L. Dokshitzer, V.A. Khoze and D.S. Koetke, Phys. Rev. Lett. 69 (1992) 3025.
- [218] Yu.L. Dokshitzer, V.A. Khoze and S.I. Troyan, J. Phys. G17 (1991) 1481; 1602.
- [219] Ya.I. Azimov, Yu.L. Dokshitzer and V.A. Khoze, Sov. J. Nucl. Phys. 36 (1982) 878.
- [220] A.V. Kisselev, V.A. Petrov and O.P. Yuschenko, Z. Phys. C41 (1988) 521.
- [221] V.A. Petrov and A.V. Kisselev, Z. Phys. C66 (1995) 453.
- [222] DELPHI Collaboration, P. Abreu et al., Phys. Lett. B479 (2000) 118.
- [223] I.M. Dremin and V.I. Yakovlev, Proc. XVII Int. Symp. on Multiparticle Dynamics, Austria, 1986, ed. M. Markityan (World Scientific, Singapore, 1987) p. 849.